Modelling and Control of Lateral Wind Turbine Tower Dynamics

Gilian G.J. Ruiterkamp

Master of Science Thesis

TU Delft Delft University of Technology

Delft Center for Systems and Control

Modelling and Control of Lateral Wind Turbine Tower Dynamics

Master of Science Thesis

For the degree of Master of Science in Systems and Control at Delft University of Technology

Gilian G.J. Ruiterkamp

June 17, 2021

Faculty of Mechanical, Maritime and Materials Engineering (3mE) · Delft University of Technology

The work in this thesis was supported by Lagerwey Wind, part of Enercon. Their cooperation is hereby gratefully acknowledged.

Abstract

In recent years wind turbines have become increasingly large to increase energy yield and cost-effectiveness. This has led to taller turbine towers, subjected to larger loads. As a result, Lagerwey turbines experience lateral tower vibrations at different resonance frequencies. These vibrations result in rotor speed measurement disturbances due to tower top roll motion. Such disturbances affect controller performance and induce undesired generator torque variations. Generator torque excites the tower, thus, a closed-loop interaction between the tower and the torque controller exists. A tower model including two resonance frequencies has been obtained through model identification in a simulation environment, which includes tower top rotational velocity as an output. A Kalman filter based on this model is able to provide an accurate estimate of tower signals using the tower top acceleration measurement and the generator torque set point. The tower top rotational velocity estimate is used to filter the rotor speed measurement. In high-fidelity simulation, it is found that in above-rated conditions (where tower vibrations are most severe) tower loads are reduced by 5.85%. In order to obtain a further load reduction, a state-feedback tower damping controller has been developed. Vibration modes are damped individually with user-defined damping ratios. For the designed controller, an average load reduction of 32.5% is achieved at the cost of a 0.8% increase in standard deviation of electric power.

Table of Contents

List of Figures

List of Tables

Acknowledgements

I would like to thank prof. dr. ir. J.W. van Wingerden for his supervision during this project. It was my strong wish to fulfil my thesis project at a company, in order to apply the theoretical knowledge gained during previous years of study. Thanks to van Wingerden's network in industry, I got in touch with Lagerwey Wind, a Dutch turbine manufacturer which is now part of Enercon. Here, i came into contact with ir. Dennis de Bot, a control engineer who had been working on the thesis subject. I would like to thank Dennis for giving me the opportunity to perform the project under his daily supervision. The assignment balances theory and application, therefore making it diverse, interesting and exactly what I had desired. Additionally, I would like to thank Dennis for the effort he put into the supervision. You were always available for a discussion on different topics. Furthermore, I would like to thank ir. Edwin Pasterkamp, who was also responsible for giving me this opportunity. During the progress meetings you provided constructive criticism which was always helpful. I would also like to thank ir. Jim Kok and ir. Mun Jung. During the days that I was able to come to office (unfortunately not as many as we had hoped), you guys were helpful and open for a discussion on the subjects I was working on and provided pleasant distraction with "gezellige" talks at the coffee machine.

Finally, I would like to thank my family and my partner who have supported me throughout my Master. Graduating in times of Corona has been challenging and their support has kept me motivated.

Delft, University of Technology
June 17, 2021

Gilian G.J. Ruiterkamp

Chapter 1

Introduction

On 22 April 2015, 195 countries signed the Paris Climate Agreement. The participants committed to keeping the increase in global average temperature well below 2°C above pre-industrial levels [18]. In order to reach this ambitious goal, the most important measure to be taken is the transition from fossil fuels to renewable energy sources. Wind energy plays an important role in achieving this goal. In 2019, wind supplied 4.7% of the world's and 15% of Europe's electrical energy consumption with a large annual growth in share [24]. Currently, wind energy is typically installed with aid of governmental subsidies. To increase the economic viability of wind energy and due to the competition among turbine manufacturers, much effort is put into decreasing the Levelised Cost Of Energy (LCOE) which expresses the cost per unit of produced energy, [€/kWh]. For this reason, wind turbines are continuously improved to increase Annual Energy Production (AEP) and decrease life-cycle cost. The increasing performance and cost reduction criteria require constant technological development.

1-1 Developments in Wind Turbine Technology

Some trends can be observed in wind turbine technology in recent years, as listed. The causes for these trends are discussed below.

- Increasingly tall turbine towers
- Introduction of more lightweight tower designs
- Increasing rotor diameters
- Increasing power ratings
- Increase in tower top mass

Wind turbine towers have become increasingly tall, see Figure 1-1. This enables access to more uniform and higher average wind speeds found at higher altitudes, therefore increasing the AEP. In the meanwhile, more lightweight tower designs are introduced to increase cost-effectiveness. Rotor diameters have experienced a great increase in size to increase rotor through-flow area and therefore energy capture. This has led to an increase in power ratings and has resulted in increased aerodynamic loads on the turbine structure. The rotor-nacelle assembly has become heavier due to the increased rotor size and larger sub-components required for increasing power. Ultimately, this has led to a taller, more flexible tower that is subjected to larger loads. As a result, wind turbine towers experience increasingly large vibrations, which negatively impact the expected structural lifespan of a wind turbine tower.

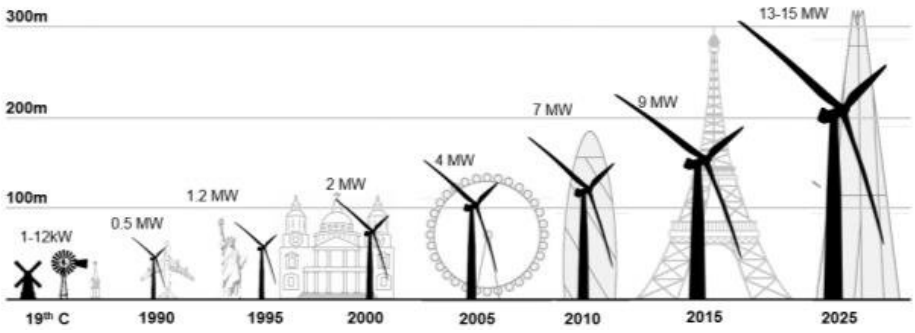

Figure 1-1: Evolution of wind turbine size and power output [12]

Due to the increased loading of structural turbine components, load reduction through advanced controller design is becoming increasingly important. This could enable further growth in wind turbine size and increase the lifetime of turbine components, therefore resulting in a decrease in LCOE. [17]

1-2 Problem Definition

In the subsequent section, background information regarding the project is provided. This leads to the research goals of the project.

The coordinate system of the turbine is defined in accordance with the system as used by Lagerwey, as shown in Figure 1-2.

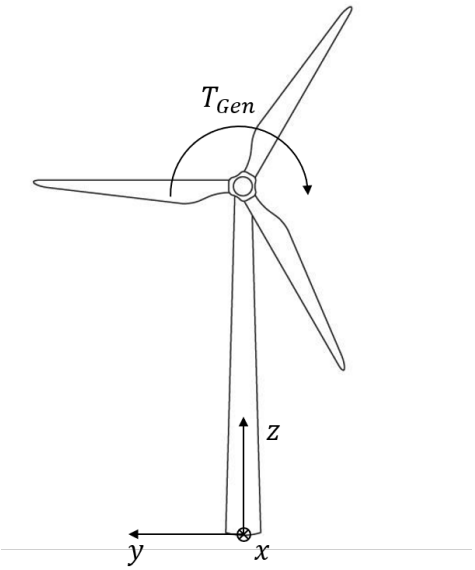

Figure 1-2: Wind turbine coordinate system

The z-axis vertically upward, the y-axis horizontally sideways and the x-axis horizontal in the wind direction. According to this coordinate system, the generator torque acting on the tower is positive in clockwise direction as shown above.

1-2-1 Background

Lagerwey turbines, in line with the trends stated above, experience increased tower loading. This has resulted in increasingly large tower vibrations. Tower vibrations in the fore-aft direction benefit from significant aerodynamic damping, however, aerodynamic damping in lateral direction is very small and sometimes even regarded negligible [27]. There have been situations in which vibrations in the lateral direction grow over a period of several minutes with no clear root cause. Possible causes suggested are a lower damping ratio in reality than in simulation, as well as closed-loop interaction of the tower and the controller.

The Lagerwey turbines exhibit a fully steel tower. Steel is known to have a relatively small damping capacity. In combination with the absence of other sources of damping, the tower basically resembles a large spring. The nacelle of the Lagerwey turbine features an accelerometer, able to measure tower top acceleration in the lateral direction. Multiple tower resonance frequencies are observed in the acceleration measurement, especially the first and second tower eigenfrequencies. Different excitation sources exist which could excite the tower in the

lateral direction. For example rotor mass imbalance, yaw misalignment, variations in the wind field and generator torque. Variations in the wind field could be the result of different phenomena, such as turbulence, tower shadow, wind shear or tower fore-aft velocity. Of these quantities, generator torque is controllable and therefore known. Generator torque results in direct excitation of the tower, since applying a torque to the rotor will result in an equally large reactive torque on the stator, which is rigidly connected to the nacelle/tower.

A possible cause for tower vibrations is interaction with the controller. Vibrations do not only result in lateral tower top displacements, they lead to tower top roll motion as well. The rotor speed Ω is measured with an encoder mounted to the stator. This means that if the stator is not a static frame of reference, this will affect the rotor speed measurement. The rotor speed measurement is the main input to the turbine controller, therefore disturbances directly affect controller performance and should be mitigated. In practice, it is observed that tower vibrations lead to disturbances in the rotor speed which result in additional pitch and torque action. With tower top rotational velocity ω, the measured rotor speed is simply: $\Omega_{meas} = \Omega - \omega$. A closed-loop interaction exists since rotor speed disturbances result in torque disturbances that could excite the tower.

The generator torque set point T_{gen} is directly related to the rotor speed measurement via a lookup-table, shown in Figure 1-3. Three regions are distinguished:

- Blue: Sub-rated
- Orange: Transient
- Green: Above-rated

In the sub-rated region generator torque is set according to the optimal power curve. At a certain rotor speed the torque-speed curve changes to a linear relation towards rated conditions. At rated conditions, the above-rated region is reached. In order to minimise power fluctuations an inverse relation is used here: $T_{gen} = \frac{P_{rated}}{\Omega}$, in which P_{rated} is rated generator power. This has a destabilising effect on rotor speed, which is compensated by the pitch controller. Finally, a transient region is used to further stabilise power output.

As shown, variations in rotor speed will have a direct effect on generator torque. Especially in the sub-rated region the slope is steep and therefore results in a large gain. In this region, a small change in rotor speed (measurement) has a significant effect on generator torque.

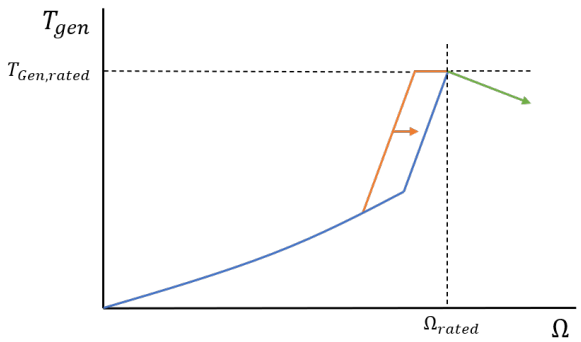

Figure 1-3: Torque-Rotor speed controller

In closed-loop, small disturbances can affect the tower's stability. This would manifest itself in reduced (or potentially negative) damping of the tower when considering the closed-loop system.

The controller gain $K_{\Omega \to T}$ equals the slope of the torque-speed curve shown above, and thus depends on operating conditions. This gain can therefore be either positive or negative. For stability, the maximum and minimum gains are of importance. These are deemed K_{SR} and K_{AR}, denoting the maximum positive gain which is obtained during sub-rated operation and the minimum negative gain, obtained above-rated.

- $K_{SR} = 34.377\ [\frac{MNm}{rad/s}]$
- $K_{AR} = -1.909\ [\frac{MNm}{rad/s}]$

Figure 1-4 shows the closed-loop interaction of the tower with the torque controller. One would expect a destabilising effect on tower vibrations in the above-rated operating region, where $K_{\Omega \to T}$ is negative. If the tower moves in the negative y-direction, the tower top rotates in positive rotor direction. The measured rotor speed, being the speed difference between rotor and stator is therefore reduced. A reduction in measured rotor speed results in an increase in generator torque in the above-rated operating region. Generator torque works in the same direction as tower movement and therefore amplifies the vibration.

This implies that in the sub-rated region, the tower is stabilised. It should be noted that tower vibrations are especially present in the above-rated operating region. The interaction can lead to both additional damping or reduced damping. Additional damping does not lead to negative effects, other than additional control action. However, regions with reduced damping are undesirable. The magnitude of this effect is yet unclear, given that no model incorporating tower rotational dynamics is available, and shall be further assessed after a sufficient tower model including rotational dynamics is obtained.

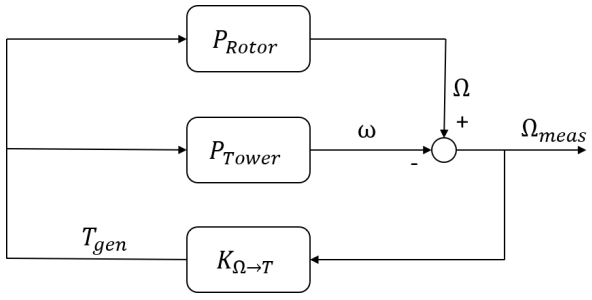

Figure 1-4: Closed-loop tower controller interaction

This interaction can be counteracted in two ways.

1. 'Break' the loop. By obtaining an estimate $\hat{\omega}$ and adding this to Ω_{meas}, the undisturbed rotor speed Ω is obtained.
2. Add artificial damping. By actively damping the tower through the controller.

In order to break the loop, typically a conventional filter, such as a notch filter, would be used to suppress disturbances at a certain frequency. A notch filter is a static filter, with a constant suppression in the frequency domain. However, this is not preferred since tower vibrations are highly variable, therefore the tuning of a filter would be difficult and could either result in insufficient suppression of the disturbance or to a loss of valuable information in the rotor speed signal. A Kalman filter is preferred, in which measurement and model information are optimally combined in order to obtain an estimate of $\hat{\omega}$. The amount of suppression in the frequency domain is therefore not static, but dependent on the estimate. Therefore this could be deemed a 'dynamic' filter. Lagerwey has developed a rotor speed measurement correction observer as shown in Figure 1-5.

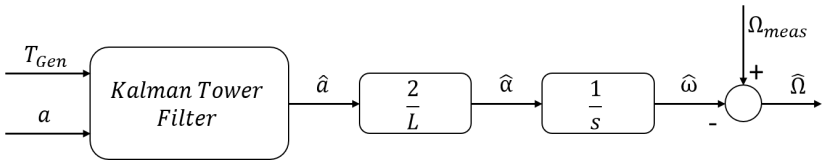

Figure 1-5: Current rotor speed measurement correction observer designed by Lagerwey

The goal is to estimate tower top rotational velocity and subtract it from the rotor speed measurement. A Discrete-Time (DT) Linear-Time-Invariant (LTI) State-Space (SS) Single-Input-Single-Output (SISO) model of generator torque to tower top acceleration has been identified using Subspace Identification with a Past-Input-Multivariable Output-Error-State-sPace (PI-MOESP) scheme in high-fidelity simulation package `Focus`. The model includes two vibration modes. A Kalman filter based on this 4^{th}-order model provides a filtered estimate of the acceleration measurement a. To obtain a relation between lateral acceleration and rotational acceleration α, a linear relation is assumed. This relation is based on the static beam bending theory of a clamped bead subjected to a torque, which will be discussed in Chapter 2. Finally, a free integrator is used to obtain an estimate of tower top rotational velocity.

Results of this filter have shown successful elimination of the fundamental (1^{st}) tower lateral resonance frequency in the rotor speed measurement. However, the observer is unable to filter a higher-order tower resonance frequency occurring in measurements. From this, it has been concluded that the linear relation $2/L$ does not hold for higher-order vibration modes. The observer has reduced torque and pitch actions as the controller is not affected by the first tower mode. Potentially, an additional increase could be attained if the Kalman filter is extended to the other observed tower resonance frequency.

As the first resonance frequency is filtered from the rotor speed measurement, the closed-loop interaction is removed. However, tower vibrations remain to exist and are still deemed too large. One possible solution could be to alter the dynamic behaviour of the tower by adjusting the mechanical design. However, this would be expensive, complicated and would likely undo the cost savings of the more lightweight tower design. Therefore, the solution is sought in controller design. A controller modification does not add additional cost to the turbine (excluding development cost). The goal is to actively damp lateral tower vibrations through a controller modification. This damping controller should be able to damp multiple modes optimally. If performed correctly, tower loads are reduced. This could enable the future design of more lightweight and cost-effective towers.

1-2-2 Research Goals

Three main research questions have been determined for the project. The first research question is as follows:

How can tower top rotational dynamics be modelled and included in a tower model?

It is unclear how tower top rotational dynamics are related to translation dynamics. Therefore, a model is to be derived which includes rotational dynamics of the tower for multiple modes. The second research question is related to breaking the loop:

How can an online estimate of tower top rotational velocity, including multiple tower vibration modes, be obtained and can it be used for rotor speed measurement correction?

Since limited sensor information is available, namely tower top acceleration and generator torque, the question is whether it is possible to obtain an accurate estimate of tower top rotational velocity ω for multiple vibrations modes, such that it reduces disturbances in the rotor speed signal. The third research goal is to add artificial damping to the tower:

Can a controller be designed, able to optimally damp multiple vibration modes?

A tower damping controller is to be designed which allows optimal damping of multiple vibration modes. This requires a model-based control design. To this extent, the model obtained from objective one is considered.

1-2-3 Case Study

For this project, a single turbine of Lagerwey's product range is studied, namely the L136 P4650 T132M BLM AW8.5 TI16.0. For this reason, a general description of this specific turbine is provided. Parameters of the turbine are provided in Table 1-1.

The Lagerwey turbine is a variable speed variable pitch turbine. As the name suggests, the turbine is designed for an annual average wind speed of 8.5 m/s and a turbulence intensity of 16%. Lagerwey turbines exhibit some features which are worth mentioning with respect to the project. The turbine features a Permanent Magnet Direct Drive (PMDD) synchronous generator, therefore the turbine lacks a gearbox. This reduces the complexity of the turbine's controller and the problem at hand. First, gearbox dynamics do not have to be modelled when assessing the effect of generator torque on the turbine tower. Secondly, gearbox loads do not have to be taken into account when designing a controller. Another feature of the Lagerwey turbines is the Modular Steel Tower (MST), a full steel tower design. This tower consists of steel plates that can be transported using regular trucks and are assembled on-site using bolted connections. The advantages of such a tower design are a decrease in transportation cost, as well as a more lightweight tower design. The tower is a soft-stiff type tower, meaning that in rated conditions the first eigenfrequency is in between the rotor and blade-passing frequencies (1P and 3P).

Table 1-1: Turbine specification

L136 P4650 T132M BLM AW8.5 TI16.0	
Parameter	Value
Power Output	4.65 MW
Rated Wind Speed	12 m/s
Rotor Speed (Rated)	11.1 RPM
Generator Torque (Rated)	4.438 MNm
Rotor Diameter	136 m
Hub Height	132 m
Cut-in Wind Speed	2.5 m/s
Cut-out Wind Speed	25 m/s
Tower Base Diameter	10.7 m
Tower Top Diameter	3.1 m
Tower structural damping ratio	0.002387

1-3 Outline

The report will discuss the design of a tower Kalman filter and tower damping controller. In Chapter 2, tower modelling techniques are assessed in order to establish a relation between tower top rotation and translation. Using this information a state-space model structure is established. Additionally, an analysis is performed on which excitation sources could potentially excite the tower in lateral direction, besides generator torque. In the next chapter, Chapter 3, a system model is to be identified. First, an experiment is designed in `Focus`. The resulting input and output data is used to derive a tower model. For this purpose, subspace identification with a Past-Output-Multivariable-Output-Error-State-sPace (PO-MOESP) scheme is used. In Chapter 4, a Kalman filter, based on the identified model is designed. Design Load Case (DLC) experiments are used for this purpose. With a Kalman gain identified, a tower damping controller is designed in Chapter 5. Final conclusions are drawn and recommendations for future research are provided in Chapter 6.

Chapter 2

Tower Modelling

In order to acquire a better understanding of the tower's dynamics, the physical equations governing tower dynamics are evaluated. By doing so, a model structure is obtained. The tower is a highly non-uniform structure, therefore the goal is not to derive a tower model analytically, as this will be obtained through a system identification procedure. Rather, the goal is to evaluate linearity of the relationship between displacement and rotation of a beam for different vibration modes and to obtain insight into the tower's dynamics in order to validate the identified model.

2-1 Euler-Bernoulli Beam Theory

As a starting point, the well-known Euler-Bernouilli (EB) beam theory is used. This theory depends on two main assumptions; one dimension of the beam is much larger than the other two and deflections are relatively small compared to the beam's length. Both assumptions are valid for a turbine tower.

2-1-1 Static Equation

The tower can be regarded as a clamped beam with a torque applied to the end. Figure 2-1 shows the turbine tower represented as such.

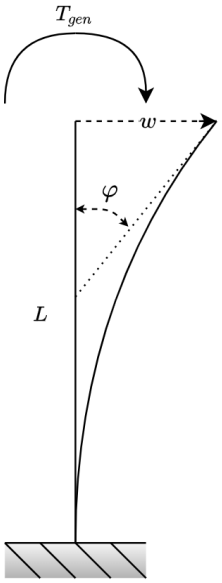

Figure 2-1: Static deformation of a clamped beam subjected to an external torque

$w(z)$ and $\varphi(z)$ are the deflection and rotation of the beam at certain height z. Note that $w(z)$ is displayed in negative y-direction in the figure. The static EB equation states:

$$\frac{d^2w(z)}{dz^2} = \frac{T_{gen}}{EI} \tag{2-1}$$

With elastic modulus E and area moment of inertia I. The second derivative of $w(z)$ with respect to z is a measure for the curvature of the beam. Upon integrating the equation once and twice, the equations for the angle φ and the displacement w are obtained respectively:

$$\varphi(z) = \frac{dw(z)}{dz} = \frac{T_{gen}}{EI}z, \quad w(z) = \frac{T_{gen}}{2EI}z^2 \tag{2-2}$$

The point of interest is the end of the beam (the nacelle). For hub height $z = L$, it can easily be seen that a linear relation exists between φ and w when a torque is applied to the end of a beam:

$$\varphi(L) = \frac{2}{L}w(L) \tag{2-3}$$

Tower top deflections can be caused by torque (T), forces (F) or distributed loads (q) acting on the tower.

$$w(L) = \frac{TL^2}{2EI}, \quad w(L) = \frac{FL^3}{3EI}, \quad w(L) = \frac{qL^4}{8EI} \tag{2-4}$$

As can be seen, their effects are linearly scaled. This relationship is typically used in literature to combine the effects of distributed loads, forces and torque acting on the tower top. [19, 16, 8]

2-1-2 Dynamic Equation

To evaluate the beam's natural frequencies and mode shapes, the dynamic EB equation for free vibration can be evaluated [11]. A viscous damping term η is assumed.

$$\rho_t A \frac{\partial^2 w}{\partial t^2} + \eta \frac{\partial w}{\partial t} + EI \frac{\partial^4 w}{\partial z^4} = 0 \tag{2-5}$$

With beam density ρ_t and cross-sectional area A. With no exogenous force applied to the beam, the following four boundary conditions can be derived:

$$for\ z = 0: \quad w(0,t) = 0,\ \frac{\partial w}{\partial z}(0,t) = 0 \tag{2-6}$$

$$for\ z = L: \quad \frac{\partial^2 w}{\partial z^2}(L,t) = 0,\ \frac{\partial^3 w}{\partial z^3}(L,t) = 0 \tag{2-7}$$

Separability of the partial differential equation allows for separation into a time-dependent and space-dependent part:

$$w(z,t) = W(z)T(t) \tag{2-8}$$

$$\rho A W \ddot{T} + \eta W \dot{T} + EI \frac{d^4 W}{dz^4} T = 0 \tag{2-9}$$

$$\frac{1}{T}\left(\ddot{T} + \frac{\eta}{\rho A}\dot{T}\right) = -\frac{EI}{\rho A}\frac{1}{W}\frac{d^4 W}{dz^4} = -\omega_n^2 \tag{2-10}$$

The time-dependent part is an Ordinary Differential Equation (ODE) with a general solution which can be determined using eigenvalues.

$$\ddot{T} + \frac{\eta}{\rho A}\dot{T} + \omega_n^2 T = 0 \tag{2-11}$$

$$\lambda^2 + \frac{\eta}{\rho A}\lambda + \omega_n^2 = 0 \tag{2-12}$$

$$\left(\lambda + \frac{\eta}{2\rho A}\right)^2 - \frac{\eta^2}{4\rho^2 A^2} + \omega_n^2 = 0 \tag{2-13}$$

$$\lambda + \frac{\eta}{2\rho A} = \pm\sqrt{\frac{\eta^2}{4\rho^2 A^2} - \omega_n^2} \tag{2-14}$$

$$\lambda_{1,2} = -\frac{\eta}{2\rho A} \pm \sqrt{\omega_n^2 - \frac{\eta^2}{4\rho^2 A^2}}i = -\sigma \pm \omega_d i \tag{2-15}$$

$$= -\zeta\omega_n \pm \omega_n\sqrt{1-\zeta^2} \tag{2-16}$$

$$\Rightarrow T(t) = e^{-\sigma}\left(a_1 cos(\omega_d t) + b_2 sin(\omega_d t)\right) \tag{2-17}$$

The constants a_1 and a_2 can be determined given the beam's initial conditions. As shown, the damped natural frequency ω_d is slightly lower than the undamped natural frequency ω_n.

The space-dependent part is a standard ODE as well and can be determined using the same principle:

$$\frac{d^4W}{dz^4} - \beta^4 W = 0, \quad \beta^4 = \frac{\rho A \omega_n^2}{EI} \tag{2-18}$$

$$W(z) = C_1 cos(\beta z) + C_2 sin(\beta z) + C_3 cosh(\beta z) + C_4 sinh(\beta z) \tag{2-19}$$

The solutions of the space-dependent part can be derived using an eigenvalue problem. Solutions exist for:

$$2\big(1 + cos(\beta L) cosh(\beta L)\big) = 0 \Rightarrow cos(\beta L) cosh(\beta L) = -1 \tag{2-20}$$

This equation has an infinite number of solutions; $\beta L = \{\pm 1.875, \pm 4.694, \pm 7.855...\}$. Given these numbers and Equation (2-18), an infinite series of undamped natural frequencies can be determined:

$$\omega_n = \left(\frac{\beta L}{L}\right)^2 \sqrt{\frac{EI}{\rho A}} \tag{2-21}$$

Given the set of boundary conditions, the following is derived:

$$C_3 = -C_1 \tag{2-22}$$

$$C_4 = -C_2 \tag{2-23}$$

$$C_2 = -RC_1, \quad with\ R = \frac{cosh(\beta L) + cos(\beta L)}{sinh(\beta L) + sin(\beta L)} \tag{2-24}$$

Yielding the following mode shape equation with ratio R:

$$W(z) = C_1 \Big(\big(cosh(\beta z) - cos(\beta z)\big) + R\big(sin(\beta z) - sinh(\beta z)\big) \Big) \tag{2-25}$$

A final scaling factor C_1 remains undetermined in this analysis, however, is sufficiently small in order to ensure only elastic deformation of the beam and is such that rotations and displacements remain small. The mode shape equation Equation (2-25) can be considered an eigenfunction related to the eigenvalues found from Equation (2-20). Given that an infinite number of eigenvalues exist, an infinite number of related mode shapes exist. In general, higher-order modes are increasingly damped and typically neither excited nor observed. For the turbine tower, the first two modes are typically observed and therefore most relevant. Additionally, the third mode is considered. In Figure 2-2, the first three mode shapes are plotted.

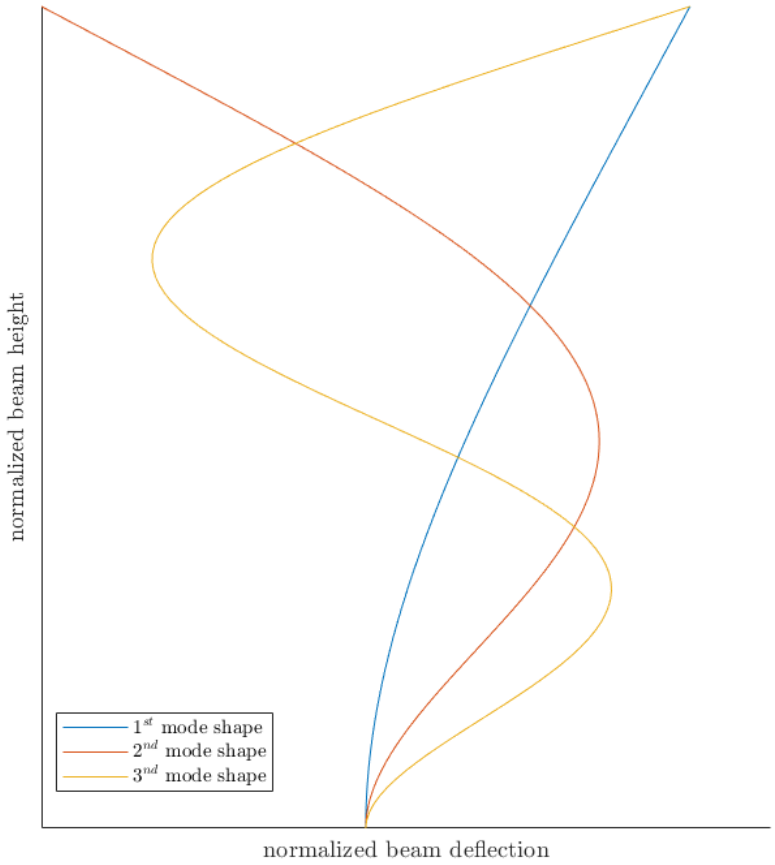

Figure 2-2: Vibration mode shapes of a clamped beam

The solution for a single eigenvalue and therefore a single vibration mode n is a product of the time-dependent (sinusoidal) part $T_n(t)$ and mode shape $W_n(z)$:

$$w_n(z,t) = T_n(t)W_n(z), \quad n = 1, 2, 3, ... \tag{2-26}$$

Subsequently, the solution of the homogeneous partial differential equation to Equation (2-5) is a linear combination of the different modes.

$$w(z,t) = \sum_{n=1}^{\infty} c_n w_n(z,t) = c_1 w_1(z,t) + c_2 w_2(z,t) + \cdots \tag{2-27}$$

Let c_n be a scalar that determines the relative contribution of the mode shape and is determined by modal mass, damping and stiffness. Due to the orthogonality of the eigenfunctions, the response of the non-homogeneous system to an exogenous input signal remains a linear combination of the mode shapes. [2, p. 705]

2-2 Timoshenko-Ehrenfest Beam Theory

A slightly more accurate beam model is the Timoshenko-Ehrenfest (TE) beam theory, which takes into account shear deformation and rotational bending effects. The most important difference is that for the EB theory: $\frac{\partial w}{\partial z} = \varphi$, whereas this is not the case for TE beam theory. Especially for beams with a larger thickness-to-length ratio and for higher-order vibration modes, the TE beam theory provides more accurate results. Additionally, it should be noted that the simulation program used for system identification experiment design, `Focus`, makes use of the TE beam theory in combination with a multi-body tower model. A summary of TE theory is provided here.

Where EB theory describes the beam's dynamics using a single Partial Differential Equation (PDE), TE theory requires a set of two coupled PDEs. For a prismatic beam:

$$\rho A \frac{\partial^2 w}{\partial t^2} + \eta_1 \frac{\partial w}{\partial t} = \kappa A G (\frac{\partial^2 w}{\partial z^2} - \frac{\partial \varphi}{\partial z}) \tag{2-28}$$

$$\rho I \frac{\partial^2 \varphi}{\partial t^2} + \eta_2 \frac{\partial \varphi}{\partial t} = EI \frac{\partial^2 \varphi}{\partial z^2} + \kappa A G (\frac{\partial w}{\partial z} - \varphi) \tag{2-29}$$

In this case, angular displacement is not approximated by the partial derivative $\frac{\partial w}{\partial z}$, which represents the slope of the deflection but by a separate variable φ. The additional parameters G and κ represent the beam's shear modulus, second moment of inertia and the (geometry dependent) Timoshenko shear coefficient respectively.

The most important observation is that the solution to these PDEs can be obtained through use of separability, by which the following can be established:

$$w(z,t) = W(z)T(t) \tag{2-30}$$

$$\varphi(z,t) = \Phi(z)T(t) \tag{2-31}$$

The time-dependent part $T(t)$ is equal for both functions. For Equation (2-28) this results in:

$$\frac{\partial^2 w}{\partial t^2} + \frac{\eta_1}{\rho A}\frac{\partial w}{\partial t} - \frac{\kappa G}{\rho}\frac{\partial^2 w}{\partial z^2} + \frac{\kappa G}{\rho}\frac{\partial \varphi}{\partial z} = 0 \tag{2-32}$$

$$W\ddot{T} + \frac{\eta_1}{\rho A} W\dot{T} - \frac{\kappa G}{\rho}\frac{d^2 W}{dz^2}T + \frac{\kappa G}{\rho}\frac{d\Phi}{dz}T = 0 \tag{2-33}$$

$$\frac{1}{T}\left(\ddot{T} + \frac{\eta_1}{\rho A}\dot{T}\right) = \frac{1}{W}\frac{\kappa G}{\rho}(\frac{d^2 W}{dz^2} - \frac{d\Phi}{dz}) = -\omega_n^2 \tag{2-34}$$

$$\Rightarrow \begin{cases} \ddot{T} + \frac{\eta_1}{\rho A}\dot{T} + T\omega_n^2 = 0 \\ \frac{d^2 W}{dz^2} + \frac{\omega_n^2 \rho}{\kappa G} W - \frac{d\Phi}{dz} = 0 \end{cases} \tag{2-35}$$

For Equation (2-29):

$$\frac{\partial^2\varphi}{\partial t^2} + \frac{\eta_2}{\rho I}\frac{\partial\varphi}{\partial t} - \frac{E}{\rho}\frac{\partial^2\varphi}{\partial z^2} - \frac{\kappa AG}{\rho I}\frac{\partial w}{\partial z} + \frac{\kappa AG}{\rho I}\varphi = 0 \tag{2-36}$$

$$\Phi\ddot{T} + \frac{\eta_2}{\rho I}\Phi\dot{T} - \frac{E}{\rho}\frac{d^2\Phi}{dz^2}T - \frac{\kappa AG}{\rho I}\frac{dW}{dz}T + \frac{\kappa AG}{\rho I}\Phi T = 0 \tag{2-37}$$

$$\frac{1}{T}(\ddot{T} + \frac{\eta_2}{\rho I}\dot{T}) = \frac{1}{\Phi}(\frac{E}{\rho}\frac{d^2\Phi}{dz^2} + \frac{\kappa AG}{\rho I}\frac{dW}{dz}) - \frac{\kappa AG}{\rho I} = -\omega_n^2 \tag{2-38}$$

$$\Rightarrow \begin{cases} \ddot{T} + \frac{\eta_2}{\rho I}\dot{T} + \omega_n^2 T = 0 \\ \frac{d^2\Phi}{dz^2} + (\frac{\omega_n^2\rho}{E} - \frac{\kappa AG}{EI})\Phi + \frac{\kappa AG}{\rho I}\frac{dW}{dz}) = 0 \end{cases} \tag{2-39}$$

Let $\eta_2 = \frac{\eta_1 I}{A}$, such that both PDEs have equal resulting eigenfrequencies. More involved, but in the same way as for the EB-equation, the solution to the set of differential equations can be obtained. The solution for a specific mode n and the total solution for the set of PDEs can be found similarly as shown in Equation (2-26) and Equation (2-27).

$$\begin{cases} w_n(z,t) = W_n(z)T_n(t) \\ \varphi_n(z,t) = \Phi_n(z)T_n(t) \end{cases} \quad , \quad n = 1, 2, 3, ... \tag{2-40}$$

Then the solution of the homogeneous partial differential equation is a linear combination of the different eigenfunctions.

$$\begin{cases} w(z,t) = \sum_{n=1}^{\infty} c_n w_n(z,t) = c_1 w_1(z,t) + c_2 w_2(z,t) + \cdots \\ \varphi(z,t) = \sum_{n=1}^{\infty} k_n \varphi_n(z,t) = k_1 \varphi_1(z,t) + k_2 \varphi_2(z,t) + \cdots \end{cases} \tag{2-41}$$

2-3 Rotational Dynamics

A relation between translation and rotation needs to be derived. For EB theory it is known that $\varphi_n = \frac{\partial w_n}{\partial z}$. The separation principle allows for the time-dependent part to be regarded as a constant with respect to z:

$$\varphi_n(z,t) = \frac{\partial w_n(z,t)}{\partial z} = \frac{\partial}{\partial z}W_n(z)T_n(t) = T_n(t)\frac{d}{dz}W_n(z) \tag{2-42}$$

Linearity of φ_n with respect to w_n can be established as follows:

$$\frac{\varphi_n(z,t)}{w_n(z,t)} = \frac{\partial w_n(z,t)}{\partial z}\Big(w_n(z,t)\Big)^{-1} = \frac{T_n(t)\frac{d}{dz}W_n(z)}{T_n(t)W_n(z)} = \frac{\frac{d}{dz}W_n(z)}{W_n(z)} \tag{2-43}$$

For any given value of z, such as $z = L$, the ratio between $W(z)$ and its derivative is constant and independent of time. This means that for the tower top, for each vibration mode, a constant linear relation exists between translation and rotation. This implies that without increasing model complexity a linear model can be used to describe not only the lateral motion of the turbine tower top but the rotational motion as well. If the mode shapes of the tower are known, the angular shape of the tower can be determined. For simplicity, C_1 is set to one. The derivative of the space-dependent part with respect to z is:

$$\frac{dW_n(z)}{dz} = sinh(\beta z) + sin(\beta z) + R(cos(\beta z) - cosh(\beta z)) \tag{2-44}$$

For the TE theory, the same can be established. For a certain tower height such as the tower top at $z = L$ the following is obtained for a single mode n:

$$\begin{cases} w_n(L,t) = W_n(L)T_n(t) \\ \varphi_n(L,t) = \Phi_n(L)T_n(t) \end{cases} \tag{2-45}$$

$$\Rightarrow \varphi_n(L,t) = \frac{\Phi_n(L)}{W_n(L)} w_n(L,t) \tag{2-46}$$

Therefore, similar to the EB beam theory, the TE beam theory results in a constant ratio between tower top displacement and rotation for a specific mode. This linear relation is established for angle φ and deflection w. Therefore it holds for its derivatives as well, given that differentiation and integration are linear operations. For the first and second vibration mode the scalars α and β can be defined and the following holds:

$$\varphi_1(t) = \alpha w_1(t) \quad \varphi_2(t) = \beta w_2(t) \tag{2-47}$$

$$\dot{\varphi}_1(t) = \alpha \dot{w}_1(t) \quad \dot{\varphi}_2(t) = \beta \dot{w}_2(t) \tag{2-48}$$

$$\ddot{\varphi}_1(t) = \alpha \ddot{w}_1(t) \quad \dot{\varphi}_2(t) = \beta \ddot{w}_2(t) \tag{2-49}$$

Thus the relation holds for (rotational) velocity and acceleration as well.

2-4 Tower Loads

Tower vibrations lead to mechanical loads. The tower base is subjected to the largest loads and is therefore typically used to quantify tower loads. For this purpose tower base bending moments are used, separated in x and y-direction. The tower bending moment in x-direction is related to lateral bending of the tower, whereas tower bending moment in y-direction is related to fore-aft bending. In this report, tower bending moment in x-direction is deemed $M(z)$, additionally, $M(0) = M$. According to EB theory, tower bending moment relates to the tower shape as follows:

$$M(z) = E(z)I(z)\frac{\partial^2 w}{\partial z^2}(z,t) \tag{2-50}$$

Thus, bending moments are linearly related to the beam's curvature $\frac{\partial^2 w}{\partial z^2}(z,t)$, since the curvature of the beam is a result of internal bending moments. From the beam's mode shapes, the curvature of the beam can be obtained for each mode.

$$M(z) = E(z)I(z)\frac{\partial^2 w}{\partial z^2}(z,t) \tag{2-51}$$

$$= E(z)I(z)\sum_{n=1}^{\infty} c_n \frac{\partial^2 w_n}{\partial z^2}(z,t) \tag{2-52}$$

$$= E(z)I(z)\left(c_1\frac{\partial^2 w_1}{\partial z^2}(z,t) + c_2\frac{\partial^2 w_2}{\partial z^2}(z,t) + \cdots\right) \tag{2-53}$$

Ultimately, it can be found that for a given height z, the dynamics of tower bending moment are a linear function of time-dependent functions $T_n(t)$.

$$M = EI\frac{\partial^2 w}{\partial z^2}(0,t) \tag{2-54}$$

$$= EI\sum_{n=1}^{\infty} c_n \frac{\partial^2 w_n}{\partial z^2}(0,t) \tag{2-55}$$

$$= EI\left(c_1 T_1(t)\frac{d^2 W_1}{dz^2}(0) + c_2 T_2(t)\frac{d^2 W_2}{dz^2}(0) + \cdots\right) \tag{2-56}$$

$$= c_{1,M}\cdot T_1(t) + c_{2,M}\cdot T_2(t) + \cdots \tag{2-57}$$

Similar to rotational dynamics, tower loads can be included in the model without increasing model complexity. Bending moments at arbitrary beam heights can be taken into account. However, in this project, a tower base moment is considered.

2-5 Linear Model

In previous sections, it has been established that a scalar relation exists between lateral and rotational dynamics for a certain tower height and vibration mode. Additionally, it is found that tower loads are linearly related to lateral tower dynamics as well. With the tower's dynamics known, a model structure of the required form can be derived. Considering the separable PDE from Equation (2-26), the dynamics of the system are only dependent on the time-dependent part $T_n(t)$. All outputs of the system are linearly related to this function through the mode shapes. As shown in Equation (2-17), the time-dependent part for each mode is a 2^{nd}-order ODE, thus a damped complex pole pair. This means that each vibration mode for a certain point on the beam can be modelled as a mass-spring-damper system.

For a given point on the beam z the space dependent part $W_n(z)$ reduces to a scalar and only the time dependent part $T_n(t)$ remains. Below, the first tower mode $w_1(z,t)$ is modelled for $z = L$:

$$a_1'\ddot{w}_1(t) + a_2'\dot{w}_1(t) + a_3' w_1(t) = a_4 T_{gen}(t), \quad w_1(t) = w_1(L,t) \tag{2-58}$$

a_1', a_2' and a_3' represent the modal mass, damping and stiffness respectively, a_4 is an arbitrary scaling factor. Given that the model will ultimately be identified, three coefficients are sufficient to obtain the same degrees of freedom. Therefore scaling factor a_4 is included in the coefficients representing modal mass, damping and stiffness.

$$\frac{a_1'}{a_4}\ddot{w}_1(t) + \frac{a_2'}{a_4}\dot{w}_1(t) + \frac{a_3'}{a_4}w_1(t) = T_{gen}(t) \tag{2-59}$$

$$a_1\ddot{w}_1(t) + a_2\dot{w}_1(t) + a_3 w_1(t) = T_{gen}(t) \tag{2-60}$$

Hence, the coefficients are not per se similar to the physical quantities, mass, damping and stiffness, as defined earlier. By defining $\mathbf{x_1}(t) = \begin{bmatrix} x_1(t) \\ \dot{x}_1(t) \end{bmatrix} = \begin{bmatrix} w_1(t) \\ \dot{w}_1(t) \end{bmatrix}$ the following state space equation is derived.

$$\dot{\mathbf{x}}_\mathbf{1}(t) = A_1\mathbf{x_1}(t) + B_1 u(t) = \begin{bmatrix} \dot{x}_1(t) \\ \ddot{x}_1(t) \end{bmatrix} = \begin{bmatrix} 0 & 1 \\ -\frac{a_3}{a_1} & -\frac{a_2}{a_1} \end{bmatrix} \begin{bmatrix} x_1(t) \\ \dot{x}_1(t) \end{bmatrix} + \begin{bmatrix} 0 \\ \frac{1}{a_1} \end{bmatrix} u(t) \tag{2-61}$$

$$y_1(t) = C_1\mathbf{x_1}(t) + D_1 u(t) = \begin{bmatrix} -\frac{a_3}{a_1} & -\frac{a_2}{a_1} \end{bmatrix} \begin{bmatrix} x_1(t) \\ \dot{x}_1(t) \end{bmatrix} + \begin{bmatrix} \frac{1}{a_1} \end{bmatrix} u(t) \tag{2-62}$$

with $u(t) = T_{gen}(t)$ and $y_1(t) = \ddot{w}_1(t)$. The 2^{nd}-order tower model, representing the fundamental vibration mode of the tower top, is used in the vast majority of studies regarding tower damping (both fore-aft and side-side) [19, 4, 1, 15, 13, 10, 23, 7, 22, 14, 16, 6, 5, 9, 26, 20, 8]. Zhang et al. [27] also uses a 2^{nd}-order tower model but separates rotational dynamics from lateral dynamics to model coupling of lateral tower dynamics with the edgewise vibration mode of the blades. Therefore, two 2^{nd}-order models are used to model the fundamental tower vibration mode.

By evaluating Equation (2-26), it is observed that the same principle applies to the second vibration mode and a similar State-Space (SS) model can be derived for $y_2(t) = \ddot{w}_2(t)$ and $\mathbf{x_2}(t) = \begin{bmatrix} x_2(t) \\ \dot{x}_2(t) \end{bmatrix} = \begin{bmatrix} w_2(t) \\ \dot{w}_2(t) \end{bmatrix}$:

$$b_1\ddot{w}_2(t) + b_2\dot{w}_2(t) + b_3 w_2(t) = T_{gen}(t) \tag{2-63}$$

$$\dot{\mathbf{x}}_\mathbf{2}(t) = A_2\mathbf{x_2}(t) + B_2 u(t) = \begin{bmatrix} \dot{x}_2(t) \\ \ddot{x}_2(t) \end{bmatrix} = \begin{bmatrix} 0 & 1 \\ -\frac{b_3}{b_1} & -\frac{b_2}{b_1} \end{bmatrix} \begin{bmatrix} x_2(t) \\ \dot{x}_2(t) \end{bmatrix} + \begin{bmatrix} 0 \\ \frac{1}{b_1} \end{bmatrix} u(t) \tag{2-64}$$

$$y_2(t) = C_2\mathbf{x_2}(t) + D_2 u(t) = \begin{bmatrix} -\frac{b_3}{b_1} & -\frac{b_2}{b_1} \end{bmatrix} \begin{bmatrix} x_2(t) \\ \dot{x}_2(t) \end{bmatrix} + \begin{bmatrix} \frac{1}{b_1} \end{bmatrix} u(t) \tag{2-65}$$

with b_1, b_2 and b_3 representing parameters equivalent to a_1, a_2 and a_3 respectively, however, in this case related to the second mode. Equation (2-27) demonstrates that the total deflection is obtained by summation of the two vibration modes.

The relationship remains valid upon differentiation.

$$w(L,t) = c_1 w_1(t) + c_2 w_2(t) \tag{2-66}$$
$$\dot{w}(L,t) = c_1 \dot{w}_1(t) + c_2 \dot{w}_2(t) \tag{2-67}$$
$$\ddot{w}(L,t) = c_1 \ddot{w}_1(t) + c_2 \ddot{w}_2(t) \tag{2-68}$$

By using Equation (2-68), a tower SS model of two vibration modes can be constructed by appending these models:

$$\dot{\mathbf{x}}(t) = A\mathbf{x}(t) + Bu(t) = \begin{bmatrix} \dot{x}_1(t) \\ \ddot{x}_1(t) \\ \dot{x}_2(t) \\ \ddot{x}_2(t) \end{bmatrix} = \begin{bmatrix} 0 & 1 & 0 & 0 \\ -\frac{a_3}{a_1} & -\frac{a_2}{a_1} & 0 & 0 \\ 0 & 0 & 0 & 1 \\ 0 & 0 & -\frac{b_3}{b_1} & -\frac{b_2}{b_1} \end{bmatrix} \begin{bmatrix} x_1(t) \\ \dot{x}_1(t) \\ x_2(t) \\ \dot{x}_2(t) \end{bmatrix} + \begin{bmatrix} 0 \\ \frac{1}{a_1} \\ 0 \\ \frac{1}{b_1} \end{bmatrix} u(t) \tag{2-69}$$

$$y(t) = C\mathbf{x}(t) + Du(t) = \begin{bmatrix} -\frac{c_1 a_3}{a_1} & -\frac{c_1 a_2}{a_1} & -\frac{c_2 b_3}{b_1} & -\frac{c_2 b_2}{b_1} \end{bmatrix} \begin{bmatrix} x_1(t) \\ \dot{x}_1(t) \\ x_2(t) \\ \dot{x}_2(t) \end{bmatrix} + \begin{bmatrix} \frac{c_1}{a_1} + \frac{c_2}{b_1} \end{bmatrix} u(t) \tag{2-70}$$

in which $y(t) = a = c_1 \ddot{w}_1(t) + c_2 \ddot{w}_2(t)$. This implies that a 4^{th} order model is required to linearly approximate the effect of two vibration modes. Corcuera et al. [3] use a linear model directly obtained from GH Bladed modelling two vibration modes. The tower model is not further specified, however is likely to be of the form as shown above, given that GH Bladed makes use of a modal tower description and is able to provide linear models directly. In Section 2-3 it has been shown that for each vibration mode a linear relation exists between translation and rotation as well as tower base moment M. This means that the following outputs can be obtained from the linear model without increasing model complexity/order:

$$\dot{\mathbf{x}}(t) = A\mathbf{x}(t) + Bu(t) = \begin{bmatrix} \dot{x}_1(t) \\ \ddot{x}_1(t) \\ \dot{x}_2(t) \\ \ddot{x}_2(t) \end{bmatrix} = \begin{bmatrix} 0 & 1 & 0 & 0 \\ -\frac{a_3}{a_1} & -\frac{a_2}{a_1} & 0 & 0 \\ 0 & 0 & 0 & 1 \\ 0 & 0 & -\frac{b_3}{b_1} & -\frac{b_2}{b_1} \end{bmatrix} \begin{bmatrix} x_1(t) \\ \dot{x}_1(t) \\ x_2(t) \\ \dot{x}_2(t) \end{bmatrix} + \begin{bmatrix} 0 \\ \frac{1}{a_1} \\ 0 \\ \frac{1}{b_1} \end{bmatrix} u(t) \tag{2-71}$$

$$y(t) = \begin{bmatrix} a(t) \\ v(t) \\ w(t) \\ \omega(t) \\ M(t) \end{bmatrix} = \begin{bmatrix} \ddot{w}(t) \\ \dot{w}(t) \\ w(t) \\ \dot{\varphi}(t) \\ M(t) \end{bmatrix} = C\mathbf{x}(t) + Du(t) \tag{2-72}$$

$$= \begin{bmatrix} -\frac{c_1 a_3}{a_1} & -\frac{c_1 a_2}{a_1} & -\frac{c_2 b_3}{b_1} & -\frac{c_2 b_2}{b_1} \\ 0 & c_1 & 0 & c_2 \\ c_1 & 0 & c_2 & 0 \\ 0 & c_1\alpha & 0 & c_2\beta \\ c_{M,1} & 0 & c_{M,2} & 0 \end{bmatrix} \begin{bmatrix} x_1(t) \\ \dot{x}_1(t) \\ x_2(t) \\ \dot{x}_2(t) \end{bmatrix} + \begin{bmatrix} \frac{c_1}{a_1} + \frac{c_2}{b_1} \\ 0 \\ 0 \\ 0 \\ 0 \end{bmatrix} u(t) \tag{2-73}$$

Tower top angular velocity $\dot{\varphi}(t)$ is included in the model and can therefore directly be used for rotor speed filtering by subtracting it from measured rotor speed. In principle, the system's

dynamics are determined by modal mass, damping and stiffness. Modal mass and stiffness are structural properties that are assumed to be invariant. Damping is a function of both structural damping and aerodynamic damping. Literature states that aerodynamic damping in side-side direction is small or even negligible [27].

2-6 Excitation Sources

The tower's internal dynamics are described by the model. Additionally, the control input T_{gen} is included in the model, which is known to excite the tower by causing a reactive torque on the tower. However, generator torque is not the sole cause of tower vibrations. The tower experiences forces caused by other unknown or stochastic excitation sources as well. An overview of such excitation sources is provided below.

The excitation sources can be divided into three categories:

- **Aerodynamic blade load imbalance**
- **Rotor mass imbalance**
- **Yaw misalignment**
- **Torsional tower mode**

If each blade is subjected to an equal relative wind speed, they produce an equal aerodynamic force in tangential rotor plane direction. These forces compensate each other, resulting in zero resultant force on the rotor and therefore on the tower in the lateral or vertical direction. Aerodynamic blade load imbalance occurs if the blades do not experience an equal relative wind speed. This can be caused by a variety of reasons. The relation between differences in wind speed and lateral forces acting on the tower is described by Pascu, Kanev, and Wingerden [19]. For blades $i = 1, 2, 3$, with number of blades B= 3 the following is stated:

$$T_{rotor}^{(i)}(U^{(i)}) = \frac{1}{2}\rho\pi R^3 (U^{(i)})^2 C_Q(\lambda^{(i)}, \theta^{(i)})/B \tag{2-74}$$

With air density ρ, rotor radius R, tip speed ratio $\lambda = \frac{\Omega R}{U}$, pitch angle θ, torque coefficient C_Q, aerodynamic torque T_{rotor} and wind speed U, in which $(\cdot)^{(i)}$ denotes that a quantity is blade-effective. Thus each blade produces a blade-effective aerodynamic torque $T_{rotor}^{(i)}$. This quantity can subsequently be used to determine a lateral force component for each blade.

$$F_{sw}^{(i)} = -\frac{1}{r} T_{rotor}^{(i)} cos(\psi^{(i)}) \tag{2-75}$$

with blade effective lateral force ${F_{sw}}^{(i)}$ and azimuth position $\psi^{(i)}$ of blade i, which is defined as zero at 12 o'clock and positive in the clockwise direction. The lateral force acts in perpendicular direction of the blade azimuth angle. The assumption is made that the lateral force

acts at a rotor-effective radius r. A simplification could be to assume $r = R/2$. These forces are subsequently combined in order to obtain the force acting on the tower: $\sum_{i=1}^{B} F_{sw}^{(i)}(t)$.

Differences in the (relative) wind field can have multiple causes:

- Turbulence
- Wind shear
- Tower shadow
- Tower fore-aft velocity
- Blade dynamics
- Yaw misalignment

First, turbulence or stochastic wind, which leads to differences in the wind field. Secondly, wind shear, due to which larger wind speeds are obtained at increasing altitudes. Wind shear is caused by the effect of the earth's surface roughness on wind speed. Typically, the power law is used to describe the effect for altitudes above 60m [20]:

$$U_{shr}^{(i)} = U(1 + \frac{r}{L} cos(\psi^{(i)})^{v} \tag{2-76}$$

In which U represents wind speed at hub height and U_{shr} the shear-induced wind speed. In similar fashion, a function can be derived for the effect of tower shadow [21]:

$$U_{shd}^{(i)} = U \frac{a^2(r_{tow}^2 sin^2(\psi^{(i)}) - x_{bl}^2)}{(r_{tow}^2 sin^2(\psi^{(i)}) - x_{bl}^2)^2}, \quad \text{for} \quad \psi^{(i)} = [90°, 270°] \tag{2-77}$$

in which r_{tow} is the tower radius, x_{bl} is the distance from blade origin to tower midline and U_{shd} is the shadow-induced wind speed. Finally, tower top fore-aft motion can cause periodic variations in wind speed. Due to fore-aft velocity $\dot{x}_{fa}$ variations in relative wind speed are induced. The rotor does not make a pure translational motion due to fore-aft movement, but also a rotational one. Therefore, The largest differences in relative wind speed are obtained when the blade is in the upper position. This can be described by the following equation [19] in which U_{tow} is the tower induced wind speed:

$$U_{tow}^{(i)} = -\dot{x}_{fa}(1 - \frac{R}{L} cos(\psi^{(i)}) \tag{2-78}$$

Therefore, coupling exists between tower fore-aft and lateral vibrations. This coupling can be especially undesirable since excitation of the lateral tower mode occurs at the tower fore-aft eigenfrequency, which approximately corresponds to the lateral eigenfrequency.

Each blade experiences the effect of shear and tower shadow once per revolution (1P). This applies to larger eddies caused by turbulence as well. Excitation due to blade effects results in periodic excitation of the tower. Since the turbine has three blades, aerodynamic effects are sampled at a rate of three times per revolution (3P).

A different source of excitation is a rotor mass imbalance. A rotor mass imbalance is caused if the Centre Of Mass (COM) of the rotor does not exactly coincide with the axis of rotation of the rotor. A centrifugal force at rotor speed frequency is present, which induces a periodic lateral force acting on the tower. The centrifugal force F_{sw}^{rot} can be modelled as a sinusoidal function:

$$F_{sw}^{rot} = a_u sin(\psi(t)) \tag{2-79}$$

with a periodic force amplitude a_u which is a function of the size of the mass imbalance. The frequency of this excitation is equal to the rotor speed (1P).

Another source of lateral tower excitation is yaw misalignment. If the undisturbed wind direction is not perpendicular to the rotor plane, the wind will exert a lateral force on the rotor and the tower directly.

A final source of excitation is torsional tower vibrations which could induce lateral vibrations. Typically, the tower's vibration modes in x- and y-direction are considered, however, the tower also has torsional vibration modes in the z-direction. For the considered tower, the torsional mode is around 1.2Hz against 0.28Hz for the lateral and fore-aft first eigenfrequencies. If the COM of the nacelle coincides with the tower z-axis, no lateral forces would be induced. In reality, the COM is in front of the tower and will therefore displace. The acceleration and deceleration of this mass induces forces in lateral direction. This is shown in Figure 2-3, which shows a top view of the tower with the COM of the rotor-nacelle assembly in front of the tower at a distance d. Torsional vibrations will lead to angular displacement ϕ of the COM and therefore also to displacement in lateral direction.

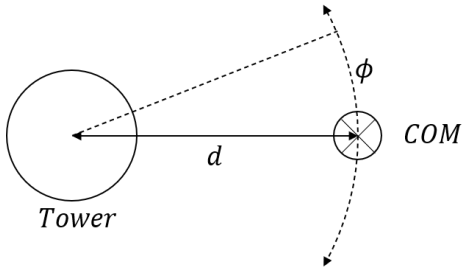

Figure 2-3: Interaction between torsional tower mode and lateral vibrations. The image shows a top view of the tower with wind direction from the right side.

The induced forces due to torsional vibrations can be described as follows:

$$F_{tors} = -sin(\phi)\ddot{\phi}dm \approx -\ddot{\phi}dm \tag{2-80}$$

Thus, the angular acceleration of the tower results in an acceleration of the mass with a component in lateral direction depending on distance d and mass m. Since ϕ is small, the sinusoidal term could be omitted.

It should be noted that other excitation sources could be present, caused by coupling with dynamics of other components. For example the effect of blade dynamics in both flap- and edgewise direction could induce additional aerodynamic imbalances.

2-7 Summary

A relation between rotational and lateral tower dynamics has been established with which rotational dynamics can be included in the tower model for different modes. It is found that the dynamic, or time-dependent part of the system is represented by a 2^{nd}-order system. Via the space-dependent part, being the mode shape, all other tower parameters can be related to the time-dependent part. This means that many additional outputs can be included in the system model without adding complexity to the system's dynamics. A SS-model representation is suitable for describing the model. Additionally, an examination is performed of which other sources of excitation could excite the tower in lateral direction and how such mechanisms can be modelled. It was found that a variety of possible sources exist.

Chapter 3

System Identification

To perform Kalman filtering and state-feedback, an adequate reduced-order linear model of the turbine tower is required. In Section 2-5, it is found that the relevant tower dynamics can be modelled using a linear State-Space (SS) model. There are multiple methods to derive such a linear model. A possibility is to derive a model from the physical equations governing the tower dynamics, which requires modes shapes from finite element tower model after which input-output relations could be derived manually. Another possibility is to perform system identification using input and output data of the system. The advantage of the latter is that coupling of the tower with other turbine components and aerodynamic effects are taken into account. This requires the conduction of an experiment in order to obtain such data. Performing experiments on operational turbines is complex, given that one does not have control or even information on external inputs to the system such as the wind field. Additionally, differences exist between different tower realisations of the same model type. Therefore, simulation package `Focus` is considered, which includes a high fidelity tower model. During the project, the assumption is made that the tower model accurately represents the dynamics of actual tower realisations. An identification experiment is designed in `Focus`. Identification will be performed using this experimental simulation data. Different system identification methods exist. Subspace identification has been selected as identification method for the following reasons:

- Subspace identification directly results in the required discrete-time linear single-input-multiple-output state-space model.
- Model order reduction is conveniently achieved with the ability to select a model order through assessment of the singular values.

In Section 3-1 the experiment design used for identification is discussed. Section 3-2 considers the identification procedure. Models of varying model order and experiment design have been identified. In Section 3-4, the identified models are validated in a specifically designed high-fidelity experiment. With a model identified, the tower-torque controller interaction mentioned in Chapter 1 can be quantified. This is performed in Section 3-5. Some final remarks considering the identification procedure are given in Section 3-6.

3-1 Experiment Design

In order to perform system identification, a suitable data set is required. Therefore, an experiment is designed. To extract the dynamics of the tower from the data set, it is important that all dynamics are excited. This so-called persistency of excitation is a requirement of the experiment input signal. An input sequence should be persistently exciting of order n in order to be able to identify a model of this order. This property is evaluated through the following rank condition of the input Hankel matrix $U_{0,n,N}$ [25, p. 358]. The subscript $0, n, N$ denotes the starting point, the number of rows and the number of columns respectively.

$$rank(U_{0,n,N}) = rank\left(\begin{bmatrix} u(0) & u(1) & \cdots & u(N-1) \\ u(1) & u(2) & \cdots & u(N) \\ \vdots & & \ddots & \\ u(n-1) & u(n) & \cdots & u(N+n-2) \end{bmatrix}\right) \geq n \tag{3-1}$$

Thus, the input Hankel matrix should be of full row rank, which can be achieved by the use of a step input signal. In `Focus`, this is achieved by simulating a stop event during normal operation. If a stop event is triggered, the generator is suddenly disabled resulting in the generator torque to be set to zero. A step input is a common identification input signal, as all dynamics are excited. Such a step down in torque results in a response of the tower which can subsequently be used as system output data. Two experiments have been designed in `Focus`:

- Partial Dynamics (PD)
- Full Dynamics (FD)

By disabling certain dynamics, it is possible to reduce the effect of disturbance inputs. For this reason, a PD experiment has been designed. In the PD experiment a series of dynamics have been disabled in order to obtain a tower response which is only a function of generator torque and the tower's internal dynamics. Additionally, an experiment is conducted with all dynamics enabled and therefore potential excitation sources and coupling with other turbine dynamics. Using the latter experiment, an assessment can be made to what extent the tower's response is affected by these other sources of excitation. Identification will be performed using both experiment types, after which the results are compared and the most suitable identification result is selected.

3-1-1 Partial Dynamics

In the PD experiment, the following parameters have been disabled:

- Blade & generator dynamics
- Tower & nacelle drag

- Tower shadow

The experiment load case is designed as follows:

Table 3-1: Experiment Design

Parameter	Value
Wind speed	12 m/s
Wind profile	Normal Wind Profile (NWP)
Stabilising time	120 s
Stop event triggered	130 s
Generator torque (130 s)	4.276 MNm
Rotor speed (130 s)	11.07 RPM

The experiment time response is shown in Figure 3-1. A detailed view of the initial response is shown in Figure 3-2.

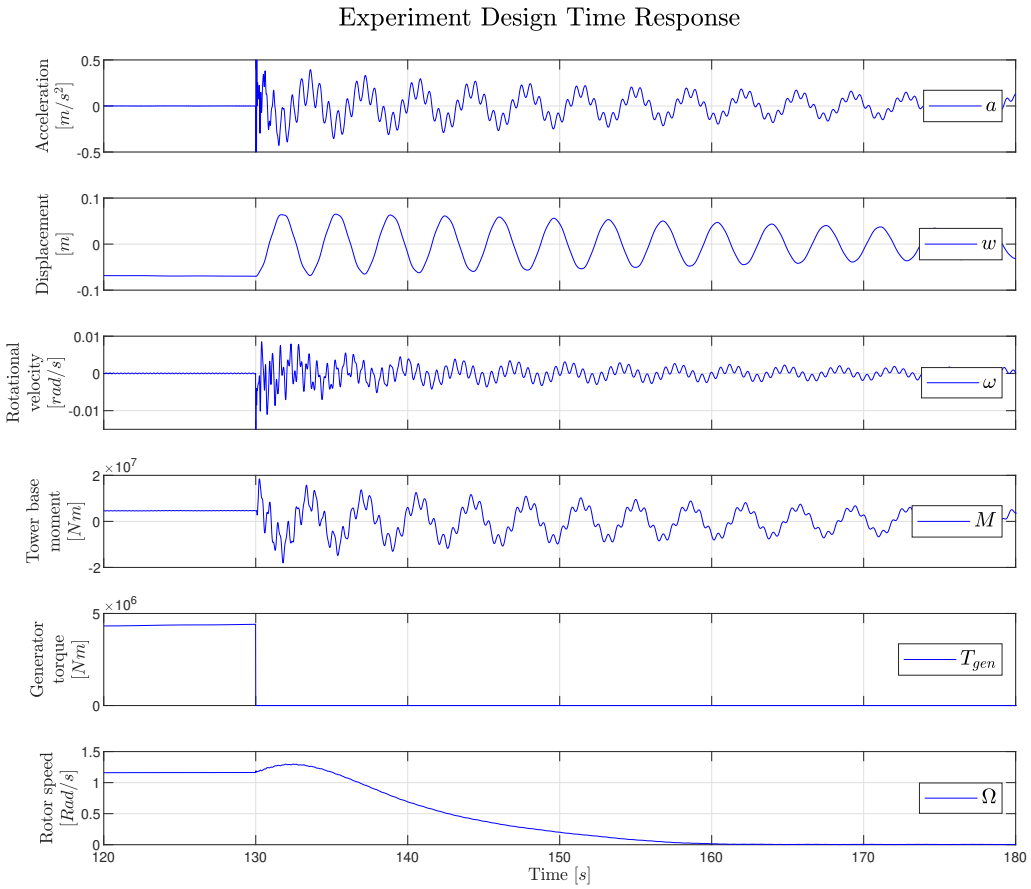

Figure 3-1: Identification experiment - PD time response identification data

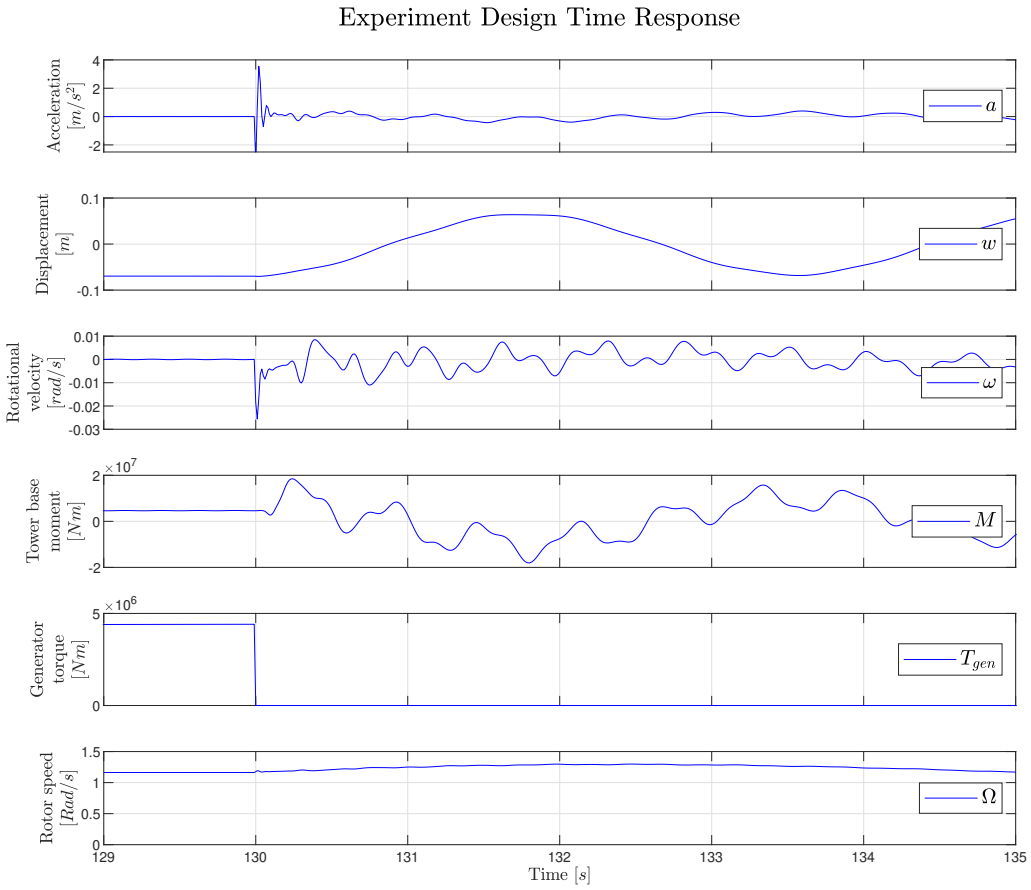

Figure 3-2: Identification experiment - PD time response identification data (detailed view)

Six parameters are logged for this experiment, namely rotor speed, generator torque, acceleration, displacement and rotational velocity of the nacelle and the tower base moment in lateral direction. Rotor speed will not be used during the identification procedure but is used to assess the effect of nacelle rotational velocity on the rotor speed measurement. Generator torque is used as the system's sole input parameter. Acceleration, displacement and rotational velocity of the nacelle and tower base moment in lateral direction are the system's output parameters. As has been stated in Section 2-4, the tower base moment is the typically used tower load indicator and is therefore included as an output of the model. This parameter could be used for online Damage Equivalent Load (DEL) estimation or for a future Model Predictive Control (MPC) controller. Preferably, lateral velocity of the nacelle is included as an output to the model, however, lateral velocity is not an available parameter in `Focus`. Hence, lateral velocity will be appended to the model afterwards.

After the stop event is triggered, the generator is disabled resulting in a step-down in generator torque. Initially, the rotor speed increases as aerodynamic torque is still exerted on the rotor. If the blades start to pitch to vane, aerodynamic torque is reduced and rotor speed decreases. The tower shows a clear response to the change in generator torque. The displace-

ment is dominated by the first tower mode. In the time response of acceleration, rotational velocity and base moment the first and second mode are distinguishable. The displacement is dominated by the first tower mode. Acceleration shows a large initial response with a peak value of 3.4 m/s^2, which damps out almost immediately. The same is observed in the rotational velocity of the nacelle, which shows a peak value of $-0.029\,rad/s$ as a the result of higher-order dynamics.

Figure 3-3 shows the estimated Power Spectral Density (PSD) of the corresponding time response signals on a logarithmic scale. In the rotor speed signal, the first four modes can be identified, which are also present in the tower output signals. In the displacement signal, only the first mode is significantly present. The higher-order modes seem to have a notably larger effect on the rotational dynamics than on lateral dynamics, given the equal effect of the first two modes on the rotational velocity of the nacelle. This is due to the mode shapes, which have larger rotation-to-deflection modes for higher-order modes.

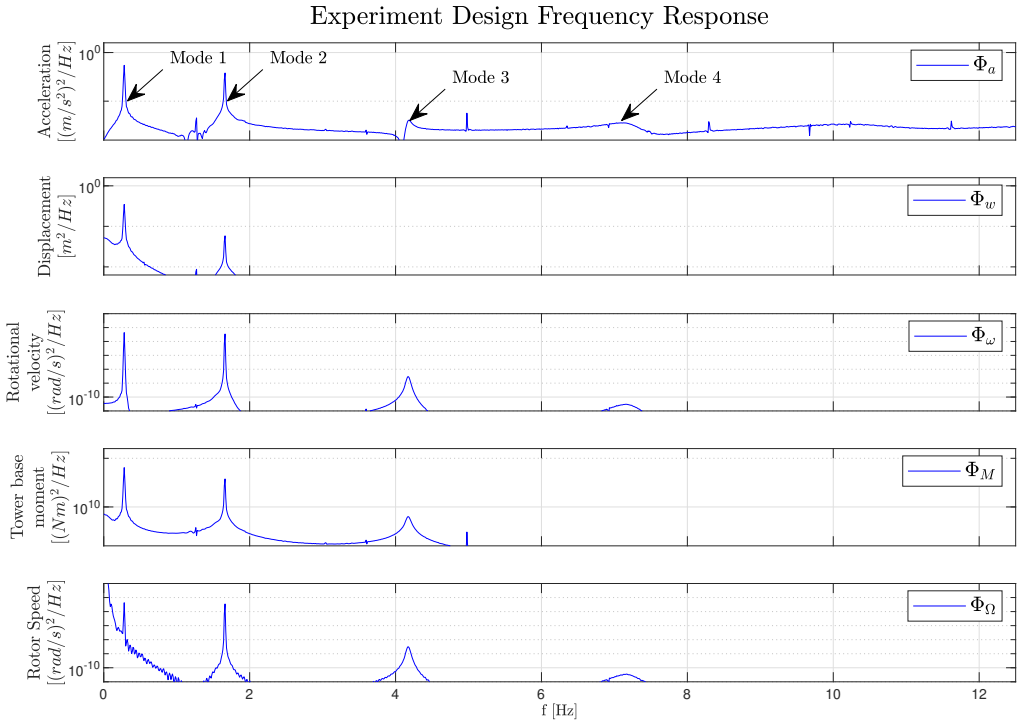

Figure 3-3: Identification experiment - Partial dynamics frequency response identification data

3-1-2 Full Dynamics

The FD experiment is similar to the PD experiment, however, with all dynamics enabled. Figure 3-4 shows the time response signals. The first difference is that the tower does not reach a steady-state at 120s, mainly due to tower shadow effects. After the stop event, the time response seems to be similar.

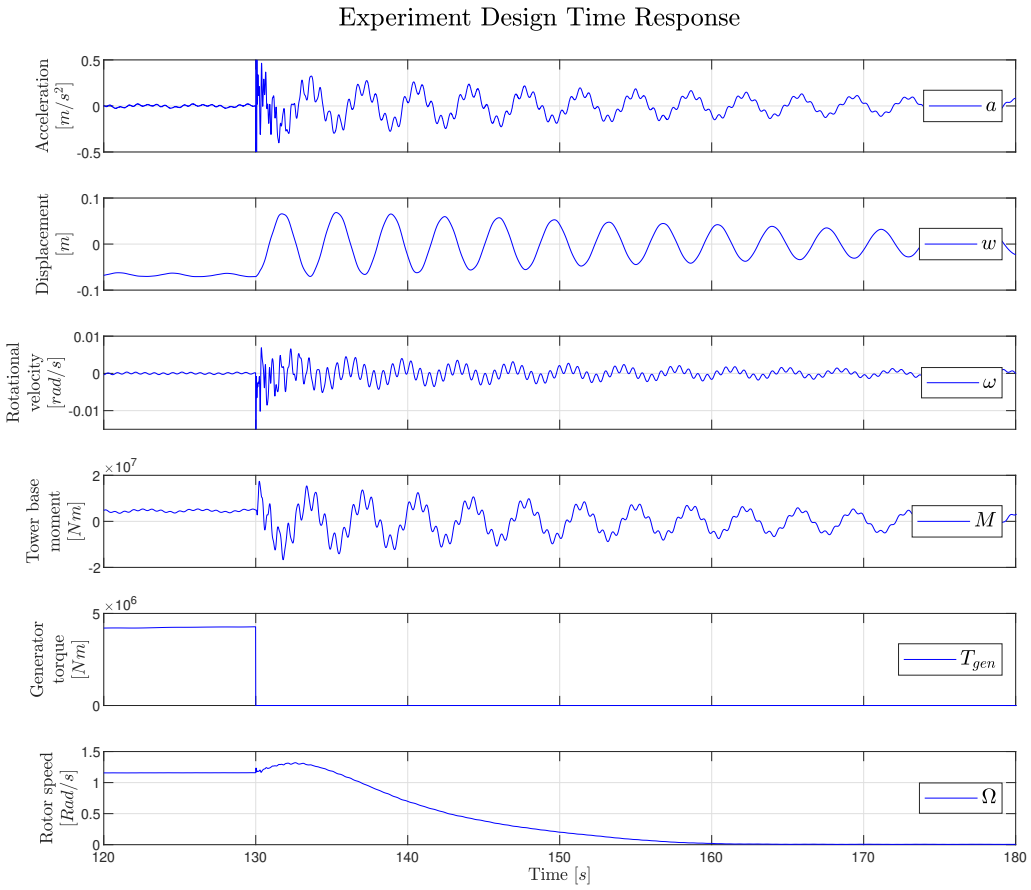

Figure 3-4: Identification experiment - Full dynamics time response identification data

Figure 3-5 shows the PSD of the corresponding signals. The signals show a more noisy response. It is also found that the second mode shows a slightly lower frequency, which will be further analysed during system identification. A lower frequency typically indicates a larger damping ratio. In the rotor speed measurement, some additional disturbances are observed due to the enabling of blade dynamics and tower shadow. At 2Hz, the blade collective edge mode is present, albeit significantly less dominant than tower induced disturbances in this experiment.

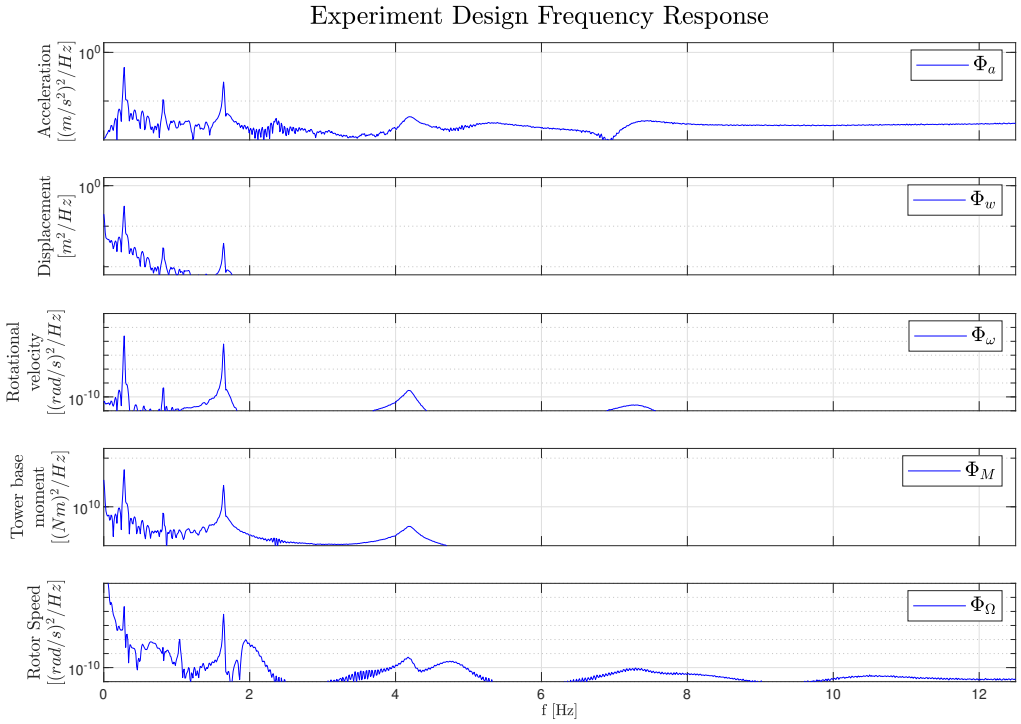

Figure 3-5: Identification experiment - Full dynamics frequency response identification data

The two designed experiments show similar results although they do differ slightly. The PD experiment is free of noise, which could be beneficial for identification accuracy. On the other hand, interaction with other turbine components might result in a more realistic situation resulting in more accurate dynamics.

3-2 Identification

In this section, the identification procedure of the identified models is discussed.

3-2-1 Subspace Identification Method

As denoted previously, the subspace identification method will be used in order to identify the required tower model. Subspace identification consists of a family of different identification method based on the same principle. The Past-Output-Multivariable-Output-Error-State-sPace (PO-MOESP) scheme has been selected, of which a summary is presented here. An advantage of this the PO-MOESP scheme is the ability to identify systems with respect to process and measurement noise $w(k)$ and $v(k)$ which are Zero-Mean-White-Noise (ZMWN), described by the following process model:

$$\tilde{x}(k+1) = A\tilde{x}(k) + Bu(k) + w(k) \tag{3-2}$$
$$y(k) = C\tilde{x}(k) + Du(k) + v(k) \tag{3-3}$$

In the case of the tower experiment with full dynamics enabled, the tower is affected by noisy inputs/disturbances which are not taken into account for identification. By using a model structure and identification scheme able to handle such disturbances in the identification data, these are (largely) filtered from the resulting model. By only considering the input-output transfer, the system can be formulated in the so-called innovation form:

$$x(k+1) = Ax(k) + Bu(k) + Le(k) \tag{3-4}$$
$$y(k) = Cx(k) + Du(k) + e(k) \tag{3-5}$$

in which $e(k)$ is a white-noise sequence and L is the Kalman gain. By use of the model representation the data equation can be formulated using the input and output block Hankel matrices $U_{i,s,N}$ and $Y_{i,s,N}$:

$$Y_{i,s,N} = \mathcal{O}_s X_{i,N} + \mathcal{T}_s U_{i,s,N} + \mathcal{S}_s E_{i,s,N} \tag{3-6}$$

A numerically efficient way of obtaining the observability matrix $\mathcal{O}_s$ is through use of the RQ factorization:

$$\begin{bmatrix} U_{s,s,N} \\ \begin{bmatrix} U_{0,s,N} \\ Y_{0,s,N} \end{bmatrix} \\ Y_{s,s,N} \end{bmatrix} = \begin{bmatrix} R_{11} & 0 & 0 \\ R_{21} & R_{22} & 0 \\ R_{31} & R_{32} & R_{33} \end{bmatrix} \begin{bmatrix} Q_1 \\ Q_2 \\ Q_3 \end{bmatrix} \tag{3-7}$$

$$\text{range}\left(\lim_{N\to\infty} \frac{1}{\sqrt{N}} R_{32} \right) = \text{range}(\mathcal{O}_s) \tag{3-8}$$

By use of a Singular Value Decomposition (SVD) of matrix R_{32}, $\mathcal{O}_s$ is determined. The singular values are used to estimate or choose a desired system order. From $\mathcal{O}_s$ the matrices A_T and C_T can easily be obtained up to a similarity transformation with matrix T, given that a state-space model is not unique. With A_T and C_T known, what remains is to determine input matrix B_T, direct feed-through matrix D_T and initial condition $x_T(0)$ by solving a Linear Least Squares (LLS) problem. The system output can be expressed in terms of B_T, D_T and $x_T(0)$ given matrices A_T and C_T as follows:

$$y(k) = C_T A_T^k x_T(0) + \left(\sum_{\tau=0}^{k-1} u(\tau)^T \otimes C_T A_T^{k-\tau-1} \right) \text{vec}(B_T) + (u(k)^T \otimes I_l)\text{vec}(D_T) \tag{3-9}$$

By defining matrix ϕ and parameter vector θ the problem can described in a LLS formulation:

$$\phi(k)^T = \begin{bmatrix} C_T A_T^k & \left(\sum_{\tau=0}^{k-1} u(\tau)^T \otimes C_T A_T^{k-\tau-1} \right) & (u(k)^T \otimes I_l) \end{bmatrix} \tag{3-10}$$

$$\theta = \begin{bmatrix} x_T(0) \\ \text{vec}(B_T) \\ \text{vec}(D_T) \end{bmatrix} \tag{3-11}$$

The solution is found through minimisation of the following objective function:

$$\min_{\theta} \frac{1}{N} \sum_{k=0}^{N-1} ||y(k) - \phi(k)^T \theta||_2^2 \tag{3-12}$$

The included estimation of initial condition $x_T(0)$ is required to filter out the effects of a non-zero initial condition. In case of the designed experiment, rated torque is applied to the tower at the start of the experiment. This results in a non-zero initial condition as can be seen by the deflection and tower base moment. Additionally, the turbine does not reach a steady-state during operation, the effect of which should be taken into account.

3-2-2 Scaling

Large differences exist between the unit scaling of the input and different outputs of the system. Especially generator torque and tower base moment, which are given in $[Nm]$, result in significant absolute values in the range of $10^6 - 10^7$. Whereas acceleration $[m/s^2]$ and displacement [m] are in the range of $10^{-1} - 10^0$ and rotational velocity $[rad/s]$ is in the range of 10^{-2}. When considering the subspace identification method for a Single-Input-Multiple-Output (SIMO) case, it becomes evident that this leads to issues in identification accuracy. The singular values would be dominated by outputs with large absolute values resulting in an affected order estimate. The subsequently solved LLS problem would also be dominated by the largest absolute output value (tower base moment in this case). Therefore, scaling has been applied.

The output value for acceleration has been chosen as a reference output. For the input and each output the absolute average value is determined:

$$\bar{u} = \text{mean}(\text{abs}(u)) \tag{3-13}$$

$$\bar{y}_i = \text{mean}(\text{abs}(y_i)), \quad \text{for } i = 1, 2, 3, 4 \tag{3-14}$$

Using these values, the input and output values are scaled such that their mean absolute values are equal to $\bar{y}_1 = \bar{a}$:

$$u_{scaled} = u \frac{\bar{y}_1}{\bar{u}} \tag{3-15}$$

$$y_{i,scaled} = y_i \frac{\bar{y}_1}{\bar{y}_i}, \quad \text{for } i = 2, 3, 4 \tag{3-16}$$

By equating all absolute average values, all outputs are given equal weight. The identification procedure is then performed using the scaled data. After identification, the corresponding rows and columns of matrices C_T, B_T and D_T are scaled inversely such that the original values are restored.

3-2-3 Identification parameters

As part of the identification procedure, a series of parameters are to be selected, namely the number of rows and columns of the Hankel matrices, s and N respectively, and the model order n. the total number of data samples is equal to $s + N$, in order to be able to construct the Hankel matrices. Furthermore, the following condition should be satisfied: $n < s \ll N$. In principle, the best results could be obtained with s and N as large as possible.

s determines the number of singular values, which are used to determine the model order. In a noise-free system $n < s$ is sufficient, as any singular values beyond model order n are equal to zero in that case. However, in the case of noise, the remaining dynamics result in non-zero singular values, which decrease for an increasing number of singular values s.

Additionally, a large number of data samples is to be taken into account such that the assumptions on white noise correlations become valid. Therefore, N should be sufficiently large. A sampling time T_s= 0.01s is used. It is important to capture the dominant dynamics of the system, given by the first tower eigenfrequency of 0.28Hz and a full cycle of 3.6s. A sufficient number of cycles is to be taken into account to get an adequate measure for damping.

Taking into account these considerations, and after manual tuning, the following values where used for the identification procedure:

- $s = 300$
- $N = 10000$ (identification time 100 s)

If the model is accurate over the specified identification time of 100 s, this is sufficient for the purpose of the model.

3-2-4 Singular Values

Analysing the model order of the system can be performed through the singular values of the observability matrix $\mathcal{O}_s$.

$$R_{32} = U_s \Sigma_s V_s^T \tag{3-17}$$

The singular values are displayed in Figure 3-6. As discussed, each vibration mode is represented by a 2^{nd}-order system. The singular values represent the relative presence of poles of the system. Thus, a set of two singular values represents one vibration mode. Additionally, noise and input disturbances lead to non-zero singular values. The first four singular values represent the first and second vibration mode, which are the most dominant. The third mode is also recognisable as a singular value pair. After the first three modes, two sets of two modes

seem to appear. The goal is not to establish the exact model order, since a large number of modes can be taken into account which are generally not excited or even distinguishable from noise. The goal is to determine a reduced model order which makes the model useful for filtering and control. Different model orders will be identified in order to compare their performance.

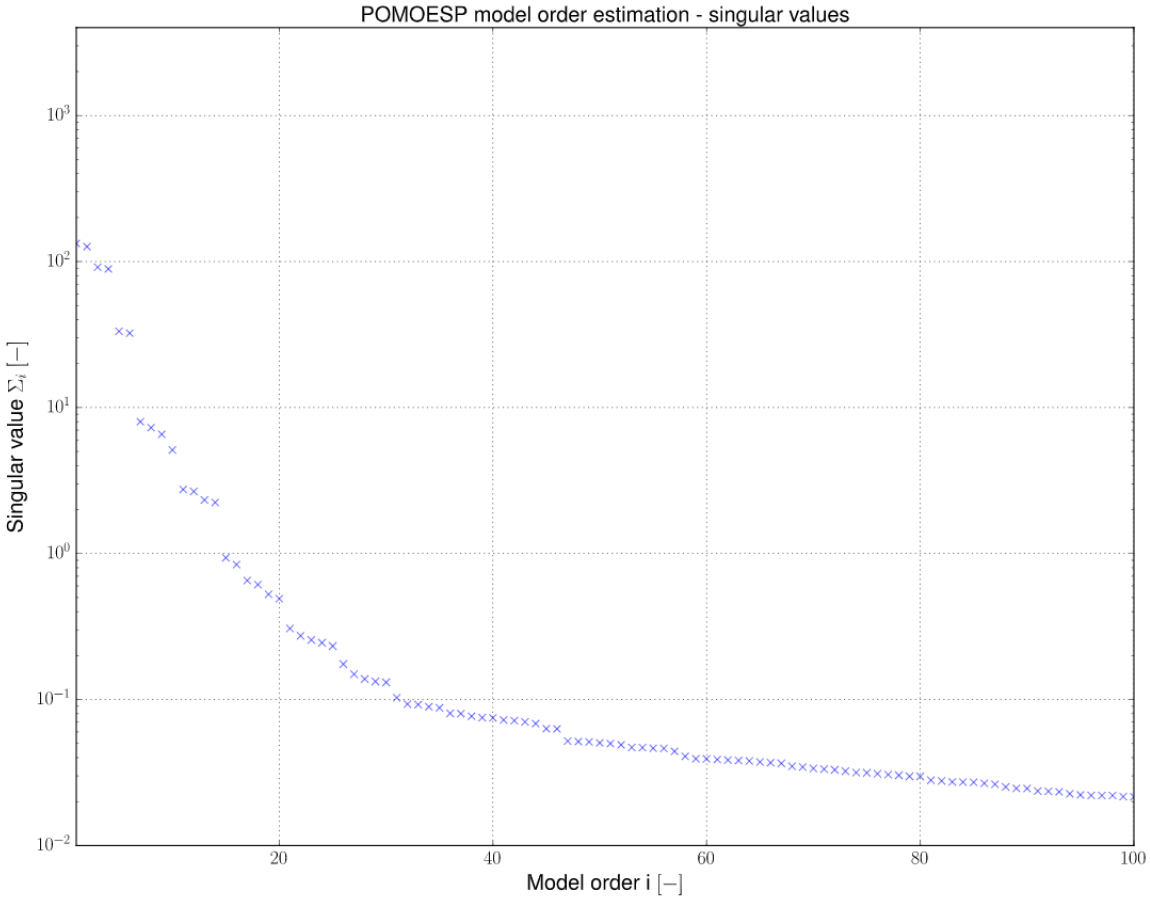

Figure 3-6: Singular Values of the observability matrix (PD)

3-2-5 Identification Result

The identification procedure is used to identify a system model using both the PD and FD experiment. Different model orders have been tested in order to assess their effect on the model fit. Based on the steps seen in singular values, the following model orders have been selected; 4, 6, 8, 10. It was found that beyond model order 10, modes were identified twice. This is so-called overfitting, in which physically invalid modes are added to the model to obtain an improved fit for the identification experiment.

The identification time responses of the 4^{th} and 10^{th}-order PD model are shown in Figure 3-7. The identified model is simulated given the torque input and initial condition. For the first two modes, both models show an accurate fit and no significant differences can be observed. A detailed view of the initial response of the signals, shown in Figure 3-8, reveals a difference

between different model orders. In the initial second of the response, modes other than the first two modes are excited. These modes are not modelled by the 4^{th}-order model, whereas the 10^{th}-order model shows a near-perfect fit. It is found that higher-order modes rapidly fade away. The identification experiment validates that it is indeed possible to include tower top rotational dynamics as well as tower base moments in a model without increasing model complexity.

Figure 3-9 shows the PSD estimates of the a 4^{th} and 10^{th}-order tower models. In a PD experiment, the tower response is almost exclusively the result of tower dynamics. This result in an accurate fit in the frequency domain. As to be expected from the time response, the first two modes are accurately modelled by both models. The 10^{th}-order model additionally models the 3^{rd} and 4^{th} tower modes accurately.

A small unmodelled frequency is observed around 1.2Hz, which matches the tower torsional eigenfrequency. As stated in Section 2-6, an interaction between tower torsional and lateral vibrations can occur. This torsional tower mode does not affect tower top rotational velocity. In the identification experiment, the torsional tower mode is negligible when compared to the effect of the tower modes.

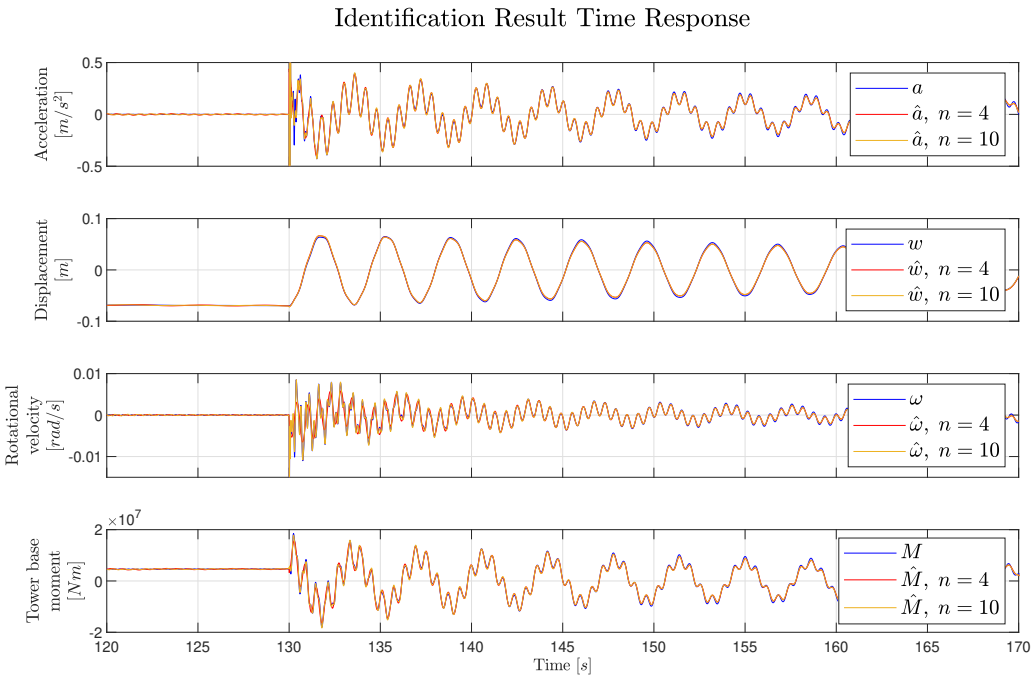

Figure 3-7: Identification Result - Time response of a 4^{th} and 10^{th}-order PD model

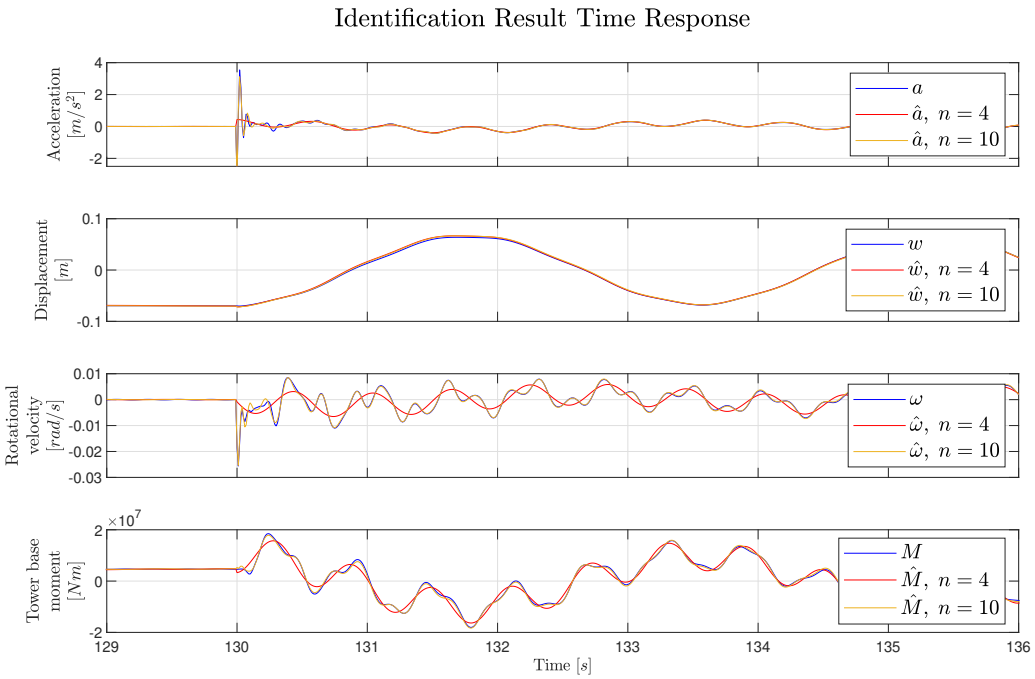

Figure 3-8: Identification Result - Zoomed time response of a 4^{th} and 10^{th}-order PD model

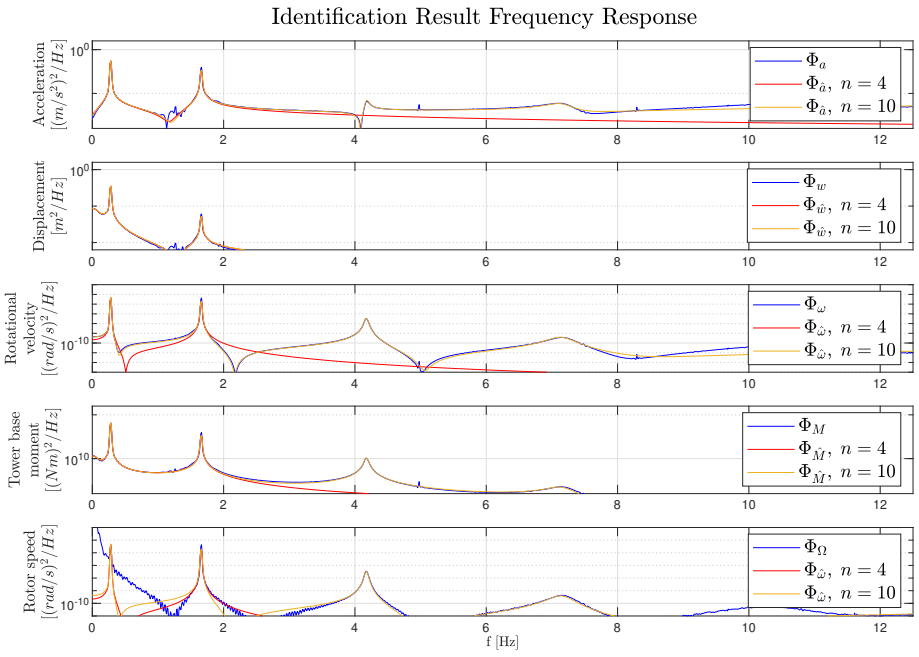

Figure 3-9: Identification result - Frequency response of a 4^{th} and 10^{th}-order PD model

In similar fashion as for the PD experiment, the time response for the FD experiment is shown

in Figure 3-10. No steady-state is reached before the step-down in torque occurs. However, since the initial state is obtained as part of the identification procedure, this is accounted for. Even though disturbances due to tower shadow and blade dynamics are present, an accurate fit is obtained for the first two modes.

Figure 3-11 shows a detailed view of the signals. The initial response looks similar to the PD model. The 3^{rd} mode is less present for the FD experiment, resulting in a better fit of the 4^{th}-order model.

Figure 3-12 shows a PSD estimate for FD experiment. In general, the response looks similar to the PD experiment, however, more disturbances are present. Nevertheless, an accurate fit is obtained at the tower eigenfrequencies.

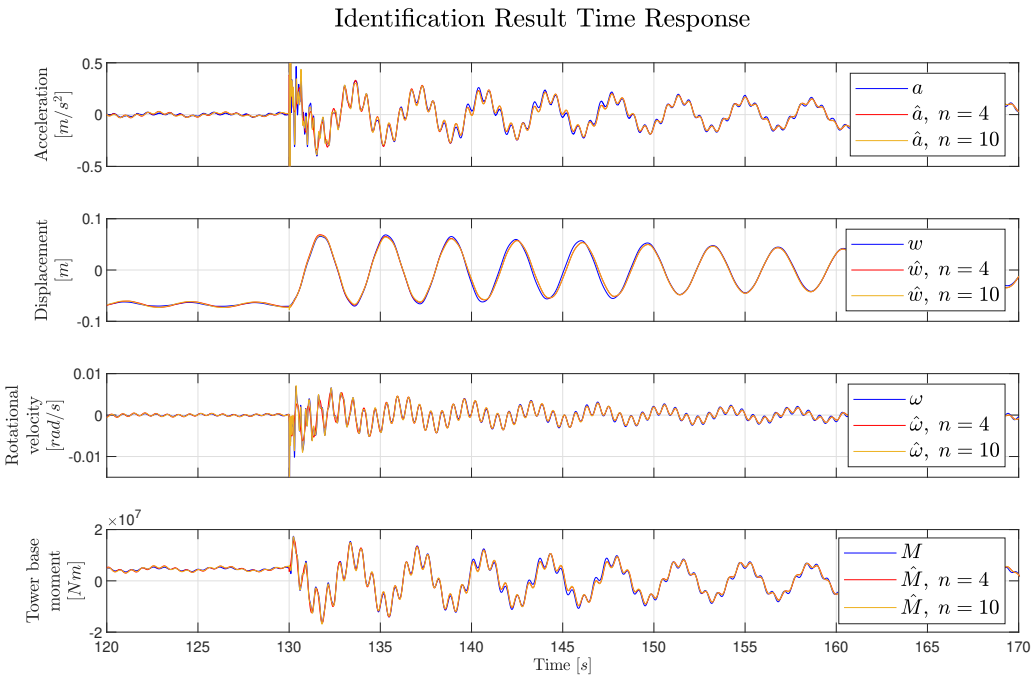

Figure 3-10: Identification Result - Time response of a 4^{th} and 10^{th}-order FD model

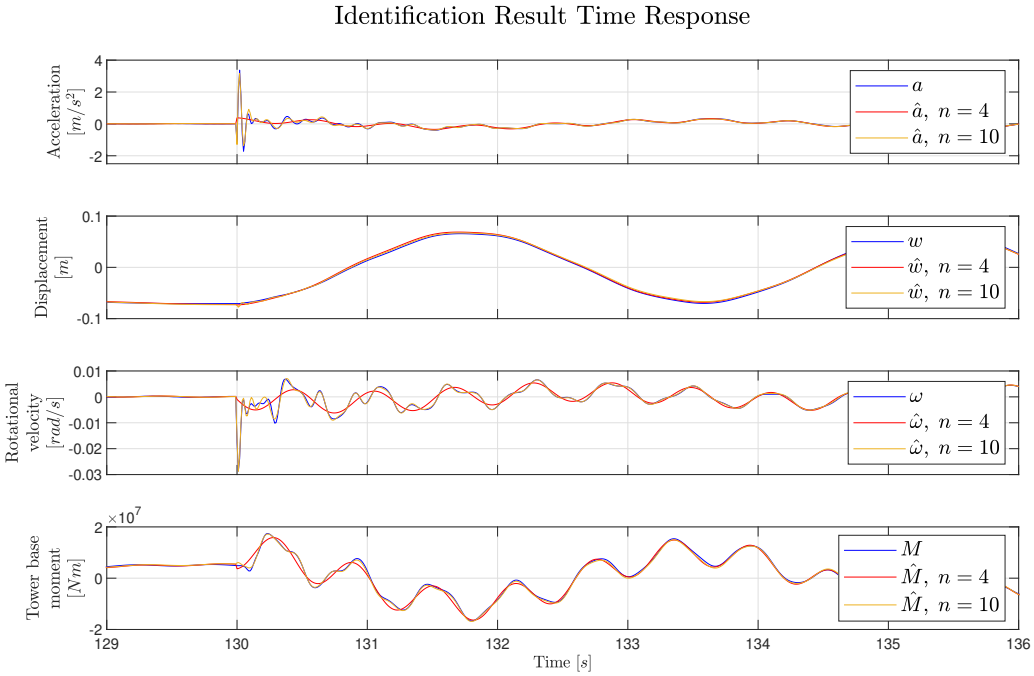

Figure 3-11: Identification Result - Zoomed time response of a 4^{th} and 10^{th}-order FD model

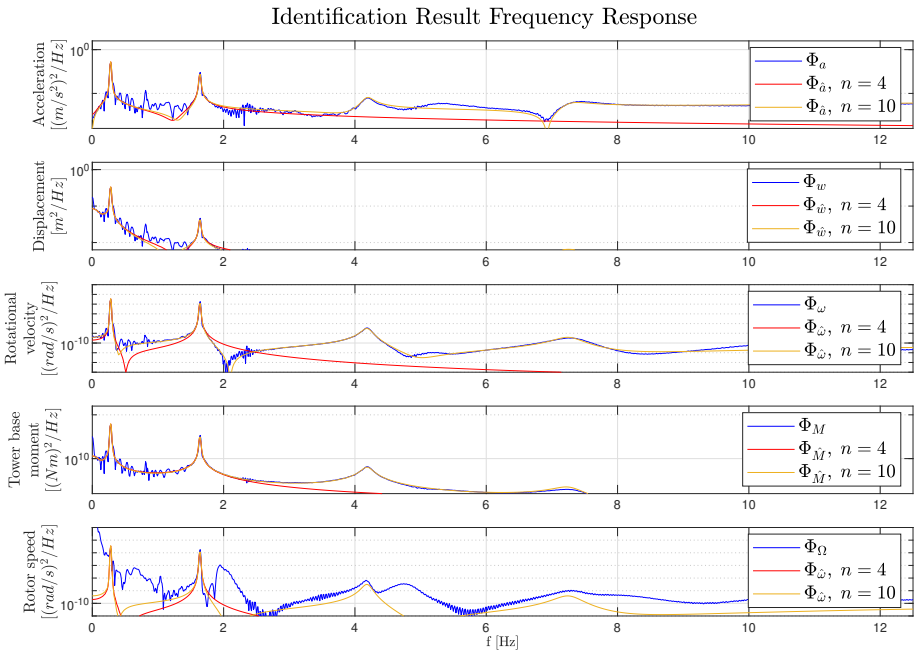

Figure 3-12: Identification result - Frequency response of a 4^{th} and 10^{th}-order FD model

In order to quantitatively compare the results, the Variance Accounted For (VAF) is used as

a performance measure:

$$VAF_i = \left(1 - \frac{\text{var}(y_i - \hat{y}_i)}{\text{var}(y_i)}\right) \cdot 100\% \tag{3-18}$$

The VAF is determined for each output value individually in order to prevent a single output from dominating the result. Identification results for the PD experiment are displayed in Table 3-2. Corresponding results for the FD experiment are displayed in Table 3-3.

Table 3-2: Identification result - VAF for different model orders [%], PD

VAF [%]				
Model Order n	a	w	ω	M
4	74.9	99.6	77.3	98.3
6	75.2	99.6	91.1	98.9
8	82.8	99.6	95.1	98.9
10	97.6	99.6	96.9	98.9

Table 3-3: Identification result - VAF for different model orders [%], FD

VAF [%]				
Model Order n	a	w	ω	M
4	72.0	99.0	79.5	98.0
6	73.2	99.0	88.3	98.3
8	76.3	98.8	93.4	98.1
10	96.7	98.6	97.6	97.9

In accordance with the time response, an increase in model accuracy is obtained for higher-order models. Displacement and tower base moment are almost exclusively a function of the first two modes and show no significant change for increasing model orders. Rotational velocity shows an increase for each additional tower mode. Acceleration only shows a clear performance increase when modelling the 5^{th} mode. The absolute values for PD versus FD are not useful for comparing the models, given that the FD experiment is subjected to more disturbances. A comparison will be made using a different validation experiment in Section 3-4.

3-2-6 Model Post-Processing

With the model identified, some additional operations are performed in order to increase the model's suitability. These three operations are:

- Transform system into real modal form

- Append velocity to system output
- Remove steady-state gain

The modal form results in a block diagonal A-matrix, for which the first two states correspond to the first mode and the second two states correspond to the second mode, etc. Velocity is appended to the model as it could be useful for modal damping. Thirdly, any steady-state gain is removed from output parameters that should not have a steady-state gain when regarding the physical model.

The model is transformed into modal form using the `MATLAB` function `modal` from the LTI-toolbox. A similarity transformation does not affect the model's dynamics.

The current model does not include velocity as an output. Typically, damping is added by applying negative feedback to the tower's velocity. In order to do so with the identified model, with a state-feedback approach, velocity is appended. The dynamics of the system are similar to the dynamics as described in Section 2-5. However, the used system identification approach does not result in a model with physical states. Therefore, after the real modal transformation, the system matrices B, C and D do not exactly match the matrices denoted previously. The C-matrix and D-matrix related to tower lateral velocity, deemed C_v and D_v, are therefore not analytically obtainable. For this reason, an open-loop simulation using the identified model is conducted.

- Iterations: $N = 1000$
- Input: for $k \geq 100, \quad u(k) = 4e6$

In this simulation, velocity is obtained using Zero-Order-Hold (ZOH) integration:

$$v(k+1) = v(k) + a(k)T_s \tag{3-19}$$

Now in order to obtain estimates for C_v and D_v, a LLS problem is solved:

$$v(k) = C_v x(k) + D_v u(k) \Rightarrow \tag{3-20}$$

$$v^T(k) - \begin{bmatrix} x^T(k) & u^T(k) \end{bmatrix} \begin{bmatrix} C_v^T \\ D_v^T \end{bmatrix} = \epsilon \Rightarrow \tag{3-21}$$

$$\min_{\theta} ||v^T - \underbrace{\begin{bmatrix} x^T & u^T \end{bmatrix}}_{\phi} \underbrace{\begin{bmatrix} C_v^T \\ D_v^T \end{bmatrix}}_{\theta} ||_2^2 \tag{3-22}$$

The obtained values for C_v and D_v are appended to the existing C and D matrices, the corresponding output is lateral velocity.

From theory, outputs related to (rotational) velocity and acceleration should have zero steady-state gain. A constant torque input would result in a steady-state deflection and base moment, but in zero velocity and acceleration. However, the identification procedure results in (very small) steady-state gains. These are removed from the model as follows:

$$K_{ss} = D + C(I - A)^{-1}B \tag{3-23}$$
$$D = D - K_{ss} \tag{3-24}$$

3-3 Model Analysis

With eight identified models, a comparison of the characteristics of the different models can be made. Each model consists solely of complex pole-pairs. The poles of the system are related to the natural frequencies and damping ratios of each mode as follows:

$$s = \sigma \pm j\omega_d \tag{3-25}$$
$$= \omega_n\Big(-\zeta \pm j\sqrt{1-\zeta^2}\Big) \tag{3-26}$$

The identified system's parameters are displayed in Table 3-4.

Table 3-4: Identification result - Pole parameters of identified models

		Partial Dynamics		Full Dynamics	
Model Order n	Mode	ω_n [Hz]	ζ	ω_n [Hz]	ζ
4	1	0.280	0.0083	0.280	0.0106
	2	1.658	0.0056	1.637	0.0068
6	1	0.280	0.0084	0.280	0.0108
	2	1.659	0.0056	1.638	0.0069
	3	4.167	0.0105	4.160	0.0296
8	1	0.280	0.0082	0.280	0.0105
	2	1.659	0.0055	1.639	0.0068
	3	4.175	0.0097	4.187	0.0246
	4	8.290	0.3715	7.642	0.1527
10	1	0.280	0.0083	0.280	0.0101
	2	1.659	0.0056	1.639	0.0066
	3	4.175	0.0100	4.188	0.0229
	4	7.146	0.0298	7.259	0.0314
	5	17.15	0.2696	14.92	0.2559

The frequency related to the first mode is accurately determined in all models (0.280Hz). The damping ratio of the first mode is slightly larger in the FD experiment. For the second mode, a slight decrease in natural frequency, as well as increased damping is observed for the FD experiment. The damping ratio of the second mode is smaller than the first mode. The third mode shows no consistent increase or decrease in natural frequency, however, damping is significantly larger for the full dynamics experiment. The parameters related to the final two

modes are rather inconsistent. In the 8^{th}-order model, the fourth mode is fitted to both the fourth and fifth mode, resulting in an increased natural frequency. In the 10^{th}-order model a more consistent estimate of the fourth mode is obtained. The frequency and damping related to the fifth mode is not consistently estimated.

Figure 3-13 shows a Bode plot of the 4^{th}-order and 10^{th}-order full dynamics models. The system output $Y(s)$ to a step response of the tower model $P_{Tower}(s)$ is $Y(s) = P_{Tower}(s)\frac{1}{s}$, and therefore $P_{Tower}(s) = sY(s)$. As expected, the Bode plot resembles the power spectral density estimates shown previously with this relation. However, the exact magnitude of each mode is shown in a bode plot. For acceleration, the second mode gain is slightly larger than the first mode. For subsequent integrals, velocity and displacement, the second mode becomes less dominant due to the low-pass filtering effect of integration. It is also observed that for rotational velocity the second mode gain is significantly larger than the first mode. Moreover, the third and fourth mode are significant in the 10^{th}-order model.

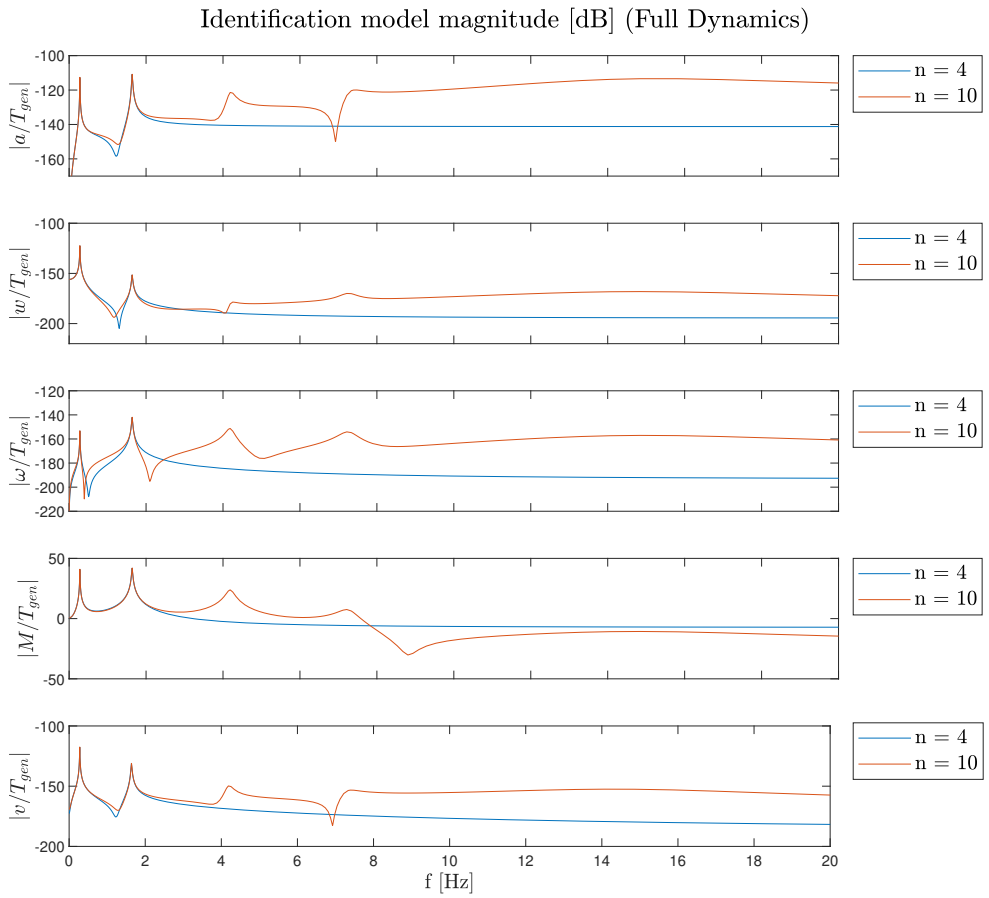

Figure 3-13: Identification result - Bode magnitude plot of full dynamics model for orders 4 and 10

3-4 Open-Loop Model Validation

A series of models has now been identified. To assess the performance of the model, an open-loop validation experiment is performed. First, a `Focus` experiment is designed in which the tower is excited. The identified tower model is subsequently simulated using generator torque input T_{gen} and an estimate of initial condition $x(0)$. The results can be compared in order to obtain a measure for model accuracy. As discussed in Section 2-6, sources of excitation other than generator torque act on the tower. If these unmodelled inputs to the system are significant with respect to generator torque, it is to be expected that the open-loop simulation will start to deviate from the actual system over time. In Chapter 4, a Kalman filter will be designed to counteract the effect of these unknown disturbance inputs. Therefore, in Chapter 4, the system model will be reevaluated using a closed-loop validation experiment.

To excite the tower, a doublet signal is used for T_{gen}. An experiment is performed at a series of different wind speeds.

- Full Dynamics: includes blade dynamics and tower shadow
- Wind speeds: 8, 12, 16, 20, 24 m/s (NWP)
- Torque rate limit: 2.5 MNm/s
- Experiment Duration 100 s
- Doublet duration: 40 s

In order to simulate actual operating conditions, a FD experiment is conducted, including blade dynamics and tower shadow. A torque rate limit has been applied, which is also part of the actual controller. Given the non-physical state of the system model, the first step is to obtain an estimate of $x(0)$. This is performed through solving a LLS problem using the first 20s of the acceleration measurement. Figure 3-16 and Figure 3-17 show the time and frequency response of the 12 m/s wind speed validation experiment for the full dynamics model with order 4. Figure 3-18 and Figure 3-19 display the corresponding response for 24 m/s wind speed. Given that the simulation is open-loop and that the actual simulation is subjected to 3P disturbances due to tower shadow, a good fit is obtained. The frequency response clearly shows disturbances at 1P, 3P and its higher harmonics (6P, 9P, 12P, 15P), as denoted in Table 3-5.

Table 3-5: Harmonic frequencies at rated rotor speed [Hz]

Harmonic	Frequency [Hz]
1P	0.183
3P	0.550
6P	1.10
9P	1.65
12P	2.20
15P	2.75

The 6P frequency is close to the first torsional tower mode with a natural frequency of 1.20Hz causing additional excitation. Moreover, it is observed that in the experiment 3P excitation seems to be the main disturbance in rotor speed, rather than tower vibrations. As expected, for 24m/s wind speed a clear increase in harmonic excitation is observed due to increased aerodynamic forces. The results for the PD model have been summarised in Table 3-6 and Figure 3-14, and for the FD model in Table 3-7 and Figure 3-15. The results show somewhat similar results. Both models show accurate results for lower wind speeds. At higher wind speeds the FD model shows an increased performance, which is mainly due to a more accurate natural frequency of the second mode. It is also found that the response is dominated by the first and second mode. This is mostly due to the torque rate limit, due to which less high-frequency content is present in the input signal. This results in decreased excitation of higher-order modes. Increasing the model order does not lead to a performance increase as higher-order modes are almost absent.

Table 3-6: Validation result (model order 4) - VAF for different wind speeds [%] (PD)

VAF [%]				
Wind speed [m/s]	a_{sw}^{tow}	w_{sw}^{tow}	ω_{roll}^{tow}	M_{base}^{tow}
8	97.2	98.9	93.9	98.2
12	97.2	97.8	94.2	97.2
16	90.6	95.5	87.7	93.9
20	83.8	93.3	83.8	91.0
24	69.7	87.4	73.7	82.6

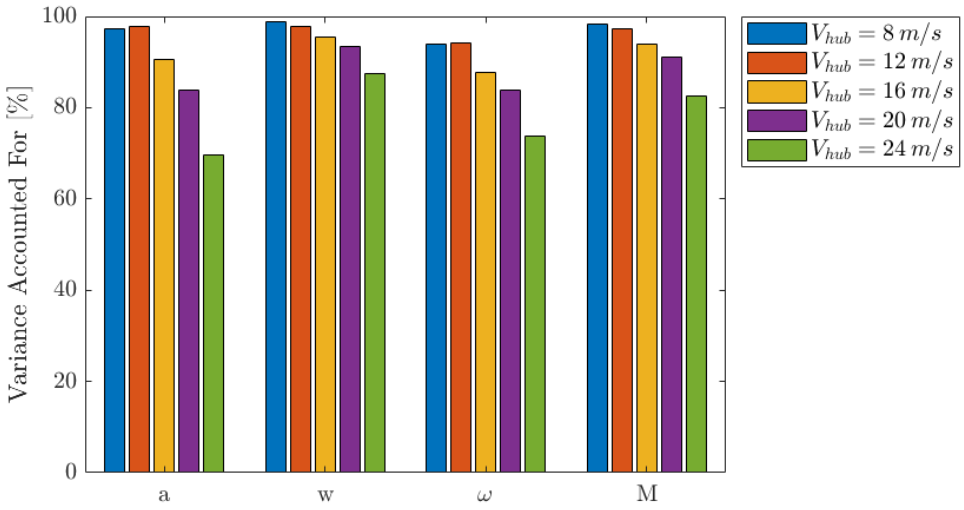

Figure 3-14: Validation Result - PD VAF [%]

Table 3-7: Validation result (model order 4) - VAF for different wind speeds [%] (FD)

VAF [%]				
Wind speed [m/s]	a_{sw}^{tow}	w_{sw}^{tow}	ω_{roll}^{tow}	M_{base}^{tow}
8	96.1	97.6	95.9	96.9
12	95.3	96.1	93.9	95.3
16	91.4	95.1	93.7	94.1
20	85.1	93.5	90.8	91.8
24	72.9	89.7	80.4	86.0

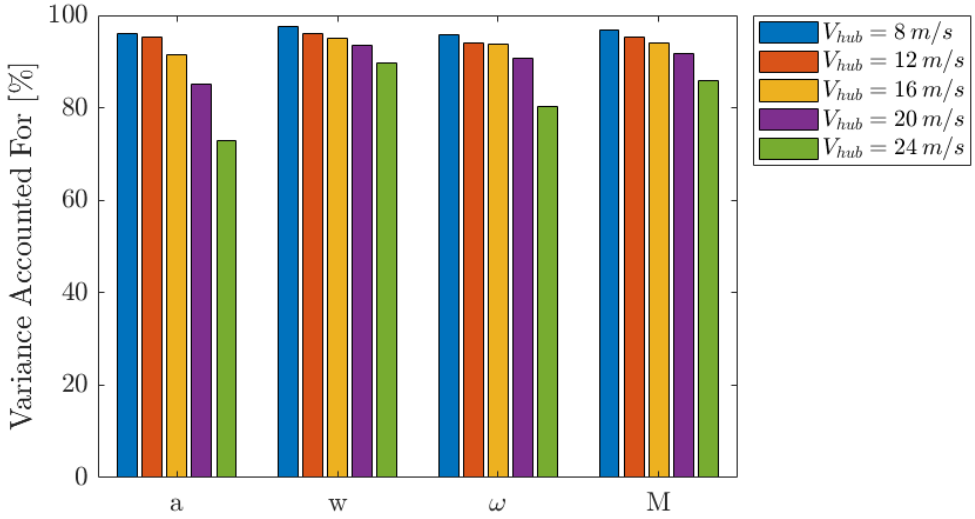

Figure 3-15: Validation Result -FD VAF [%]

The set of FD models has been chosen for the continuation of this project. A definite decision on model order is made during the Kalman filter design, as other operating conditions could lead to increased excitation of higher-order dynamics.

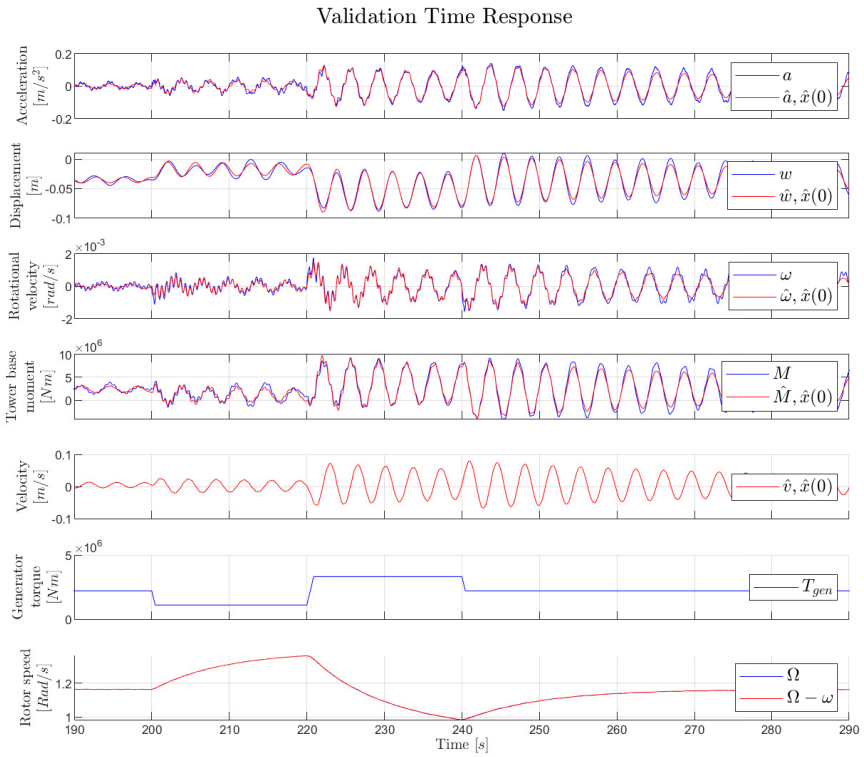

Figure 3-16: Validation Result - FD Time response 12 m/s using model order 4

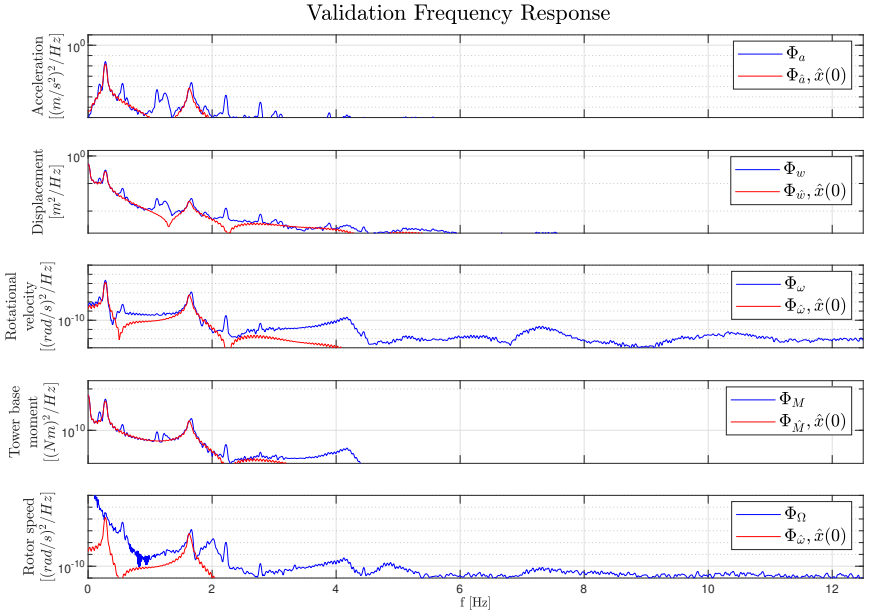

Figure 3-17: Validation Result - FD Frequency response 12 m/s using model order 4

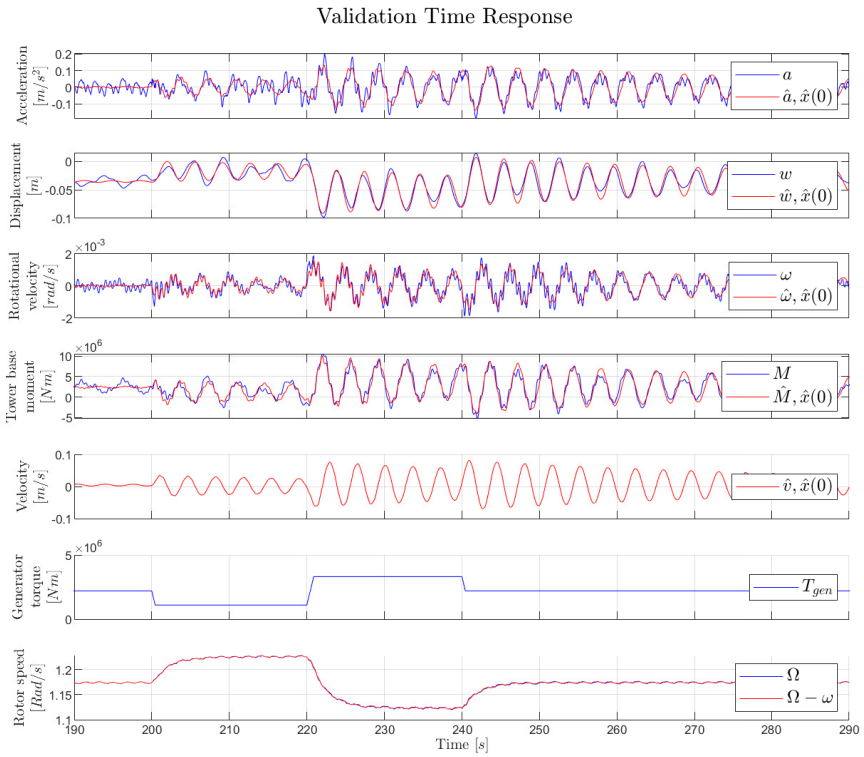

Figure 3-18: Validation Result - FD Time response 24 m/s using model order 4

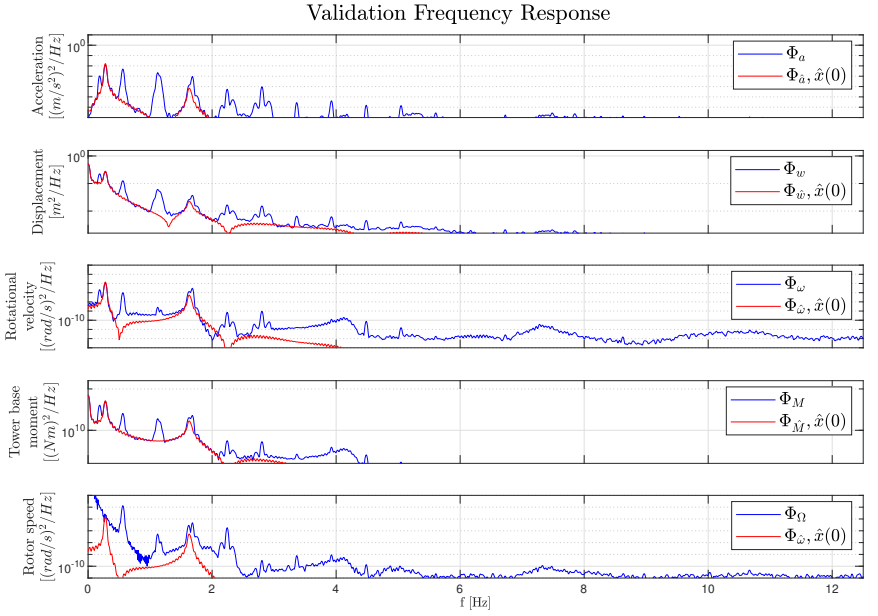

Figure 3-19: Validation Result - FD Frequency response 24 m/s using model order 4

3-5 Closed-Loop Tower Stability

In Chapter 1, the interaction of the tower with the torque controller has been discussed. With a tower model P_{Tower} now identified, this relation can be quantified. This is performed for the 4^{th}-order FD model. Additionally the rotor model $P_{Rotor} = \frac{-1}{Js}$ has been taken into account, with moment of inertia J. Considering Figure 1-4, the poles of the closed-loop system can be obtained for:

$$1 - (P_{Rotor} - P_{Tower})K_{\Omega \to T} = 0 \tag{3-27}$$

Two values are used for gain $K_{\Omega \to T}$, namely the maximal positive gain in the sub-rated region, K_{SR}, and the maximal negative gain in the above-rated region, K_{AR}. The results for the values considered are shown in Table 3-8. The damped natural frequencies and damping ratios are determined for three cases: one without controller interaction, thus yielding the nominal tower model, and two with interaction.

Table 3-8: Closed-loop tower dynamics

$K_{\Omega \to T}$	Mode	ω_d [Hz]	ζ
0	1	0.280	0.0106
	2	1.637	0.0068
K_{SR}	1	0.279	0.0170
	2	1.629	0.0241
K_{AR}	1	0.280	0.0102
	2	1.638	0.0058

It is found that the closed-loop interaction does have an effect on the tower's dynamics, albeit a relatively small effect. Rotor speed filters are not taken into account in this analysis. As expected, in above-rated conditions this results in a (slight) decrease in damping. In sub-rated conditions, the effect is reversed and the torque controller provides additional damping. The damping effect sub-rated is significantly larger than the decrease in damping above-rated due to the larger absolute gain value. It should be noted that the large gain value sub-rated is obtained only in a small section of the torque-speed curve.

It should be noted that the damping ratio is a combination of structural and aerodynamic damping. Parallel to this project, Lagerwey is performing field tests in order to obtain more accurate damping values for the tower. Preliminary results show that damping for actual towers in the field could be 50% less than used in simulation. This could increase the negative consequences of this effect.

3-6 Conclusion

The chapter validates the theoretical background of Chapter 2. It is possible to identify a reduced-order tower model including rotational dynamics as well as tower (base) bending moments, which can be done with a relatively simple linear SS model. The subspace identification method proves to be an effective way of identifying such a model. The advantages of the method, such as directly resulting in the required model in desired form, as well as model order reduction proved to be useful. On the other hand, it should be noted that the identified SS model matches the form derived in Chapter 2, up to a similarity transformation.

Chapter 4

Kalman Filter

In this chapter, a Kalman filter is designed based on the identified models from the Full Dynamics (FD) experiment. The rotational velocity estimate is used for rotor speed measurement filtering, the effect of which shall be assessed in this chapter. The state estimate is used for active tower damping in Chapter 5. In Section 4-1, the design of the Kalman filter is discussed. In Section 4-2, the results are evaluated for a series of different cases. First, data is post-processed. The Kalman filter is subsequently implemented in the controller to assess the closed-loop response and whether effect on turbine operation can be observed.

4-1 Design

The main use of an observer is to estimate the state of a system under presence of noise. A Kalman filter is able to do so in a statistically optimised manner.

The system matrices are assumed to be Linear-Time-Invariant (LTI) and subjected to process and measurement noise, similar to Equation (3-3).

$$x(k+1) = Ax(k) + Bu(k) + w(k) \tag{4-1}$$

$$y(k) = Cx(k) + Du(k) + v(k) \tag{4-2}$$

$$E\left[\begin{bmatrix} v(k) \\ w(k) \end{bmatrix} \begin{bmatrix} v(j)^T & w(j)^T \end{bmatrix}\right] = \begin{bmatrix} R(k) & S(k)^T \\ S(k) & Q(k) \end{bmatrix} \delta(k-j) \geq 0 \tag{4-3}$$

$$\begin{bmatrix} R(k) & S(k)^T \\ S(k) & Q(k) \end{bmatrix} \geq 0, \quad R > 0 \tag{4-4}$$

An asymptotic observer with observer gain L based on this model would result in the following state estimation error $x_e(k) = \hat{x}(k) - x(k)$:

$$\hat{x}(k+1) = A\hat{x}(k) + Bu(k) + L(y(k) - \hat{y}(k)) \tag{4-5}$$
$$x_e(k+1) = \hat{x}(k+1) - x(k+1) \tag{4-6}$$
$$= A\hat{x}(k) + Bu(k) + L(y(k) - \hat{y}(k)) - Ax(k) - Bu(k) - w(k) \tag{4-7}$$
$$= A(\hat{x}(k) - x(k)) + L(Cx(k) + Du(k) + v(k) - C\hat{x}(k) - Du(k)) - w(k) \tag{4-8}$$
$$= A(\hat{x}(k) - x(k)) + L\big(Cx(k) + Du(k) + v(k) - C\hat{x}(k) - Du(k)\big) - w(k) \tag{4-9}$$
$$x_e(k+1) = (A - LC)x_e(k) - w(k) + Lv(k) \tag{4-10}$$

$x_e(k)$ does not converge to zero for $k \to \infty$ with asymptotically stable $A - LC$, due to the presence of noise terms $w(k)$ and $v(k)$. Therefore, the objective is to minimise $x_e(k)$. In order to do so, two parameters are used. The estimate is unbiased, thus the mean value of $x_e(k)$ should be zero: $E[x_e(k)] = E[\hat{x}(k) - x(k)] = 0$. Secondly, the state-error covariance matrix $E[x_e(k)x_e(k)^T]$ is minimal. For a time-varying system different methods exist to solve this problem, for example the conventional and the square root implementation [25]. The state-error estimation covariance matrix is continuously updated and minimised resulting in an optimised time-varying Kalman gain.

For a time-invariant system with constant noise covariance matrices, the covariance matrix converges:

$$P(k|k-1) = E\big[\big(x(k) - \hat{x}(k|k-1)\big)\big(x(k) - \hat{x}(k|k-1)\big)^T\big] \tag{4-11}$$
$$\lim_{k\to\infty} P(k|k-1) = P \tag{4-12}$$

and P is obtained through solving the Discrete-Algebraic-Ricatti-Equation (DARE), resulting in a constant Kalman gain L.

$$P = APA^T + Q - (S + APC^T)(CPC^T + R)^{-1}(S + APC^T)^T \tag{4-13}$$
$$L = (S + APC^T)(CPC^T + R)^{-1} \tag{4-14}$$

A statistically optimal asymptotic observer is given by:

$$\hat{y}(k) = C\hat{x}(k|k-1) + Du(k) \tag{4-15}$$
$$\hat{x}(k+1|k) = A\hat{x}(k|k+1) + Bu(k) + L(y(k) - \hat{y}(k)) \tag{4-16}$$

The system matrices are considered LTI in this project as stated in Section 2-5. This is one condition in order to use a constant Kalman gain. Another condition is that process and measurement noise covariance matrices are time-invariant. Disturbances acting on the system other than generator torque are regarded as noise inputs. Typically, these disturbances stem from aerodynamic effects (tower shadow and wind shear). This means that for higher wind speeds more disturbances are present, as confirmed during model validation. In theory,

process and noise covariance matrices could therefore not be perfectly time-invariant. To assess time-invariance and the validity of using a constant Kalman gain, tuning is performed for a set of different wind speeds.

It should be noted that acceleration is the only measured output of the system, therefore y_a will represent acceleration a. Cross-covariance matrix S is set to zero. As feedback is only performed with one output: $R \in \mathbb{R}^{1x1}$, $Q \in \mathbb{R}^{nxn}$, $L \in \mathbb{R}^{nx1}$

$$\hat{y}(k) = C\hat{x}(k|k-1) + Du(k) \tag{4-17}$$

$$\hat{x}(k+1|k) = A\hat{x}(k|k+1) + Bu(k) + L(y_a(k) - \hat{y}_a(k)) \tag{4-18}$$

Measurement noise covariance matrix $R = 0.05$, based on sensor information. However this value is somewhat arbitrary. Q is a diagonal process noise covariance matrix which is tuned to maximise the Variance Accounted For (VAF) of the estimated outputs and actual outputs. This is performed for a series of different wind speeds and for different model orders according to the same procedure. The system models have been transformed into modal form. This means that the A-matrix is block-diagonal and that states x_i and x_{i+1} are related to mode i. The following procedure is followed for tuning the Kalman gain using Q:

- $Q = \text{diag}(Q_{diag})$
- Set $Q_{diag} = k \cdot \begin{bmatrix} 1 & 1 & \cdots & 1 & 1 \end{bmatrix}$, Optimise VAF for scalar k.
- Set $Q_{diag} = \begin{bmatrix} k_1 \cdot \begin{bmatrix} k & k \end{bmatrix} & \cdots & k_i \cdot \begin{bmatrix} k & k \end{bmatrix} \end{bmatrix}$. Optimise each mode individually using k_i.
- Set $Q_{diag} = \begin{bmatrix} \begin{bmatrix} r_1 k_1 k & \frac{1}{r_1} k_1 k \end{bmatrix} & \cdots & \begin{bmatrix} r_i k_i k & \frac{1}{r_i} k_i k \end{bmatrix} \end{bmatrix}$. Tune ratio r_i between elements related to a single mode.

The advantage of tuning the Q matrix is that for a positive semi-definite Q matrix, the Kalman gain is guaranteed to be stable. The Kalman gain is derived through manual tuning and a reference data set which represents typical turbine operation over a variety of conditions. A set of Design Load Case (DLC) experiments is used. DLCs are used for certification purposes and therefore provide an accurate depiction of turbine behaviour. The used DLC experiments have the following characteristics:

- Experiment duration: 600s
- Wind field: Normal Turbulence Model (NTM)
- Average wind speed: 3-25m/s
- Yaw misalignment: -8°, 0°, 8°
- Rotor mass imbalance: Blade 2 mass is 1% larger

For tuning the Kalman gain the following wind speeds have been selected with no yaw misalignment: 8, 12, 16, 20, 24 m/s. The results of the tuning approach are displayed in Table 4-1. For each wind speed, a Kalman gain is obtained through tuning Q. Additionally the corresponding maximum VAF for outputs a, w, ω and M are displayed. It should be noted that the VAF related to a is not used as a performance measure. The acceleration signal is the result of all inputs acting on the tower. The Kalman filter extracts the effect of the tower modes on acceleration and rejects other inputs to the acceleration signal. The VAF related to the other three outputs can be considered a performance measure. Some observations can be made here.

- Higher wind speeds result in larger vibrations. Larger vibrations result in larger vibration-to-noise ratios and therefore in improved estimation accuracy.
- For higher wind speeds, the Kalman gain related to mode 1 is tuned slightly more aggressively.
- Inclusion of vibration modes beyond the second mode does not lead to a performance increase.

In general, the performance of the Kalman filter increases for higher wind speeds. As will be shown in the subsequent section, tower vibrations increase significantly for increasing wind speeds. For increased tower vibrations, the tower modes are more significantly present in the acceleration signal in comparison to external excitation. As shown by the large increase in VAF related to acceleration.

Table 4-1: Filtering result - Kalman gain tuning results, model order 4

DLC type	Q_{diag}	L	VAF
8	$\begin{bmatrix}0.001\\0.004\\0.01\\0.01\end{bmatrix}$	$\begin{bmatrix}-0.1095\\0.2993\\0.3018\\2.5151\end{bmatrix}$	$\begin{bmatrix}16.9\\72.9\\70.1\\65.1\end{bmatrix}$
12	$\begin{bmatrix}0.0013\\0.005\\0.01\\0.01\end{bmatrix}$	$\begin{bmatrix}-0.1251\\0.3339\\0.2996\\2.5398\end{bmatrix}$	$\begin{bmatrix}22.4\\75.5\\63.1\\69.0\end{bmatrix}$
16	$\begin{bmatrix}0.0013\\0.005\\0.0075\\0.0033\end{bmatrix}$	$\begin{bmatrix}-0.1257\\0.3337\\0.2543\\2.1445\end{bmatrix}$	$\begin{bmatrix}34.8\\72.9\\73.8\\73.0\end{bmatrix}$
20	$\begin{bmatrix}0.0008\\0.02\\0.005\\0.005\end{bmatrix}$	$\begin{bmatrix}-0.2022\\0.5389\\0.1934\\1.7840\end{bmatrix}$	$\begin{bmatrix}42.1\\77.1\\73.8\\76.8\end{bmatrix}$
24	$\begin{bmatrix}0.0021\\0.0233\\0.0056\\0.0056\end{bmatrix}$	$\begin{bmatrix}-0.2465\\0.6074\\0.2028\\1.9452\end{bmatrix}$	$\begin{bmatrix}60.5\\83.9\\80.0\\83.3\end{bmatrix}$

Each of these five Kalman gains is tested for every DLC experiment, thus for a total of 69 experiments (23 wind speeds for 3 yaw angles). At higher wind speeds, tower vibrations significantly larger, illustrated in Figure 4-1. In this plot, the standard deviation of four output parameters is denoted for each experiment. Each wind speed shows three experiments, one for each yaw angle. This clearly shows an almost linear increase in the standard deviation of vibration-related tower outputs. At higher wind speeds, between 15 and 25m/s, tower vibrations are especially large. Therefore, rotor speed measurement correction is particularly usefull in this region.

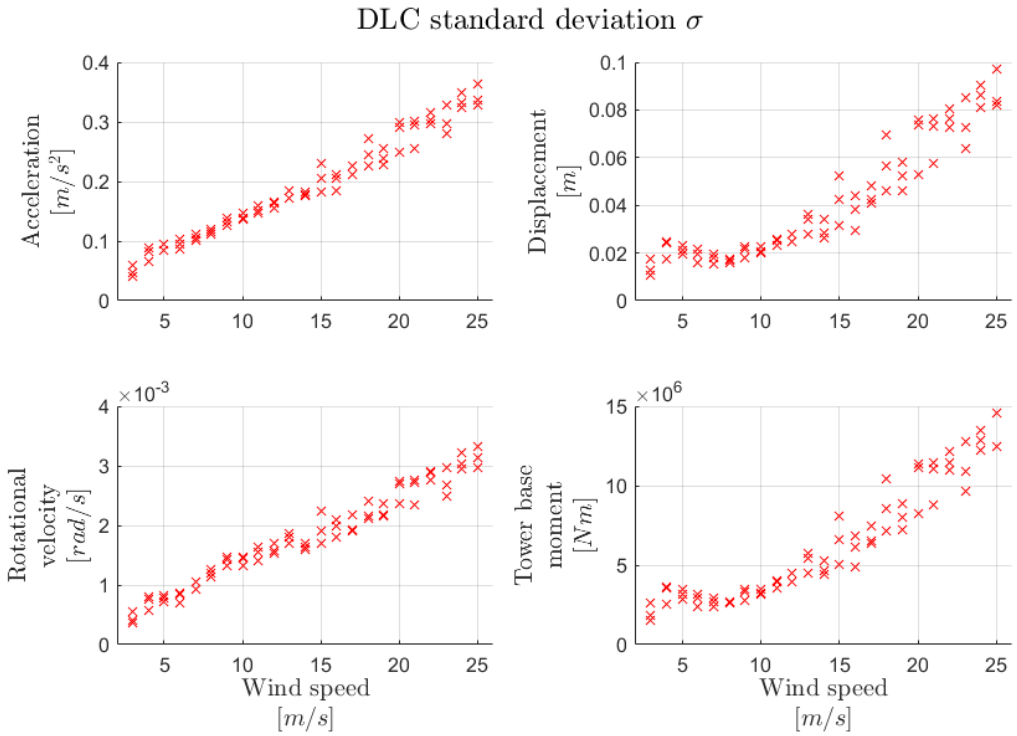

Figure 4-1: DLC experiment standard deviations

The average VAF over all 69 experiments has been determined for each Kalman gain, as is displayed in Table 4-2.

Table 4-2: Filtering result - Kalman gain tuning results, model order 4

VAF [%]				
Kalman gain	a	w	ω	M
L_8	41.4	81.2	72.5	77.7
L_{12}	41.6	81.4	72.7	77.9
L_{16}	41.3	81.4	73.0	78.2
L_{20}	41.9	81.2	73.5	78.9
L_{24}	42.3	80.7	73.6	78.7

The gains tuned at different wind speeds perform very similar. Kalman gain L_{20} is chosen, which shows the best results when regarding the VAF. The Kalman gain is tuned for a 20m/s wind speed, which is in the middle of the high wind speed range and therefore the region with largest vibrations. The dynamics of the Kalman filter can be described as follows:

$$\hat{x}(k+1) = (A - LC)\hat{x}(k) + \begin{bmatrix} B - LD & L \end{bmatrix} \begin{bmatrix} u(k) \\ y_a(k) \end{bmatrix} \tag{4-19}$$

$$\hat{y} = C\hat{x}(k) + Du(k) \tag{4-20}$$

The poles of the observer can be compared to the poles of the system, shown in Table 4-3. The observer poles are required to be faster than the system poles in order to obtain adequate state estimation. The speed of the system poles is determined by the real part of the poles. The observer poles for the first mode are significantly faster with a ratio of 34.3. The second mode is also faster with a ratio of 5.5. Considering Equation (4-10), it can be seen that a smaller Kalman gain results in a slower observer, therefore allowing for more process noise. A larger Kalman gain would result in amplification of measurement noise.

Table 4-3: Kalman result - system poles vs. observer poles

Poles of the system		
	Mode 1	Mode 2
A	$-0.0187 \pm 1.756i$	$-0.0699 \pm 10.288i$
A-LC	$-0.6412 \pm 1.705i$	$-0.3840 \pm 10.286i$
σ_A/σ_{A-LC}	34.3	5.5

Figure 4-2 shows a bode plot of the Kalman filter's dynamics. Frequency content in the acceleration signal related to the tower modes is transferred to the estimate whereas other frequency content is suppressed. It can be found that generator torque results in more excitation of the second mode. In practice, the torque signal contains significantly less frequency content at the second mode frequency than at the first mode due to the controller and the torque rate limit.

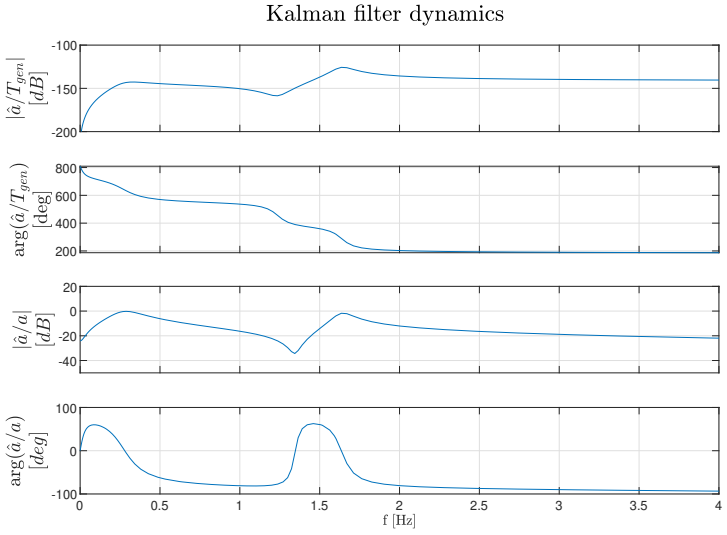

Figure 4-2: Bode plot of Kalman Filter dynamics

The magnitude of $|\hat{a}/a|$ at the tower frequencies shows the estimation magnitude per mode, as shown in Table 4-4. Both modes are estimated with zero phase delay.

Table 4-4: Kalman result (model order 4) - Magnitude of $|\hat{a}/a|$ for mode 1 and 2

$\lvert\hat{a}/a\rvert$		
Gain	[dB]	[%]
Mode 1	-0.222	97.48
Mode 2	-1.77	81.56

A gain of 0dB would result in a perfect estimate at tower frequencies. However, in order to achieve this for higher frequencies such as the second frequency, a significantly larger Kalman gain would have to be designed, which results in increased amplification of measurement noise. A larger Kalman gain therefore results in decreased estimation accuracy.

4-2 Evaluation

With a Kalman gain selected, the results are analysed in more detail for several different test cases:

- DLC post-processing
- DLC controller implementation
- Field data post-processing

The first case allows for the analysis of observer estimation accuracy, without closed-loop effects. In the second case, the Kalman filter is implemented in the controller, therefore closed-loop tower-controller interaction is considered. Hence, the effect of filtering the rotor speed signal on tower stability can be assessed. Thirdly, field data is post-processed in order to assess similarity between simulation and field.

4-2-1 DLC Post-Processing

DLC data is post-processed using the Kalman filter. First, some examples are used. The first example is for the DLC experiment at 9 m/s wind speed. A segment of the time response of the experiment with relatively large vibrations is displayed in Figure 4-3. The related frequency response is shown in Figure 4-4 (note the logarithmic scale). The acceleration signal shows significant disturbances. The Kalman filter optimally separates the effect of the tower's state on acceleration from other inputs. In the frequency response, it is found that the effect of the first and second mode are extracted from the signal. Additionally the 1P and 3P effects can be observed (0.18 and 0.54Hz) as well as the effect of the 1^{st} tower torsional mode (1.20Hz). At higher frequencies, noise caused by the stochastic wind field remains present in the signal.

The displacement signal is estimated quite accurately, although it is noisier than the actual displacement. In the displacement signal, only the effect of the first mode is significant. Opposite to displacement, rotational velocity is dominated by the second mode, which shows the benefit of taking into account this additional mode.

The first and second mode are also present in the tower base moment. Although the second mode is insignificant in the tower top displacement, it is very significant for tower base moments which is ultimately determines the amount of fatigue damage caused. Additionally, the velocity estimate is shown, which is mainly dominated by the first tower mode. In the final plot of Figure 4-4, the frequency response of the filtered rotor speed is compared to the measured rotor speed. The effect of rotor speed filtering is clearly observed. For the first mode a decrease of 93.9% is obtained in Power Spectral Density (PSD). For the second mode a reduction of 99.5% is obtained (!). Other disturbances remain present in the rotor speed signal as these disturbances are not caused by tower vibrations. The 1P and 3P disturbances can be distinguished, as well as the collective blade edge mode (2Hz).

Figure 4-5 and Figure 4-6 show the same results for 24 m/s wind speed, where all parameters are dominated by the first tower mode. As the tower modes become more dominant with respect to noise in the acceleration measurement, the estimates become more accurate at higher wind speeds. For the first and second mode the reduction in rotor speed disturbance is 90.7% and 90.5% respectively. As illustrated in Figure 4-8 on a linear scale for reference.

Figure 4-7 shows the average VAF per wind speed for different wind speeds with 3 m/s increments. It is found that at very low wind speeds, high performance is obtained. This is caused by a lack of disturbance inputs to the system and tower vibrations in general at low wind speeds. Then a steep decline is observed for wind speeds at around 9-12 m/s, caused by the increasing presence of harmonic excitation. For high wind speeds the VAF increases again, as tower vibrations become more dominant with respect to input disturbances. As seen in Figure 4-1, tower vibrations become especially significant at wind speeds $\geq$ 15 m/s, therefore accuracy in this region is required.

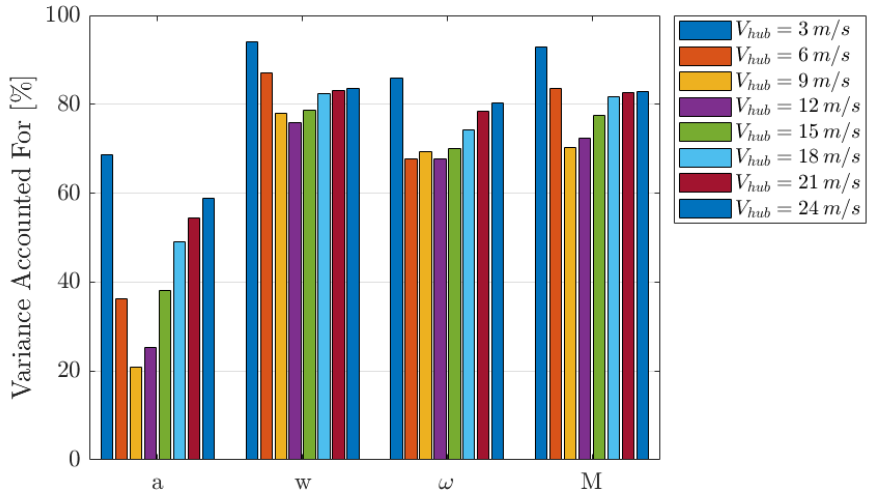

Figure 4-7: Kalman Filter Performance - Average VAF [%] at different wind speeds

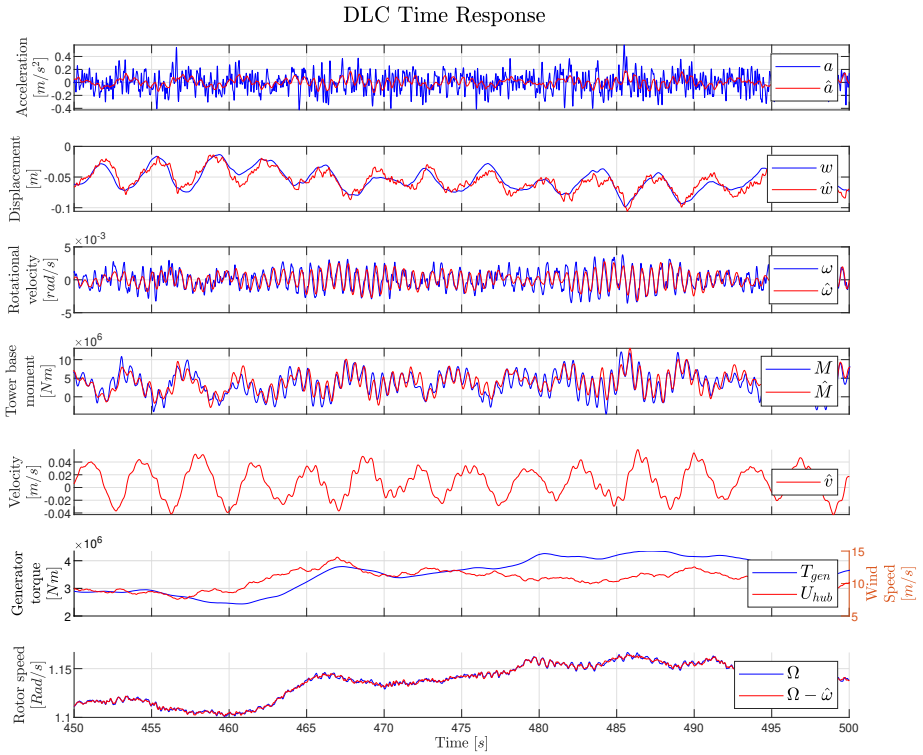

Figure 4-3: Kalman filter performance - DLC 9 m/s time response

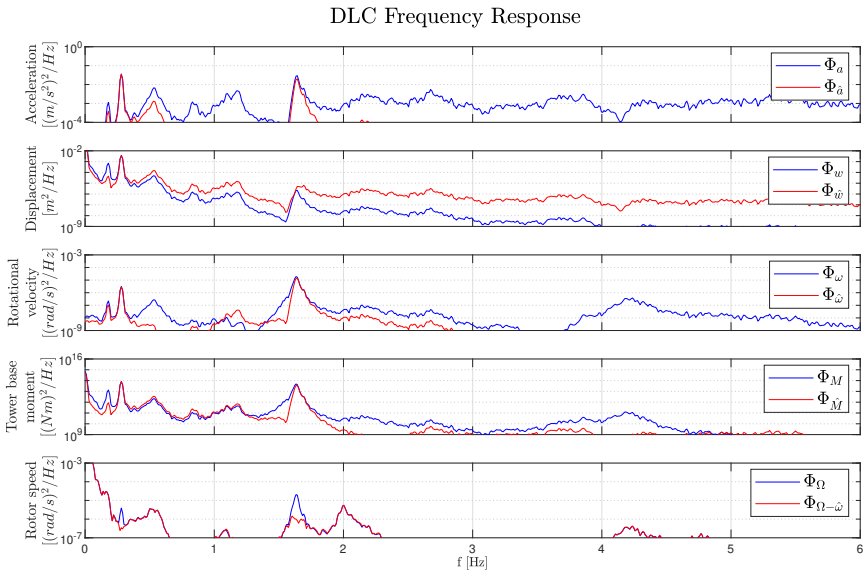

Figure 4-4: Kalman filter performance - DLC 9 m/s frequency response

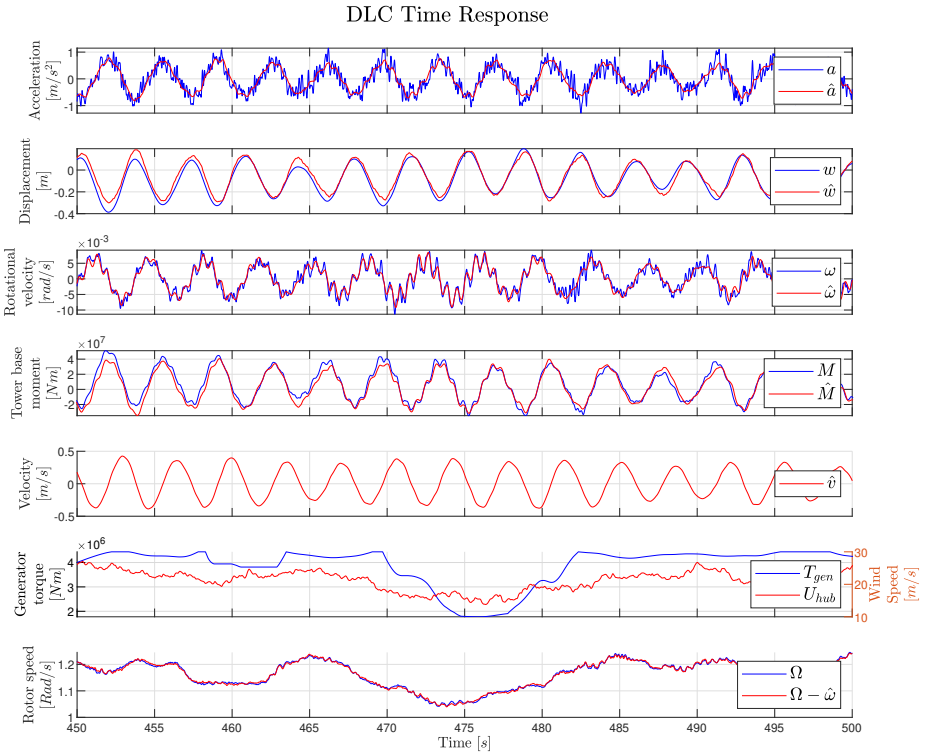

Figure 4-5: Kalman filter performance - DLC 24 m/s time response

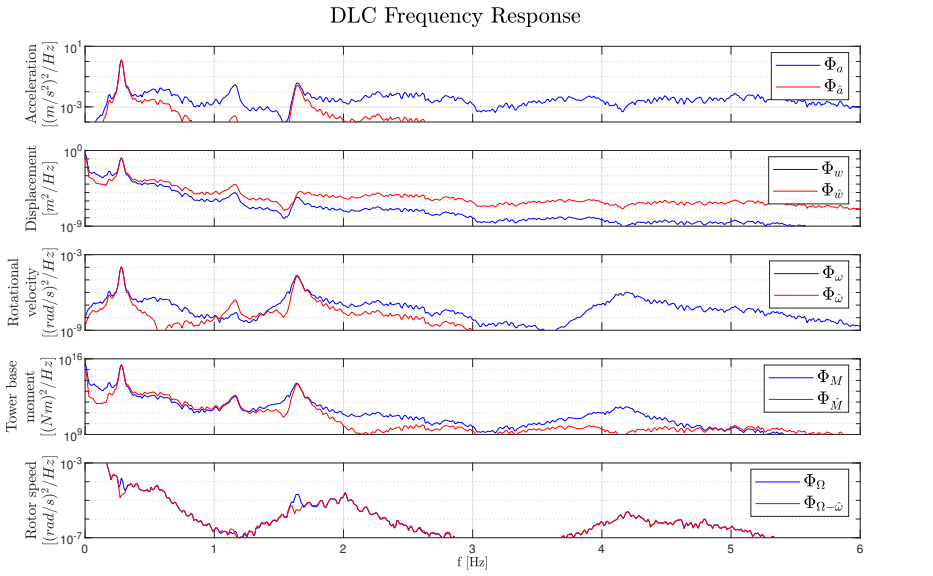

Figure 4-6: Kalman filter performance - DLC 24 m/s frequency response

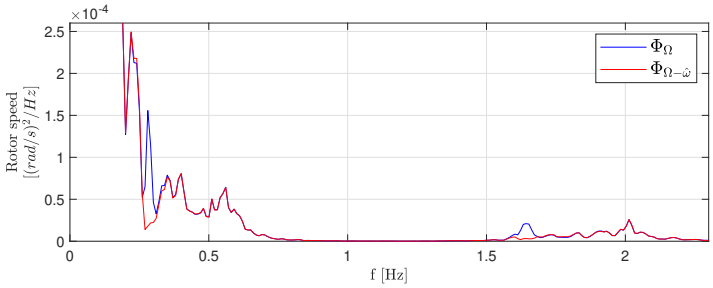

Figure 4-8: Kalman filter performance - DLC 24 m/s frequency response of filtered rotor speed with a linear scale

The average reduction in PSD of the rotor speed signal at the tower eigenfrequencies due to filtering is determined and shown in Table 4-5. The average reduction for the second mode is slightly higher than for the first mode. This can be explained by the frequency content which is present in the rotor speed signal itself. Therefore not all content in the signal at this frequency stems from the tower modes and a 100% reduction is not possible. The amount of frequency content in the rotor speed signal is higher at lower frequencies, therefore the reduction at the first tower mode is slightly less. The average reduction has been determined for different cases, which all show very similar results. Yaw misalignment and different wind speeds do not affect the Kalman filter's performance, which is an important observation regarding robustness.

Table 4-5: Kalman result (model order 4) - PSD reduction for mode 1 and 2

PSD reduction [%]		
	Mode 1	Mode 2
Average	89.1	93.5
Yaw 0°	89.7	93.3
Yaw -8°	89.2	93.7
Yaw 8°	88.4	93.4
Wind speeds 3-14 m/s	89.0	95.2
Wind speeds 15-25 m/s	89.2	91.6

Table 4-6 shows the VAF for the three different yaw angles. Other than expected, the Kalman filter performance improves for situations with a yaw misalignment. Possibly this is caused by a reduced tower shadow (3P) disturbance due to a larger distance between blade and tower in case of yaw misalignment.

Table 4-6: Kalman result (model order 4) - VAF for different yaw angles

VAF [%]				
Yaw [°]	a	w	ω	M
0	40.2	79.6	72.8	77.7
-8	42.7	81.6	73.8	79.5
8	42.8	82.4	74.0	79.5

4-2-2 Controller Implementation

Next, the Kalman filter is implemented in the controller. The first and second tower mode are removed from the rotor speed measurement during the experiments rather than through post-processing, thus affecting turbine operation. From Section 3-5, it was found that rotor speed measurement disturbances cause additional damping in the sub-rated region, whereas it causes a slight decrease in damping in the above-rated region. Therefore, depending on the operating region, removing tower disturbances from the rotor speed measurement might have either a positive or negative effect on tower loads. In both cases the interaction happens unknowingly and is therefore undesired. The implementation is tested in two experiments:

- Staircase normal wind profile with steps of 1 m/s
  - Low wind speeds. Wind speed increases between 5-12 m/s, turbine operates in sub-rated conditions
  - High wind speeds. Wind speed increases between 12-19 m/s, turbine operates in above-rated conditions
- DLC

In the first experiment, a staircase normal wind profile is used, such that the turbine is in either sub-rated or above-rated conditions, while in a DLC experiment these regions alternate due to the variable wind speed. For the first case, wind speed increases from 5 to 12 m/s, with the turbine acting in sub-rated conditions. For the second case, winds speed increases from 12 to 19 m/s and thus the turbine operates in above-rated conditions. Each experiment is conducted with and without rotor speed measurement correction, after which the results are compared. Figure 4-9 shows the time response of the signal for wind speeds between 12 and 19 m/s. The steps in wind speed cause torque actions, which lead to tower excitation. Additionally the effect of 3P excitation is present.

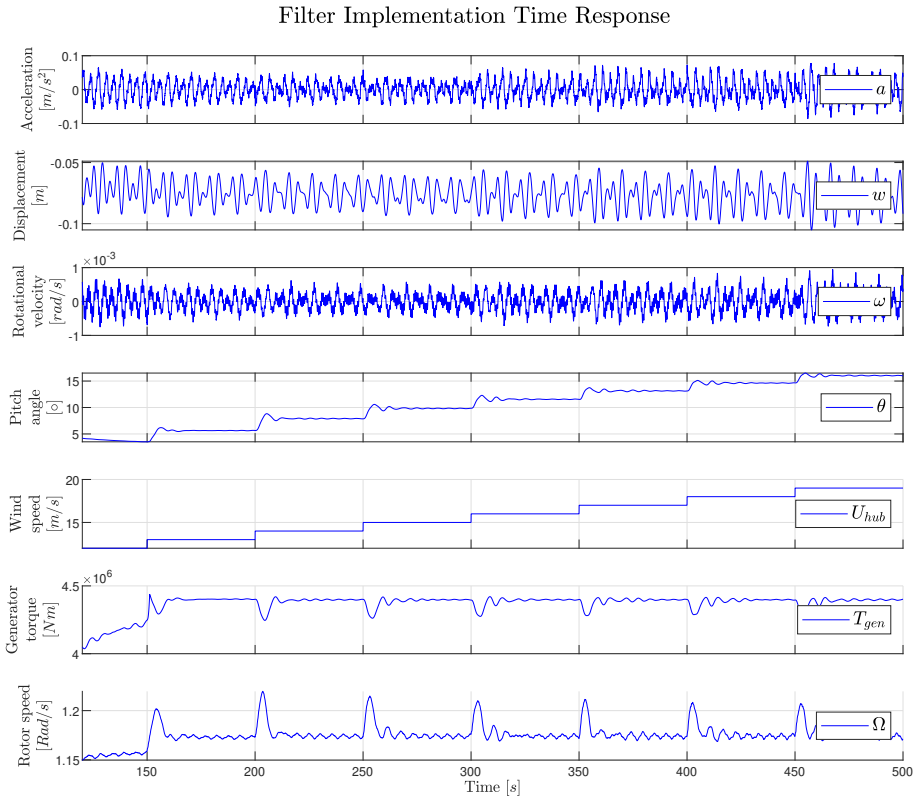

Figure 4-9: Filter Implementation - Time response to a staircase wind profile

In order to assess the effect of rotor speed measurement correction, a set of performance parameters have been determined. The Damage Equivalent Load (DEL) value is obtained through first performing a rainflow counting procedure, which provides the number of full and half cycles for certain load amplitudes. The Palmgren-Miner rule is subsequently used to obtain the final value:

$$\sigma_v = (\sum_{i=1}^{n}(\sigma_i^m n_i)/n_v)^{1/m} \tag{4-21}$$

σ_v is proportional to the ratio between cycles experienced versus the total number of cycles to failure at the stress level. Therefore $\sigma_{v,Kalman}/\sigma_{v,nominal} = DEL_{Kalman}/DEL_{nominal}$. The ratio is independent of value n_v. m is determined by material properties. For the steel tower, values between 3-5 are used. $m = 3$ has been used in this case. The results are shown in Table 4-7

Table 4-7: Filter implementation - PSD reduction of control action for mode 1 and 2

Ratio(Kalman/nominal) [%]		
Parameter	5-12 m/s	12-19 m/s
$DEL(M)$	104.88	94.15
$\sigma(a)$	106.92	92.60
$\sigma(T_{gen})$	100.01	100.14
$\sigma(\theta)$	99.94	100.00

In line with expectation, when filtering is applied, damping is reduced in sub-rated conditions and increased in above-rated conditions. In sub-rated conditions a DEL increase of 4.88 % is observed, while in above-rated conditions a decrease of 5.85% is obtained. These results clearly show the effect of tower-torque controller interaction. It should be noted that although an increase in DEL is obtained in sub-rated conditions, tower vibrations are especially present for high wind speeds and thus in above-rated conditions. For above-rated conditions, the effect of filtering is also observed in the frequency response of the control signals, as shown in Figure 4-10. Torque and pitch action is reduced at the tower frequencies, the rate of which is denoted in Table 4-8. For sub-rated conditions, this effect is not clearly observed, since pitch angle is constant and tower vibrations are relatively small.

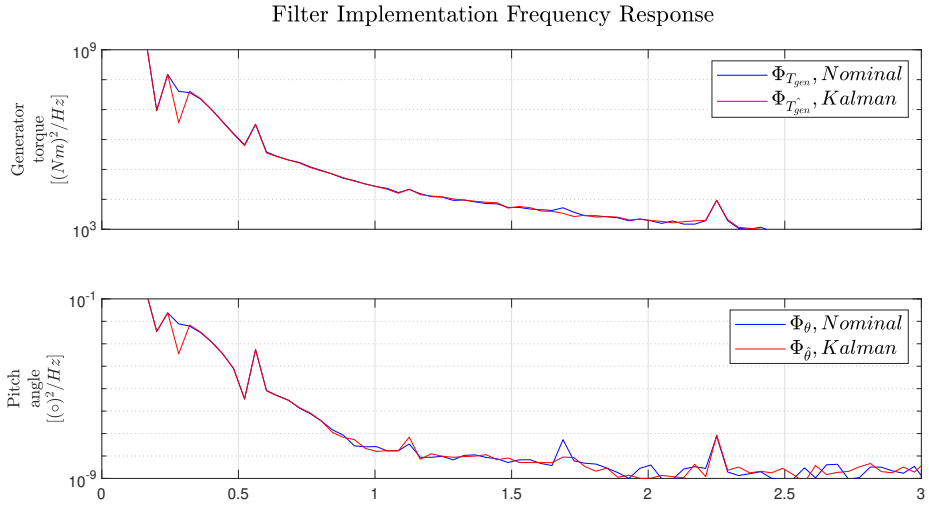

Figure 4-10: Filter Implementation - Effect of Kalman filtering on control action

Table 4-8: Filter implementation - Power Spectral Density reduction of control action for mode 1 and 2

PSD reduction [%]		
	Mode 1	Mode 2
Generator torque	91.0	34.8
Pitch angle	95.3	83.1

In a DLC experiment, the turbine alternates between operating regions. Therefore the effect is expected to be less consistent, as shown in Table 4-9. Positive effects are denoted in green, negative effects in red. The parameters have been determined for each of 69 experiments, after which the average is determined over all these experiments. On average, the effects are rather insignificant. It is observed that tower vibrations slightly increase, caused by the significant loss of damping when the turbine is operating in the sub-rated region of the torque controller. A slight decrease in control action for both torque and pitch is observed as well. Upon dividing the results into a low wind speed and a high wind speed category, the results reveal a more clear effect. For low wind speeds, a predominantly negative effect is observed with increases in vibration-related parameters. For high wind speeds, the opposite is observed and the effect on all parameters except for tower fore-aft moments is positive. The positive effect for high wind speeds is less than the negative effect at lower wind speeds, which is caused by the highly turbulent wind used in a DLC. At low wind speeds, the turbine operates exclusively in the sub-rated region of the torque control curve. At high wind speeds, in principle, the turbine operates in the above-rated region. However, due to large variations in wind speed, rotor speed regularly drops, causing sub-rated operation. Taking into consideration the presence of tower vibrations for different wind speeds as shown in Figure 4-1, the effect is especially important for wind speeds larger than 15 m/s. Without rotor speed measurement correction, the tower exhibits different damping ratios, whereas with this filtering an approximately constant damping ratio is obtained. The extreme load value is expected to be largest in case of minimal tower damping ratio. For this reason, the maximum tower base moment has been determined. As can be seen, during low wind speeds this value is on average increased with 1.93%, while for high wind speeds this value is reduced with 1.98%.

Table 4-9: Filter implementation - DLC performance analysis

Ratio(Kalman/Nominal) [%]			
Parameter	Average	Wind speeds 3-14 m/s	Wind speeds 15-25 m/s
$\sigma(a)$	100.41	101.65	99.04
$\sigma(w)$	102.95	106.26	99.34
$\sigma(\omega)$	100.24	101.53	98.82
$\sigma(M)$	102.56	105.66	99.18
DEL(M)	101.77	104.27	99.04
max(M)	100.06	101.93	98.02
$\sigma(M_{tower\ base,fore-aft})$	100.80	100.72	100.88
$\sigma(M_{tower\ base,torsional})$	100.02	100.29	99.72
$\sigma(M_{blade,leadwise})$	99.90	99.95	99.85
$\sigma(M_{blade,flapwise})$	99.51	100.31	98.64
$\sigma(\theta)$	99.25	98.94	99.60
$\sigma(\Omega)$	99.88	101.32	98.31
$\sigma(P_{gen})$	99.86	100.43	99.24
$\mu(P_{gen})$	99.77	99.47	100.10
$\sigma(T_{gen})$	99.83	100.47	99.14

4-2-3 Field Data Post-Processing

The Kalman filter can be tested through post-processing actual field data. In the field, only acceleration data is available. Therefore, it is not possible to assess the performance using the estimated output parameters. A section of the time response is shown in Figure 4-11. It shows that the first tower mode is significantly more present than the second mode, whereas in simulation also the second mode is significant. Figure 4-12 shows the corresponding PSDs. The first mode shows a clear reduction of 92.7% in PSD. A small peak seems to remain. This can be explained, as the Kalman filter only filters tower movement from the rotor speed. These rotor speed measurement disturbances lead to torque and pitch action at the tower's frequency as is shown in the lower two plots. These will induce actual rotor speed disturbances at this frequency. Such disturbances remain as they are not directly an effect of tower top rotational velocity. An actual implementation results in a reduction or removal of torque and pitch disturbances at the tower's natural frequency and would therefore also reduce this actual rotor speed disturbance. As stated, the second mode is hardly present. Although a reduction in PSD is seen at the exact second tower mode, a slight increase is observed at adjacent frequencies. Moreover, no effects of the second mode on generator torque and pitch angle are observed.

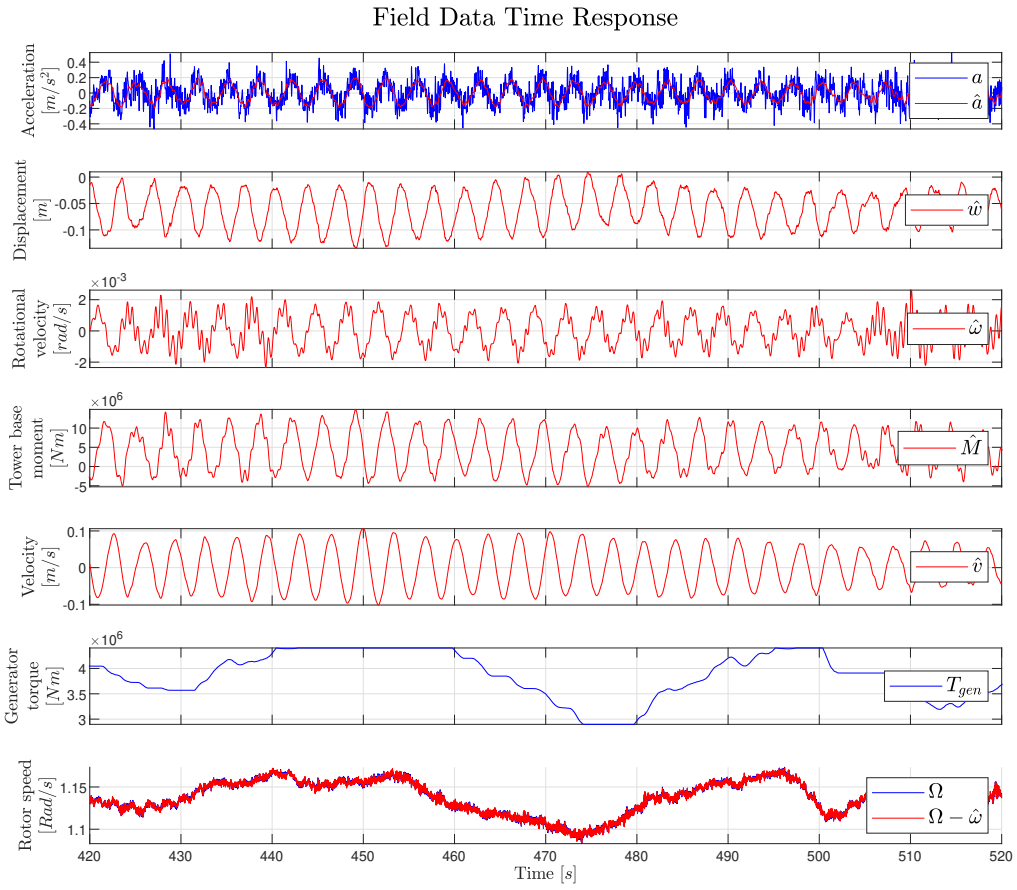

Figure 4-11: Kalman filter performance - Field data time response

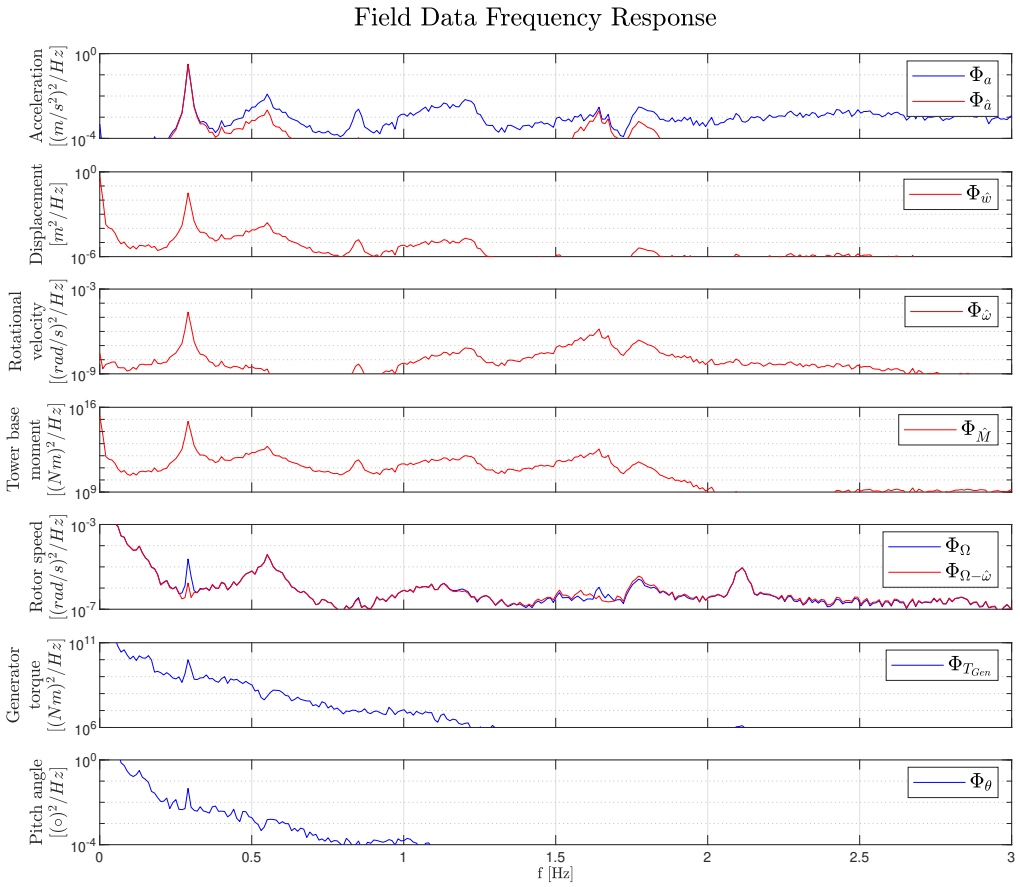

Figure 4-12: Kalman filter performance - Field data frequency response

4-3 Conclusion

Excitation sources other than generator torque have been regarded as noise inputs. This noise poses a limit in Kalman gain tuning, since a more aggressive (larger) Kalman gain would result in amplification of noise. Nevertheless, a Kalman filter has been designed which shows adequate results in state estimation. Tower disturbances can be successfully removed from the rotor speed measurement using the tower top rotational velocity estimate. It has been shown that filtering the rotor speed does not always lead to a decrease in tower vibrations. Depending on the operating region, the controller already acts as an active tower damper or reduces damping. The controller typically adds damping in sub-rated conditions for lower wind speeds with only small tower vibrations. However, a tower-controller interaction that reduces damping is particularly undesirable, which happens at high wind speeds and thus in situations with large vibrations. Rotor speed disturbances lead to additional undesired control actions, which are removed by rotor speed measurement correction. This is seen more clearly in field data than in simulation. In the next chapter, a state-feedback tower damping controller is designed, using the Kalman filter state estimate.

Chapter 5

Modal Damping Control

In preceding chapters, it has been established that tower vibrations do affect rotor speed measurements and therefore affect controller performance. In closed-loop, this effect can be both positive or negative. To mitigate the problem of extreme side-side vibrations, an active tower damping control strategy is required. The developed control strategy is based on state feedback control. The reason for choosing state feedback is simplicity and ease of implementation, therefore lowering the bar for implementation in the field. In the case of state feedback, additional damping can effectively be added to both modes individually. Alternatively one could think of linear Model Predictive Control (MPC),which has the advantage of including (soft) constraints. Therefore a controller can be designed which keeps vibrations within certain bounds while allowing for small vibrations. Advantages are; more freedom in designing a controller which satisfies the objective of load reduction while not affecting nominal performance. A disadvantage of MPC is computational complexity. For an MPC controller to be viable, sampling time and prediction horizon would have to optimised to keep computation time within certain bounds, while effectively controlling two modes. As side-side damping is not the main objective of the controller but rather an additional feature, a more simple and intuitively comprehensive damping method is preferred for implementation.

The state feedback controller has been deemed Modal Damping Control, as damping is added to each individual mode. Tuning is performed using pole placement since a direct relation between damping ratios and pole locations can be established.

5-1 Design

The procedure is as follows:

- Define desired damping ratios $\zeta_{K,1}$ and $\zeta_{K,2}$ for each mode
- Determine natural frequencies from the system model
- Determine desired complex pole locations using damping ratios and natural frequencies

- Determine feedback gain through pole-placement

Tower damping is performed through inducing generator torque variations. To prevent rotor speed variations, these are to be kept minimal. Therefore only a limited amount of damping is added to the tower. $\zeta_{K,1} = \zeta_{K,2} = 0.03$ results in a 183% and a 417% increase of damping for the first and second mode respectively. With $\omega_{n,1} = 0.28$ and $\omega_{n,2} = 1.637$ the new pole locations can be determined:

$$p_K = -\zeta_{K,i}\omega_{n,i} \pm i\omega_{n,i}\sqrt{1-\zeta_{K,i}}, \quad \zeta_{K,i} < 1 \tag{5-1}$$

A diagram of the control system is shown Figure 5-1.

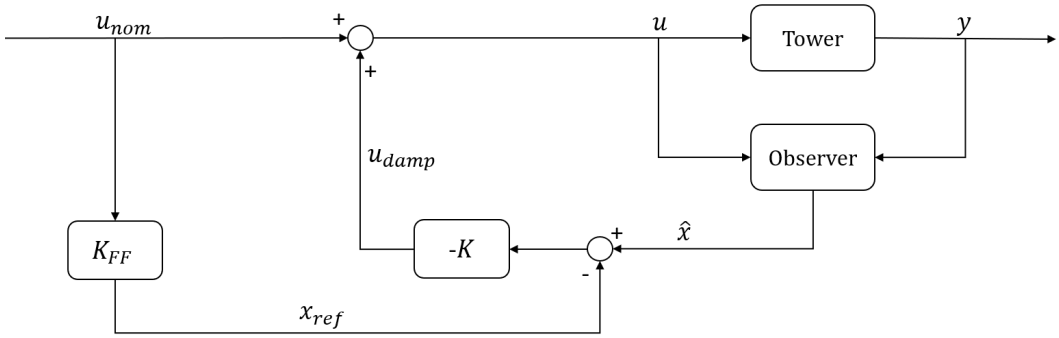

Figure 5-1: Diagram of Modal Damping Control system

Through pole-placement, a state feedback gain K is determined for which the pole locations of $A-BK$ match the desired poles. The controller attempts to reach a steady-state of the tower. When adding damping, typically velocity feedback is performed. In a steady-state, velocity is zero. Therefore, in principle, no steady-state reference would be required. However, the identification procedure led to a very small steady-state gain regarding velocity, which has been removed from the model by adding this gain value to the direct feed-through term D of the model. This has removed the gain from the output of the system, however, not from the states. Due to this slight model inaccuracy, a steady-state reference is required. In steady-state, u should equal u_{nom}. The derivation below shows how the model's steady-state gain results in a steady-state generator torque error:

$$u = u_{nom} + u_{damp} = u_{nom} - Kx_{ss} \tag{5-2}$$

$$x_{ss} = (I-A)^{-1}Bu_{nom} \tag{5-3}$$

$$u = u_{nom} - K(I-A)^{-1}Bu_{nom} = (I - K(I-A)^{-1}B)u_{nom} \tag{5-4}$$

From the derivation, it is observed that a zero steady-state gain is obtained if the term $K(I-A)^{-1}B$ equals zero. However, for the identified model the term $K(I-A)^{-1}B = -0.0027$, thus resulting in a 0.27% torque increase in steady-state: $u = 1.0027u_{nom}$. The gain is small,

but undesired and is therefore removed by setting a reference state equal to the steady-state given a nominal generator torque. This results in a Feed-Forward (FF) gain K_{FF}:

$$x_{ref} = Ax_{ref} + Bu_{nom} \tag{5-5}$$
$$x_{ref} = (I - A)^{-1}Bu_{nom} = K_{FF}u_{nom} \tag{5-6}$$

The resulting FF gain K_{FF} results in zero steady-state gain as $KK_{FF} = -0.0027$. State feedback is applied to the error between estimated tower state and reference state as follows:

$$u_{damp} = -K(\hat{x} - x_{ref}) \tag{5-7}$$

The dynamics of the closed-loop system including observer can be assessed regarding stability. The feedforward part of the system does not affect the system poles.

$$Tower: \quad \begin{cases} x(k+1) = Ax(k) + Bu(k) \\ y(k) = Cx(k) + Du(k) \end{cases} \tag{5-8}$$
$$Observer: \quad \begin{cases} \hat{x}(k+1) = (A - LC)\hat{x}(k) + (B - LD)u(k) + Ly(k) \\ y(k) = C\hat{x}(k) + Du(k) \end{cases} \tag{5-9}$$
$$Control: \quad \begin{cases} u(k) = -K\hat{x} \end{cases} \tag{5-10}$$

Using the relations above, the closed-loop system dynamics can be obtained through appending system and observer dynamics:

$$\begin{bmatrix} x(k+1) \\ \hat{x}(k+1) \end{bmatrix} = \begin{bmatrix} A & 0 \\ LC & A - LC \end{bmatrix} \begin{bmatrix} x(k) \\ \hat{x}(k) \end{bmatrix} + \begin{bmatrix} B \\ B \end{bmatrix} u(k) \tag{5-11}$$
$$u(k) = -K \begin{bmatrix} 0 & 1 \end{bmatrix} \begin{bmatrix} x(k) \\ \hat{x}(k) \end{bmatrix} \tag{5-12}$$
$$\begin{bmatrix} x(k+1) \\ \hat{x}(k+1) \end{bmatrix} = \begin{bmatrix} A & 0 \\ LC & A - LC \end{bmatrix} \begin{bmatrix} x(k) \\ \hat{x}(k) \end{bmatrix} - \begin{bmatrix} 0 & BK \\ 0 & BK \end{bmatrix} \begin{bmatrix} x(k) \\ \hat{x}(k) \end{bmatrix} \tag{5-13}$$
$$\begin{bmatrix} x(k+1) \\ \hat{x}(k+1) \end{bmatrix} = \underbrace{\begin{bmatrix} A & -BK \\ LC & A - BK - LC \end{bmatrix}}_{A_{CL}} \begin{bmatrix} x(k) \\ \hat{x}(k) \end{bmatrix} \tag{5-14}$$

Through the coordinate transform $e = x - \hat{x}$, the closed-loop system can be written in block-diagonal form:

$$\begin{bmatrix} x(k) \\ e(k) \end{bmatrix} = \begin{bmatrix} I & 0 \\ I & -I \end{bmatrix} \begin{bmatrix} x(k) \\ \hat{x}(k) \end{bmatrix} = T \begin{bmatrix} x(k) \\ \hat{x}(k) \end{bmatrix} \tag{5-15}$$
$$T \begin{bmatrix} A & -BK \\ LC & A - BK - LC \end{bmatrix} T^{-1} = \begin{bmatrix} A - BK & BK \\ 0 & A - LC \end{bmatrix} \tag{5-16}$$

The poles of A_{CL} are the poles of the closed-loop system, which is a result of the feedback system and the observer. Through the coordinate transform, the system is in block diagonal form. Therefore the eigenvalues of the closed-loop system are equal to the eigenvalues of $A-BK$ and $A-LC$. The poles of the closed-loop system and different subsystems are shown in Table 5-1. This is the separation principle, which allows for a separate design of a feedback controller and an observer. Thus, also in combination with an observer, the same damping values are obtained.

Table 5-1: Modal Damping Control - Poles of the system, the feedback system, the observer and the total closed-loop system

Poles of the system		
	Mode 1	Mode 2
A	$-0.0187 \pm 1.756i$	$-0.0699 \pm 10.288i$
A-BK	$-0.0527 \pm 1.755i$	$-0.3086 \pm 10.284i$
A-LC	$-0.6412 \pm 1.705i$	$-0.3840 \pm 10.286i$
A_{CL}	$-0.0527 \pm 1.755i$ $-0.6412 \pm 1.705i$	$-0.3086 \pm 10.284i$ $-0.3840 \pm 10.286i$
ζ_{CL}	0.03	0.03

A step response of the damped tower is displayed in Figure 5-2. It can be seen that a significant amount of damping is added to the tower at the cost of small torque variations. Additionally, it can be seen that damping is effectively added to both the first and second mode.

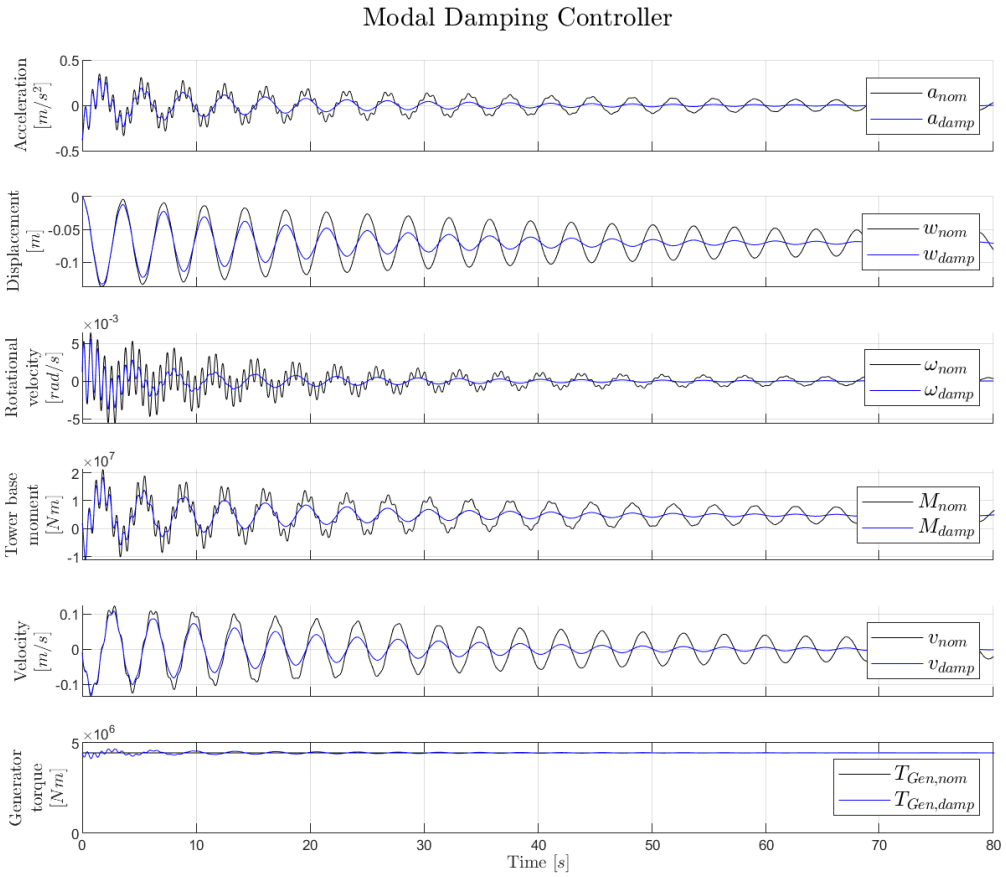

Figure 5-2: Modal Damping Control - Step response simulation

5-2 Implementation

The modal damping controller has been implemented in the Lagerwey controller. A Design Load Case (DLC) experiment consisting of 69 experiments is conducted in `Focus` to assess its performance. For reference, the experiment is compared with an experiment with an equal wind field but without tower damping. Initially, no saturation functions are implemented to assess pure controller performance. The goal is to reduce tower loads at a minimal cost. Therefore, for each experiment a series of performance parameters are determined. The ratio between these parameters with and without tower damping can be determined as a performance measure. By averaging the result over 69 experiments, the significance of the results can be assessed. The results are shown in Table 5-2. Standard deviation is used as main performance parameter, additionally mean power, Damage Equivalent Load (DEL), maximal tower base moment and maximal torque exceedance have been determined. Significant positive effects are shown in green, whereas negative effects are shown in red. Parameters with a very small deviation from nominal are shown in black. Furthermore, the results have been divided into a low wind speed and a high wind speed region.

A significant effect is observed for all parameters related to lateral tower dynamics. Tower base bending moment standard deviation is decreased by 33.5%. It can be noted that the relative decrease in base moment standard deviation and related DEL value are similar. The maximal tower base moment is determined by comparing maximal values for both experiments. These ratios are subsequently averaged over all experiments. On average, the maximal tower base moment is reduced by 23.9%.

Tower top acceleration shows a moderate decrease of 15.4%, which can be explained as external sources of excitation causing tower top acceleration remain equal for both experiments. The additional control action required for tower damping causes a slight increase of 1% in generator torque standard deviation, which is concentrated at the tower frequencies as will be treated shortly. For high wind speeds, this increase is larger, caused by increased vibrations and therefore increased control action. The induced torque variations are of relatively high frequency. Due to the large inertia of the rotor, it acts as a mechanical low-pass filter and torque variations lead to negligible rotor speed variations. Additionally, rotor speed disturbances due to tower top rotational velocity are reduced because of tower damping. Generator power is simply the product of generator speed and generator torque. Generator torque variations therefore directly induce power variations, although power variations are slightly lower due to decreased rotor speed variations. Since tower damping control action is simply added to nominal generator torque and no saturation function is implemented, generator torque can exceed rated torque. The maximum exceedance for all cases is determined from the experiments. For low wind speeds a maximum exceedance of 3.56% is obtained, for high wind speeds 8.42%. It should be noted that the performed DLC experiment is a scenario with significantly larger turbulence intensity than typically observed in the field. Moreover, torque exceedance happens temporarily at the tower frequency and is alternated by torque undershoots. No significant effect is observed in the pitch control action, as no negative effect is seen for rotor speed. Hence, the tower damping controller does not have a detuning or destabilising effect on rotor speed control.

Table 5-2: Modal Damping Control - DLC performance analysis

Ratio(Damping/Nominal) [%]			
Parameter	Average	Wind speeds 3-14 m/s	Wind speeds 15-25 m/s
$\sigma(a)$	84.64	85.40	83.82
$\sigma(w)$	67.82	67.80	67.84
$\sigma(\omega)$	72.75	72.08	73.48
$\sigma(M)$	66.49	64.82	68.32
$DEL(M)$	67.46	66.48	68.54
$\max(M)$	76.11	75.88	76.36
$\sigma(M_{tower\ base,fore-aft})$	100.00	100.04	99.95
$\sigma(M_{tower\ base,torsional})$	99.72	99.77	99.66
$\sigma(M_{blade,leadwise})$	99.93	99.96	99.91
$\sigma(M_{blade,flapwise})$	100.00	99.98	100.03
$\sigma(\theta)$	99.98	100.11	99.83
$\sigma(\Omega)$	99.87	99.95	99.79
$\sigma(P_{gen})$	100.82	100.21	101.49
$\mu(P_{gen})$	99.97	100.00	99.94
$\sigma(T_{gen})$	100.98	100.29	101.72
$\max(T_{gen})$	108.42	103.56	108.42

The standard deviation of the control action u_{damp} can be assessed to analyse the average the size of control action, as shown in Table 5-3. The average control action, and therefore deviation from nominal torque, is 1.23% of rated torque.

Table 5-3: Modal Damping Control - Average control action

Size of damping generator torque			
Parameter	Average	Wind speeds 3-14 m/s	Wind speeds 15-25 m/s
$\sigma(u_{damp})$ [Nm]	54575	27361	84262
$\sigma(u_{damp})/T_{Gen,rated}$ [%]	1.23	0.62	1.90

Figure 5-3 shows a set of parameters for different average wind speeds. First, the standard deviation of damping control action. The figure shows that more control action is required at higher wind speeds and follows a line that corresponds to Figure 4-1. The second graph shows the DEL ratio for all experiments. It is found that for almost all experiments, a ratio in the range of 60-80% is obtained, with no experiments that show a reduction of less than 20%. The third graph shows the standard deviation ratio of generator torque, which is a sum of

nominal generator torque and damping torque. At higher wind speed some experiments show a significant increase, whereas others show a moderate decrease. Finally, the mean power is shown, which, in general, is not affected. Only two outlier experiments show a decrease of 1%. Some experiments show a small increase.

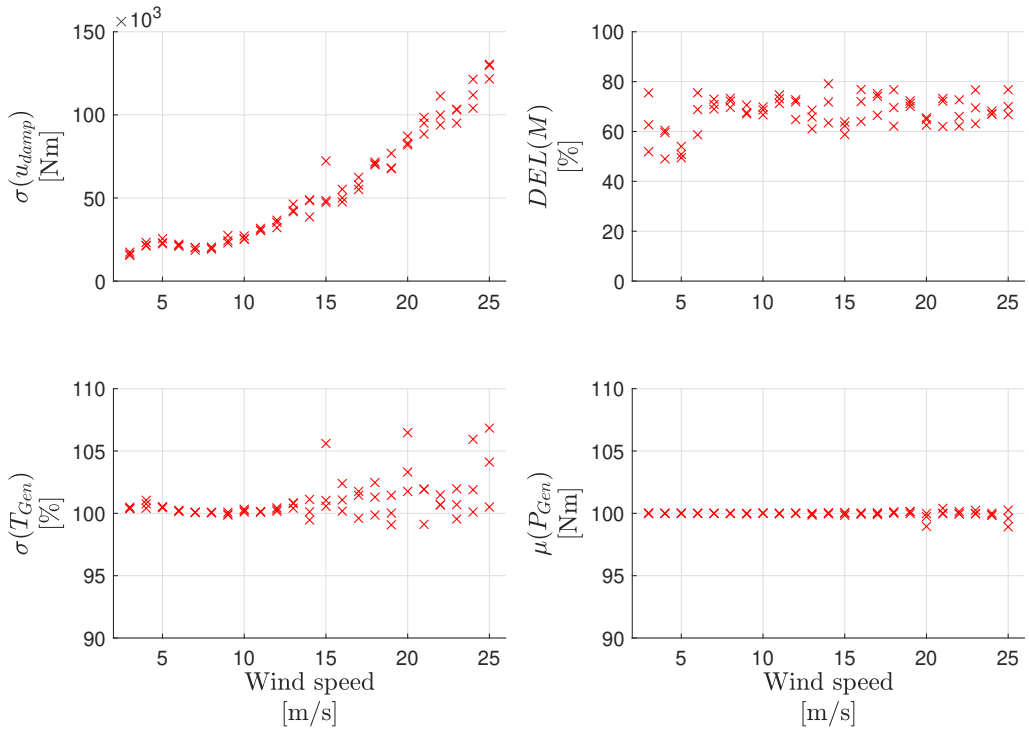

Figure 5-3: Modal Damping Control - Damping control action standard deviation, DEL ratio, generator torque standard deviation ratio and average power shown for different wind speeds

Figure 5-4 shows a typical time response with relatively large vibrations. Tower damping effectively adds damping to both modes. In the displacement signal, where especially the first mode is present this can be clearly observed. The second mode is more dominant in the rotational velocity signal, where effective damping is observed as well. Due to the turbulent wind conditions vibrations never fully dampen out. The torque signal clearly shows the effect of tower damping control action. In general, control action is small and results in small deviations from nominal torque. Rotor speed is unaffected as was observed in the overall results. Figure 5-5 shows the frequency response of the corresponding (complete) time series. It is observed that the controller modification results in different results at the tower frequencies while remaining approximately equal otherwise. Both the first and second mode show a clear reduction in lateral dynamics at tower frequencies, resulting in an increase in generator torque variations.

To be able to assess the effect of modal damping of the first and second mode, another experiment has been performed in which the damping ratio of the only the first mode is altered. The results provide a measure for the contribution of damping the second tower mode and are displayed in Table 5-4. Parameters that change are shown in this table. As expected the effect of damping is slightly reduced.

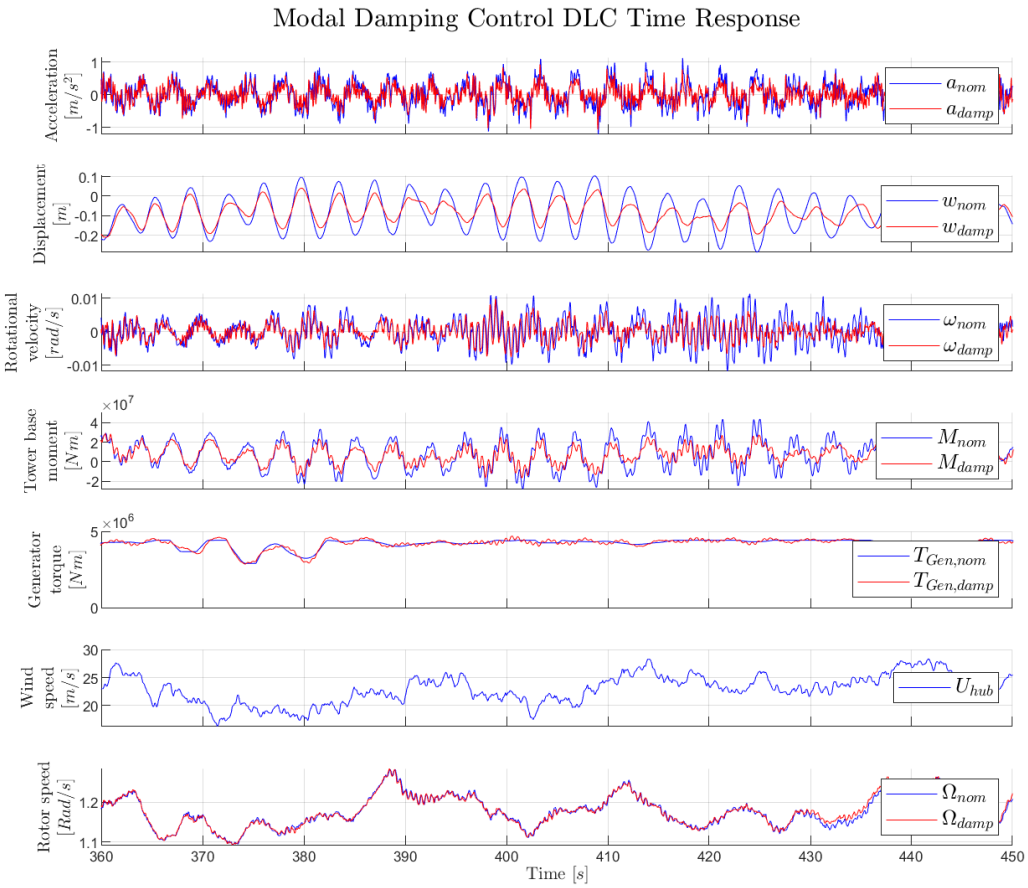

Figure 5-4: Modal Damping Control - DLC1.2 Time response 22 m/s

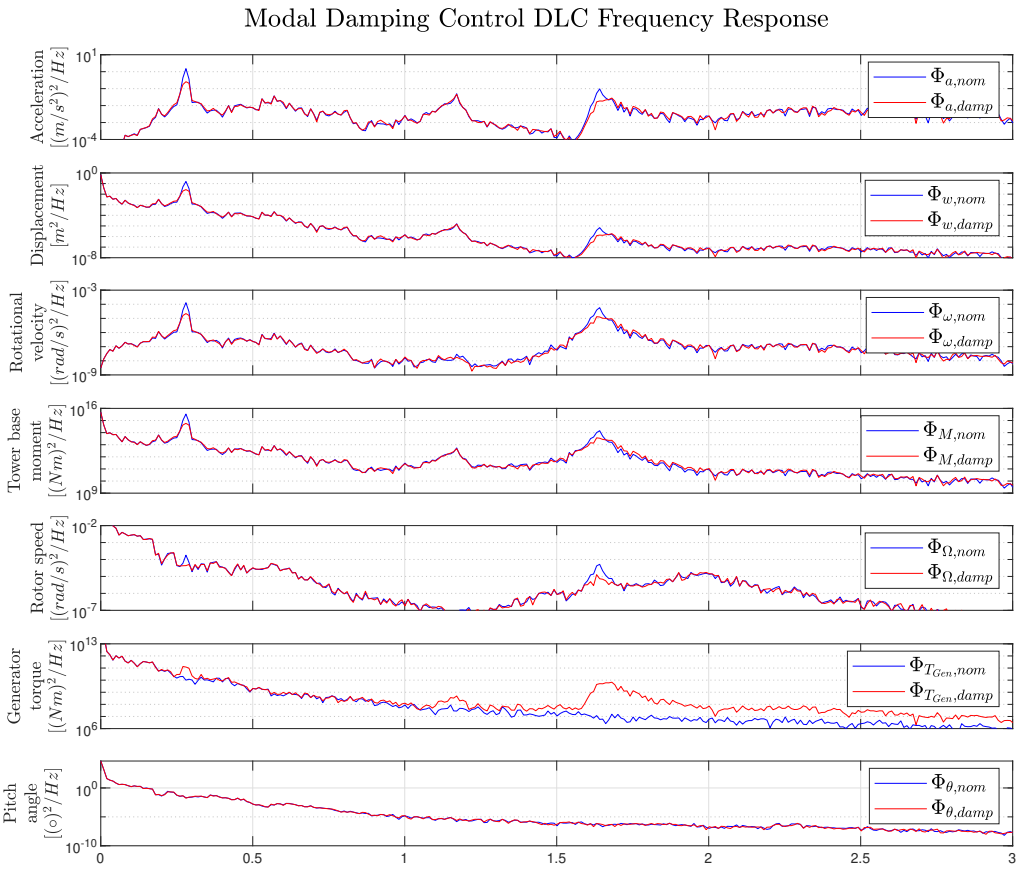

Figure 5-5: Modal Damping Control - DLC1.2 Frequency response 22 m/s

Table 5-4: Modal Damping Control - DLC performance analysis without damping of the second vibration mode

Ratio(Damping/Nominal) [%]			
Parameter	Average	Wind speeds 3-14 m/s	Wind speeds 15-25 m/s
$\sigma(a)$	86.20	87.26	85.04
$\sigma(w)$	67.78	67.82	67.74
$\sigma(\omega)$	86.36	87.47	85.16
$\sigma(M)$	70.56	70.51	70.61
$DEL(M)$	75.80	77.22	74.26
$\max(M)$	80.34	81.04	79.58
$\sigma(\theta)$	99.88	99.95	99.80
$\sigma(\Omega)$	99.90	99.97	99.82
$\sigma(P_{gen})$	100.77	100.17	101.42
$\mu(P_{gen})$	99.96	100.00	99.92
$\sigma(T_{gen})$	100.91	100.24	101.63
$\max(T_{gen})$	107.84	102.80	107.84

The displacement signal shows almost no difference since it is dominated by the first mode. Whereas in the previous experiment, the base moment standard deviation and the DEL seemed to be similar, now a larger difference is observed. Omitting the second mode damping leads to a moderate decrease in the reduction of the standard deviation, but does lead to a more significant decrease of DEL reduction. Therefore, the second mode has a more significant contribution to the DEL than can be observed from the standard deviation of tower base moment. These results are summarised in Table 5-5. Here, the total DEL reduction is listed along with the DEL reduction in case of only mode 1 damping. The difference between these two results is attributed to damping of the second mode. For high wind speeds, the DEL is to a larger degree dominated by the first mode.

Table 5-5: Modal Damping Control - DEL reduction as a result of modal damping

DEL Reduction [%]			
Case	Average	Wind speeds 3-14 m/s	Wind speeds 15-25 m/s
Total	32.54	33.52	31.46
Mode 1	24.20	22.88	25.74
Mode 2	8.34	10.74	5.72

A time and frequency response are shown in Figure 5-6 and Figure 5-7 respectively. In the time response, it is observed how the first mode is effectively damped, whereas the second

mode remains unchanged. The frequency response only shows a difference at the first tower frequency. Hence, damping can be added to each mode individually while not affecting another mode.

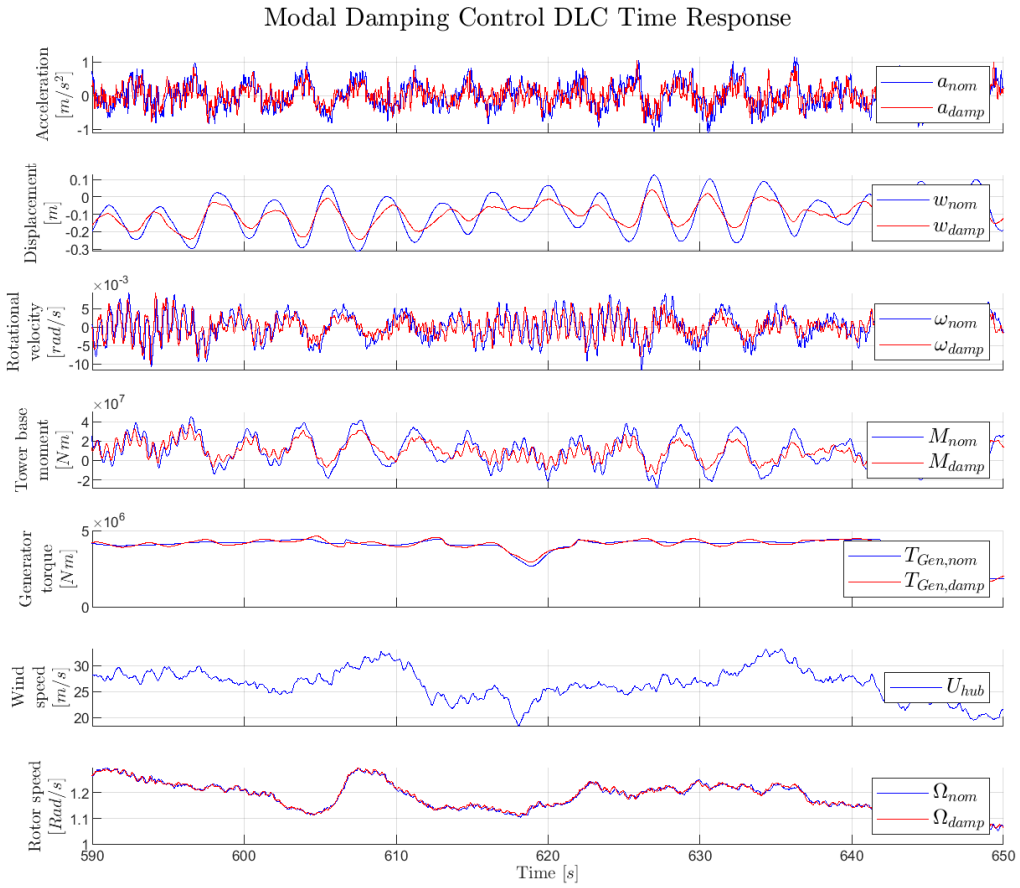

Figure 5-6: Modal Damping Control - DLC1.2 Time response 25 m/s without damping of the second vibration mode

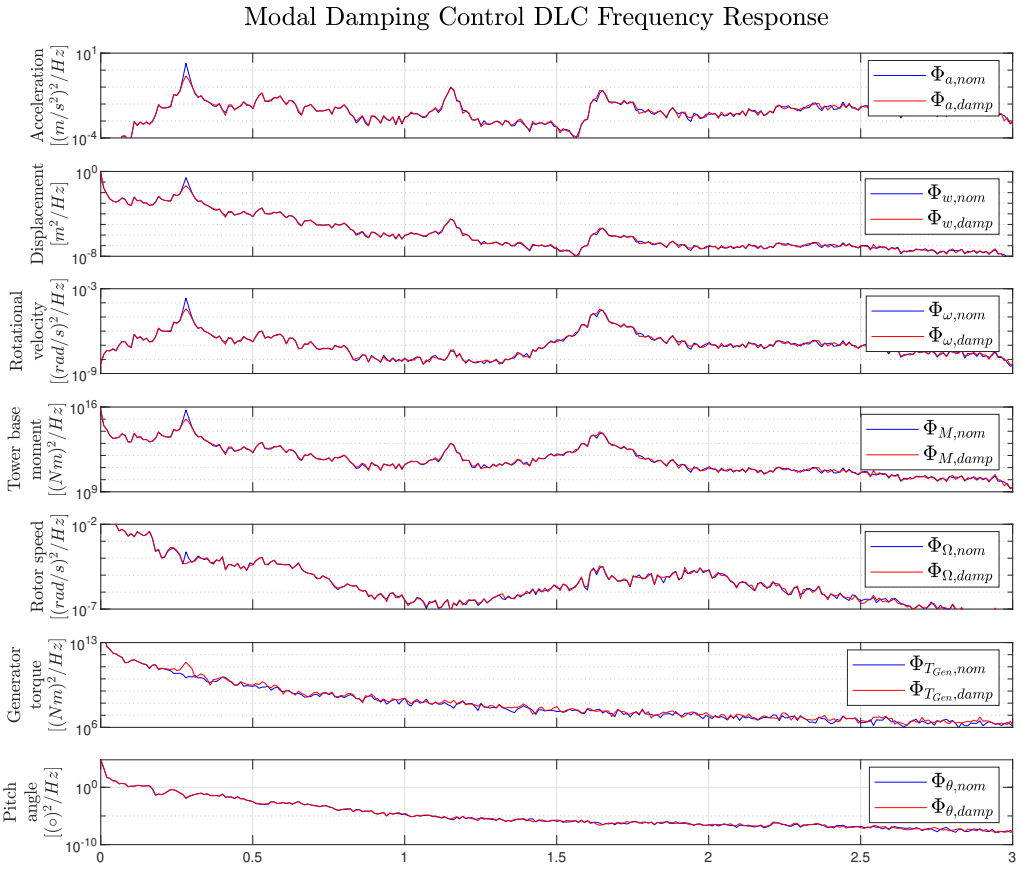

Figure 5-7: Modal Damping Control - DLC1.2 Frequency response 25 m/s without damping of the second vibration mode

Finally, two more controllers have been designed with different damping ratios, being $\zeta = 0.05$ and $\zeta = 0.1$. The most important results are compared in Table 5-6. As expected, increasing the damping ratio leads to a further decrease in tower loads. However, the decrease in tower loads is not linearly related to the increase in damping ratio. For $\zeta = 0.03$, the damping ratio is tripled which resulted in a decrease of 32% of the DEL. For $\zeta = 0.1$, a tenfold increase in damping ratio is obtained, which results in a further decrease of only 12% of the DEL. Power variations show a significant increase from 0.8% to 3.54%. It appears that adding any damping is beneficial since the tower damping ratio is not a constant parameter but dependent on aerodynamic conditions. Therefore situations of negligible damping can occur during which tower vibrations caused by external excitation sources are hardly damped. With added damping, these vibrations are counteracted and the tower is brought back into a steady-state at all times. Once the tower reaches a steady-state, no more fatigue damage is caused. Increasing the damping ratio decreases the settling time of the tower and therefore results in a further decrease in fatigue damage. However, this decrease is limited and does not weigh up to the additional control effort which is required.

Table 5-6: Modal Damping Control - DLC performance comparison for different damping ratios

Ratio(Damping/Nominal) [%]				
Parameter	Damping ratio ζ	Average	Wind speeds 3-14 m/s	Wind speeds 15-25 m/s
$\sigma(a)$	0.03	84.64	85.40	83.82
	0.05	82.20	83.60	80.68
	0.1	80.67	82.65	78.50
$DEL(M)$	0.03	67.46	66.48	68.54
	0.05	61.02	60.85	61.22
	0.1	55.65	56.38	54.85
$\sigma(\Omega)$	0.03	99.87	99.95	99.79
	0.05	99.98	99.96	100.00
	0.1	100.04	99.88	100.23
$\sigma(P_{gen})$	0.03	100.82	100.21	101.49
	0.05	101.53	100.46	102.70
	0.1	103.54	101.10	106.20
$\sigma(T_{gen})$	0.03	100.98	100.29	101.49
	0.05	101.92	100.67	103.28
	0.1	104.51	101.66	107.62
$\max(T_{gen})$	0.03	108.42	103.56	108.42
	0.05	113.28	105.42	113.28
	0.1	122.32	109.35	122.32
$\sigma(u_{damp})/T_{Gen,rated}$	0.03	1.23	0.62	1.90
	0.05	1.90	0.94	2.94
	0.1	3.02	1.52	4.65

5-3 Conclusion

From the results, it is found that the tower response is dominated by the first mode. Therefore damping of only the first mode already leads to significantly improved results. Although in practice, problems typically stem from the first mode, damping can be effectively added to the second mode which results in an additional decrease in loads. The project considers only one turbine type with a 132m tower height. Currently, Enercon/Lagerwey produces turbines with tower heights up to 166m and with increasing rotor diameters. As towers become taller and more flexible, the natural frequencies will decrease, resulting in increased tower excitation since tower frequencies lie closer to periodic excitation sources. The need for tower control in general increases, and the advantages of damping of the second mode will increase.

In the tuning process of the damping controller, the negative effects of the controller have to be taken into consideration. As mentioned previously, tower damping is not the main controller objective, but rather an additional feature. The induced torque variations should be kept minimal to prevent too large power variations. Although damping is modelled as a

constant value, it is to a large degree the result of aerodynamic damping, while structural damping is rather small. Due to turbulent wind conditions, this aerodynamic damping ratio can be inconsistent, which might result in moments of decreased damping. Active damping is consistent, thus resulting in a guaranteed amount of damping at all times. It is observed that increasing damping to a still moderate value results in a great decrease of loads. This does go at the cost of increased torque/power variations. The DLC data set can be considered a worst-case scenario since a blade mass imbalance is present (one blade is 1% heavier) and turbulence intensity is high (16% versus 10% in typical site conditions), which leads to continuous excitation of the tower. In the field, conditions are typically less turbulent and thus tower vibrations are somewhat more occasional depending on operational conditions. In a situation without tower vibrations, the controller does not affect performance. One could imagine situations in which the tower is temporarily excited after which the excitation source disappears again, for example due to a gust or eddies in the wind field. In such a case, the damping controller results in a faster return to a stable tower state and therefore prevents undesired disturbances due to tower vibrations.

The design method provides great freedom in tuning the amount of damping for each mode and might allow for site-specific damping ratios. Thus increasing damping for more turbulent sites and decreasing damping for less turbulence.

Chapter 6

Conclusions

6-1 Conclusions

Three main research questions have been defined in this project. The first question is:

How can tower top rotational dynamics be modelled and included in a tower model?

The first step of the project was to derive a tower model which includes rotational dynamics. It was found, using Euler-Bernouilli and Timoshenko-Ehrenfest beam theories, that the dynamics of a tower can be separated into a time-dependent and space-dependent part. The time-dependent part is represented by a mass-spring-damper system for each vibration mode, and is independent of tower height. All output parameters regarding the tower are related to the time-dependent system via the mode shapes. This allows the inclusion of lateral and rotational dynamics as well as bending moments at arbitrary heights into the model without increasing model complexity. During the identification procedure, it was found that an accurate model can be obtained and that the previously established relations are valid.

The model has been obtained through a black-box identification procedure. The main advantage of the method is that it directly resulted in the required discrete-time linear-time-invariant single-input-multiple-output state-space model. Additionally, the singular value decomposition could be used effectively to estimate an adequate model order. The effect of aerodynamic damping and coupling with other turbine components, such as the blades, is taken into account. This resulted in more accurate estimation of damping ratios and natural frequencies. This resulted in an accurate model, however, not in the exact form as derived from physical equations. Additionally, very small steady-state gains are obtained in the model due to numerical inaccuracy. This leads to the use of a feedforward term for the state-feedback controller.

With the model identified, the closed-loop interaction between the tower and the torque controller is quantified. In the sub-rated operating region, where the torque-speed curve has a positive gain, the interaction has a damping effect on the tower. In the above-rated

operating region, the effect is opposite and damping is reduced. It is found that due to the absolute gain values in respective regions, the effect of damping in a part of the sub-rated region is significantly larger than the destabilising effect above-rated. It should be noted that tower vibrations are especially large at high wind speeds, where the turbine operates predominantly in the above-rated region of the torque-speed curve.

How can an online estimate of tower top rotational velocity, including multiple tower vibration modes, be obtained and can it be used for rotor speed measurement correction?

A static Kalman filter has been designed using this model. Using tower top acceleration and generator torque as inputs, adequate state/output estimates can be obtained. In a Design Load Case (DLC) experiment, the tower is mainly excited by external sources of excitation, rather than generator torque. Therefore, the state estimates are mainly determined by the acceleration signal. These periodic and stochastic excitation sources are typically zero-mean. Generator torque is not, therefore resulting in steady-state values for displacement and tower base bending moment. Taking into account generator torque is therefore important in order to accurately estimate these signals. The Kalman gain has been carefully tuned using DLC data, which resembles actual turbine operation with significant turbulence. Noise in the acceleration signal due to external excitation sources limits the Kalman gain. Especially the torsional tower mode is present in the acceleration signal. The disturbance is amplified in the state estimates for more aggressive Kalman gains, therefore posing a limitation. It has been shown that both the first and second vibration mode can be removed from the rotor speed measurement using the tower top rotational velocity estimate. The Kalman filter has been implemented in the Lagerwey controller and tested in `Focus`. The implementation removes the closed-loop tower-controller interaction. This leads to a constant damping ratio over the entire operating region. In an experiment with a staircase wind profile, this effect could be observed. The Damage Equivalent Load (DEL) showed a 6.9% increase in sub-rated conditions and a 7.4% decrease in above-rated conditions.

Can a controller be designed, able to optimally damp multiple vibration modes?

With rotor speed measurement correction, a constant damping ratio is obtained throughout the entire operating region. The damping ratio could be increased through active damping in order to reduce tower fatigue damage. Hence, a modal damping controller has been developed. In principle, it is a state-feedback controller with a pole-placement tuning method, which allows to select damping ratios for each mode individually. It is found that the method is intuitive and effective. For the designed controller a DEL reduction of 32.5% is obtained with a 1% increase in generator torque standard deviation. It was found that the second mode contributes to approximately 25% of this reduction. A further increase in damping ratio can be attained, however, this will lead to a disproportionate increase in control action.

In summary:

- Tower top rotational velocity and tower base bending moment can be included in a tower model without increasing model complexity.

- Accurate state estimation can be performed using only tower top acceleration and generator torque. A tower top rotational velocity estimate can effectively be used to remove disturbances in rotor speed.
- Active damping can be added to individual modes using state-feedback.

6-2 Recommendations

Recommendations for future work based on the research are denoted here:

1. **Derive a tower model based on physical equations:**
   The first recommendation regards the derivation of the tower model. As mentioned, identification has led to a black-box model with no physical states. Therefore the model does not correspond to the model form as stated in Chapter 2. This makes using the model less intuitive. Identification led to small steady-state errors in the model which were removed with a feedforward term in the state-feedback controller. One could also derive a model using physical equations. Modes shapes, derived from a Finite-Element-Model (FEM) could be used to establish relations for rotational dynamics and bending moments. Alternatively, one could use a grey-box model identification method. Therefore only estimating a set of parameters from data, rather than the entire model. This would not result in any steady-state errors.
2. **Add additional excitation sources to the model:**
   In the current Kalman filter, all excitation sources other than generator torque are modelled as Zero-Mean-White-Noise (ZMWN) noise. The reason for doing so is that typically no information is available of these other sources, whereas generator torque is a control parameter. Possibly, estimates can be obtained of these unknown input sources, given that some are to a certain extent deterministic and/or periodic. For example, the effects of tower shadow and wind shear is for a large part dependent on wind speed (of which an estimate can be obtained) and azimuth position of the rotor. A feedforward estimate could be derived and taken into account, which would reduce the amount of excitation considered as stochastic. This could increase the performance of the Kalman filter. Since a large part of tower excitation is periodic, another possibility is to use Gaussian processes to obtain an online estimate of a periodic input disturbance using the estimation error.
3. **Control tower base bending moments using Model Predictive Control (MPC):**
   The currently designed state feedback controller is always active if vibrations are present. However, steel has a certain fatigue limit, a load limit below which no damage is caused. This means that small vibrations do not lead to fatigue damage. An MPC controller could be designed which keeps tower base bending moments within certain bounds. In such a scenario, the controller would only become active if tower vibrations are large enough. The advantage is that nominal turbine performance is not affected in the case of small tower vibrations.

Bibliography

[1] E. A. Bossanyi. "Wind Turbine Control for Load Reduction". In: *Wind Energy* (June 2003). DOI: 10.1002/we.95.

[2] William E Boyce and Richard C. DiPrima. *Elementary Differential Equations and Boundary Value Problems*. WILEY, 2012. ISBN: 978-0-470-45831-0.

[3] Asier Diaz de Corcuera et al. "H_∞ Based Control for Load Mitigation in Wind Turbines". In: *Energies* (Dec. 2012). DOI: 10.3390/en5040938.

[4] Martin A. Evans, Mark Cannon, and Basil Kouvaritakis. "Robust MPC Tower Damping for Variable Speed Wind Turbines". In: *IEEE Transactions on Control Systems Technology* (Jan. 2015). DOI: 10.1109/TCST.2014.2310513.

[5] Adrian Gambier. "Simultaneous Design of Pitch Control and Active Tower Damping of a Wind Turbine by using Multi-objective Optimization". In: *IEEE* (Aug. 2017). DOI: 10.1109/CCTA.2017.8062698.

[6] M. Geyler and P. Caselitz. "Robust Multivariable Pitch Control Design for Load Reduction on Large Wind Turbines". In: (Aug. 2008). DOI: 10.1115/1.2931510.

[7] Lars Christian Henriksen. "Model Predictive Control of Wind Turbines". In: (Oct. 2011).

[8] E.L. van der Hooft, P. Schaak, and T.G. van Engelen. "Wind turbine control algorithms". In: (Dec. 2003).

[9] Stoyan Kanev. "Towards new industrial software for advanced wind turbine control". In: (Mar. 2011).

[10] Anne Koerber and Rudibert King. "Combined Feedback–Feedforward Control of Wind Turbines Using State-Constrained Model Predictive Control". In: (June 2013). DOI: 10.1109/TCST.2013.2260749.

[11] Paul A. Lagace. *Vibration of Continuous Systems[Lecture Slides]*. 2001.

[12] Michael Liebreich. "London summit 2017". In: (Sept. 2017).

[13] Wai Hou Lio, J.A. Rossiter, and Bryn L. Jones. "A Review on Applications of Model Predictive Control to Wind Turbines". In: (July 2014). DOI: 10.1109/CONTROL.2014.6915220.

[14] Eduardo José Novaes Menezes et al. "Active load control of large wind turbines using state-space methods and disturbance accomodating control". In: (May 2018). DOI: 10.1016/j.energy.2018.02.143.

[15] Sebastiaan Paul Mulders et al. "Preventing wind turbine tower natural frequency excitation with a quasi-LPV model predictive control scheme". In: *Wind Energy* (2020). DOI: 10.1002/we.2447.

[16] Yoonsu Nam, Phan Trung Kien, and Yo-Han La. "Alleviating the Tower Mechanical Load of Multi-MW Wind Turbines with LQR Control". In: (Nov. 2013). DOI: 10.6113/JPE.2013.13.6.1024.

[17] Lucy Y. Pao and Kathryn E. Johnson. "Control of Wind Turbines". In: (Apr. 2011). DOI: 10.1109/MCS.2010.939962.

[18] *Paris Agreement*. 2015.

[19] Valentin Pascu, Stoyan Kanev, and Jan-Willem van Wingerden. "Adaptive tower damping control for offshore wind turbines". In: *Wind Energy* (Oct. 2016). DOI: 10.1002/we.2058.

[20] B Ritter et al. "The design of nonlinear observers for wind turbine dynamic state and parameter estimation". In: (2016). DOI: 10.1088/1742-6596/753/5/052029.

[21] Surya Santoso, Neeraj Karnik, and Swagata Das. "Time-Domain Modeling of Tower Shadow and Wind Shear in Wind Turbines". In: *Hindawi* (2011). DOI: 10.5402/2011/890582.

[22] David Schlipf, Dominik Johannes Schlipf, and Martin Kühn. "Nonlinear model predictive control of wind turbines using LIDAR". In: (Oct. 2013). DOI: 10.1002/we.1533.

[23] Mohsen Soltani et al. "Load Reduction of Wind Turbines Using Receding Horizon Control". In: (Sept. 2011). DOI: 10.1109/CCA.2011.6044407.

[24] *Statistical Review of World Energy*. 2020.

[25] Michel Verhaegen and Vincent Verdult. *Filtering and System Identification[A least squares approach]*. Cambrige University Press, 2007. ISBN: 978-1-107-40502-8.

[26] Alan D Wright. "Modern Control Design for Flexible Wind Turbines". In: (July 2004). DOI: 10.2172/15011696.

[27] Zili Zhang et al. "Dynamics and Control of Lateral Tower Vibrations in Offshore Wind Turbines by means of Active Generator Torque". In: *energies* (Nov. 2014). DOI: 10.3390/en7117746.

Glossary

List of Acronyms

LLS	Linear Least Squares
DLC	Design Load Case
COM	Centre Of Mass
EB	Euler-Bernouilli
TE	Timoshenko-Ehrenfest
VAF	Variance Accounted For
PSD	Power Spectral Density
DEL	Damage Equivalent Load
LCOE	Levelised Cost Of Energy
AEP	Annual Energy Production
PMDD	Permanent Magnet Direct Drive
MST	Modular Steel Tower
DT	Discrete-Time
LTI	Linear-Time-Invariant
SS	State-Space
SISO	Single-Input-Single-Output
SIMO	Single-Input-Multiple-Output
PI-MOESP	Past-Input-Multivariable Output-Error-State-sPace
PO-MOESP	Past-Output-Multivariable-Output-Error-State-sPace
SVD	Singular Value Decomposition
ODE	Ordinary Differential Equation
PDE	Partial Differential Equation
PD	Partial Dynamics
FD	Full Dynamics

NWP	Normal Wind Profile
NTM	Normal Turbulence Model
MPC	Model Predictive Control
ZOH	Zero-Order-Hold
DARE	Discrete-Algebraic-Ricatti-Equation
FF	Feed-Forward
FEM	Finite-Element-Model
ZMWN	Zero-Mean-White-Noise

List of Symbols

$(\cdot)^{(i)}$	Blade-effective ..
α	Rotational acceleration
$\dot{x}_{fa}$	Tower top fore-aft velocity
η	Viscous tower damping ratio
κ	Timoshenko shear coefficient
λ	Tip speed ratio
$\mathcal{O}_s$	Observability matrix
Ω	Actual rotor speed (as seen from earth)
ω	Tower top rotational velocity in (lateral) x-direction
ω_d	Damped natural frequency
ω_n	Undamped natural frequency
Ω_{meas}	Measured rotor speed (as seen from generator stator)
ϕ	Angular displacement of the tower in (torsional) z-direction
ψ	Rotor azimuth
ρ_t	Beam mass density
θ	Pitch angle
φ	Tower top angular displacement
$\varphi(z)$	Tower angular displacement at height z
ζ	Damping ratio
A	Cross-sectional area
A	System state matrix
a	Tower top lateral acceleration
a_u	Periodic centrifugal force amplitude due to rotor mass imbalance
B	Input matrix
B	Number of blades
C	Output matrix
C_Q	Torque coefficient

C_v	Velocity output matrix
D	Feedthrough matrix
d	Distance from tower midline to centre of mass of rotor-nacelle assembly
D_v	Velocity feedthrough matrix
E	Elastic Modulus
F	Force
F_{sw}^{rot}	Centrifugal force-induced lateral force acting on the tower
F_{sw}	Resultant lateral force acting on the rotor plane
G	Shear modulus
I	Area moment of inertia
J	Moment of inertia
K	State Feedback gain
$K_{\Omega \to T}$	Torque controller gain
K_{AR}	Minimal torque controller gain (found above-rated)
K_{FF}	Feed-forward gain
K_{SR}	Maximal torque controller gain (found sub-rated)
L	Hub height
L	Kalman gain
M	Tower base bending moment
m	Mass of rotor-nacelle assembly
$M(z)$	Tower bending moment at height z
N	Number of columns of the Hankel Matrix
n	Model order
P	State-error covariance matrix
P_{rated}	Rated generator power
P_{Rotor}	Rotor plant model
P_{Tower}	Tower plant model
Q	Process noise covariance matrix
q	Distributed load
R	Measurement noise covariance matrix
R	Rotor radius
r	Rotor effective radius
r_{tow}	Tower radius
S	Cross-covariance matrix
s	Number of rows of the Hankel Matrix
T	Torque
T_s	Sampling time
T_{gen}	Generator torque set point
T_{rotor}	Aerodynamic torque
U	Wind Speed at hub height

u_{damp}	Tower damping control action
U_{shd}	Shadow-induced wind speed
U_{shr}	Shear-induced wind speed
U_{tow}	Tower-induced wind speed
$v(k)$	Measurement noise
$w(k)$	Process noise
$w(z)$	Tower displacement at height z
x	System state
x_e	State estimation error
x_{bl}	Distance from blade origin to tower mid line
z	Height along tower z-axis